UNDERSTANDING NANOEMULSIONS

BY

LAURA LEE

A thesis submitted to
The University of Birmingham
for the degree of
Doctor of Philosophy

Microstructure Group
School of Chemical Engineering
College of Engineering and Physical Sciences
University of Birmingham
February 2015

Abstract

Nanoemulsions have many advantages: enhanced creaminess, better stability and more efficient delivery of neutraceuticals to the body. All these advantages give incentives for food companies to replace existing micron-sized emulsions with nanoemulsions.

This work has developed the understanding of how to produce nanoemulsions efficiently using two high pressure devices: the industrially used high pressure valve homogeniser (HPH) and the efficient but hard to scale Microfluidizer. A range of different oil to aqueous phase viscosity ratios, emulsifier types, pressure drops and number of passes through the devices were tested. It was shown for O/W nanoemulsions the Microfluidizer produces the final droplet size after one pass whereas in the HPH coalescence was shown to be prevalent thus requiring several passes to get to the final droplet size and a tight droplet size distribution. The geometry of these devices was shown to be the largest influence on homogenisation efficiency. Upon lowering the viscosity ratio (increasing the continuous phase viscosity), coalescence in the HPH was reduced and for the W/O emulsions produced, the efficiency was matched to the Microfluidizer, with both producing minimum droplet diameters of 50 nm. The oil continuous nanoemulsions produced here would be a good oil mimetic.

Flavour/volatile release was measured from a series of O/W emulsion droplet sizes, ranging from 150 nm up to 40 μm, and detected using a mass spectrometer. It is shown that with increasing droplet size the continuous phase volatile release increases, as there is less oil-water interface for the volatile to get trapped (partitioned) into and a lower number of droplets to reduce the transfer through the continuous phase. The dispersed phase volatile detection was similar for all emulsion droplet sizes and oil phase fractions.

This thesis concludes by researching an application of nanoemulsions: inclusion of oil within fluid gels to reduce the bland flavour associated with fluid gels only. It was shown that up to 30% oil can be incorporated within the polysaccharide particles although the viscosity reduces with increasing oil inclusion. Additionally, the emulsifier type used to stabilise the oil influences the fluid gel properties with sodium caseinate producing the highest elastic modulus, compared to Tween 20 and to the least SDS.

Acknowledgements

I would like to acknowledge the exceptional support that I have had throughout my PhD from my immediate supervisors Professor Ian Norton, Dr Ian Noble, Dr Robin Hancocks and Dr Jennifer Norton. Their support has helped me to publish and present several papers, and produce a thesis that I am proud of.

My appreciation goes to the department of Chemical Engineering at The University of Birmingham for funding this work.

Friends and family are so important and mine have been exceptional. Thank you to Mum and Dad, Kayleigh and Clare, Sue and Steve, and Taj (especially if you read my thesis drafts!).

Finally, I want to thank those who made the lab a fun as well as productive environment to work in throughout my PhD.

Contents

List of Figures

List of Tables

Nomenclature

Fluid Mechanics

c_∞	solubility of droplet in continuous phase	mol/m^3
D	diffusion co-efficient	m^2/s
d	droplet diameter	m
$d_{3,2}$	Sauter mean diameter (weighted for volume to surface area)	m
F	force	N
g	gravity	m/s^2
G'	storage or elastic modulus	Pa
G"	loss or viscous modulus	Pa
IMax	maximum ion intensity	arbitrary units
k	kinetic energy	J
K	mass transfer co-efficient	kg/m^2
L	length	m
m/z	mass to charge ratio	kg/C
P_L	Laplace pressure	Pa
p	statistical significance	dimensionless
r	droplet radius	m
rcf	relative centrifugal force	N
Re	Reynolds Number	dimensionless
R_g	ideal gas constant	J/mol.K
T	temperature	K
t	time	s
U	velocity	m/s
v	molar volume of particle material	m^3/mol
v_s	separation velocity	m/s
ε	energy dissipation	W/kg
η	viscosity	Pa.s
η_{ratio}	viscosity ratio	dimensionless
θ	wetting angle	^{o}
λ_K	Kolmogorov length scale	m
ν	kinematic viscosity	m^2/s
ρ	density	kg/m^3
σ_{OW}	oil-water interfacial tension	mN/m
$\dot{\gamma}$	shear rate	s^{-1}
∇v	velocity gradient	m/s

Subscripts

A	air
c	continuous phase
d	dispersed phase
E	emulsion

O	oil
W	water

Abbreviations

APCI	atmospheric pressure chemical ionisation
CFD	computational fluid dynamics
cps	corrected particle scattering
FG	fluid gel
HLB	hydrophilic-lipophilic balance
HPH	high pressure valve homogeniser
HPPS	High Performance Particle Sizer
HS	headspace
LE	lipid effect
MF	Microfluidizer
MS	mass spectroscopy
O/W	oil-in-water emulsion
PEG	polyethylene glycol
PGPR	polyglycerol polyricinoleate
PTR	proton transfer reaction
RANS	Reynolds averaged Navier-Stokes
RNG	Reynolds normalisation group
SDS	sodium dodecyl sulphate
W/O	water-in-oil emulsion
κ-c	kappa carrageenan

CHAPTER 1. INTRODUCTION

1.1 Motivation for thesis and background

Consumers are getting more conscious about the ingredients in the food they are consuming leading to a consumer pull towards formulation and production changes to increase the benefit of food on their health by including higher quantities of vitamins and minerals, and lowering the numbers and quantities of additives along with lowering the fat content.

With the rising levels of obesity in the developed world the governments have started pressuring food manufacturers to reduce the calorie content of food. According to national statistics, over the two decades between 1993 and 2014 obesity levels in England have increased from 14.8% to 24.8% (hscic.gov, 2014). Obesity is a disease that causes many other health issues: type II diabetes, coronary heart disease, hypertension and stroke, asthma, depression, metabolic syndrome, dyslipidaemia, certain cancers, gastro-oesophageal reflux disease, gallbladder disease, reproductive problems, osteoarthritis and back pain, obstructive sleep apnoea, breathlessness, and psychological distress (NHS, 2012). Obesity and its related diseases are currently estimated to be costing the NHS £5 billion per year (GOV.UK, 2013). The government are reacting to these increasing obesity levels and the associated costs by, among other methods, investing in research to develop lower fat, lower sugar and/or lower carbohydrate foods that can be consumed as alternatives to the higher calorie versions. Fat reduction has been prioritised as the most beneficial component in food to be reduced since it has the highest energy density at 9 kcal/g, compared to 4 kcal/g for protein and 3.75 kcal/g for carbohydrate (Norton, 2011).

Despite excessive dietary consumption, someone suffering with obesity is also likely to have high rates of micronutrient deficiencies. If specific vitamins and minerals are found to be deficient in the consumer's diet this can lead to problems with glucose metabolism and insulin signalling pathways thus leading to the development of type II diabetes (Via, 2012). Therefore, in addition to developing reduced fat foods, there is motivation to develop structures which also aid in the delivery of nutrients and minerals more efficiently to the body.

Lower fat products are being researched and developed with the aim of replacing the fuller fat version in the overweight consumer's diet. One of the challenges of researching and developing new products is to preserve the consumer's satisfaction in the product, through maintaining the sensory quality (Tuorila and Cardello, 2002).

1.1.1 Approach for researching and developing new products

A generally accepted approach for engineering new lower fat products is the 'Microstructure approach', see Figure 1.1.

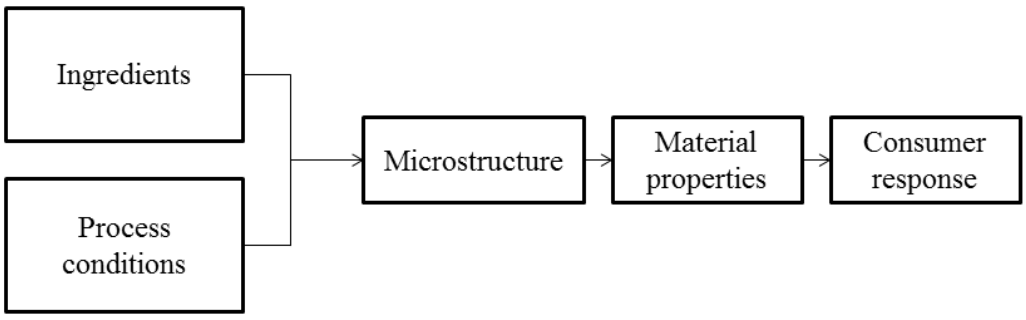

Figure 1.1: Microstructure approach for food engineering

This approach acknowledges that a formulation or processing change influences the microstructure which in turn affects the material properties and the consumer response. In the case of fat reduction in foods, it would be desirable to maintain a similar microstructure despite the formulation change, thus maintaining the consumer response. Alternatively, novel microstructures can be designed to provide similar material properties and consumer responses to the fuller fat product.

1.1.2 Nanoemulsions and their relevance

Products containing both oil/fat and water are known as emulsions. They are found in many industries including food, personal care, pharmaceuticals, agro-chemicals and cosmetics, although this thesis had a bias towards emulsions in food. Emulsions are dispersions of oil and water, with either the oil dispersed (oil-in-water emulsions or O/W) or water dispersed within oil (water-in-oil emulsions or W/O). Mayonnaise, salad dressings, milk, cream liqueurs and soups are some examples of O/W emulsions. There are fewer examples of emulsion products that are oil or fat continuous (W/O) however; margarine and the oil mimetic, Flora Cuisine, are typical.

An approach of enhancing the acceptance of emulsion based products whilst reducing the fat content is to produce nanoemulsions. Nanoemulsions have droplet diameters of 20 – 200 nm and have many advantages. The sensory benefits of the smaller droplets are that they are perceived as creamier or fattier in the mouth (Lett *et al.*, 2014). This benefit can be exploited by reducing the fat content of the product to match the creaminess to the fuller fat product. Additionally, the smaller droplet sizes lead to extended physical stability and therefore, providing that the product is chemically stable, the shelf life of the product can be extended. It

is claimed that nano-sized droplets allow for a higher proportion of oil soluble nutrients to adsorb through the gut wall into the blood stream (McClements, 2011), and if the droplets are small enough (below 50 nm), they deliver oil soluble micronutrients and bio-actives via a translucent emulsion. The notable advantage here is that nanoemulsions can be used to deliver nutrients commonly absent in western diets to help reduce malnutrition related diseases or metabolic disorders, for example type II diabetes (Via, 2012). Faster flavour release is also often quoted as an additional advantage of nanoemulsions however this has not been researched fully. As a consequence of the many advantages that nanoemulsions provide, existing micron-sized emulsion products are being superseded by sub-micron or nano-sized alternatives.

Nanoemulsions can be produced using low energy techniques by exploiting chemistry to cause phase inversion, although this method commonly produces less stable nanoemulsions and restricts the ingredients that can be used (Tadros *et al.*, 2004, Solans *et al.*, 2005). More frequently, nanoemulsions are produced using high pressure homogenisers which create a large amount of pressure energy that dissipates as turbulent kinetic energy causing droplet deformation and break-up (Jafari *et al.*, 2007b). There are two main high pressure homogenisers: a high pressure valve homogeniser (HPH) or a high pressure impinging jet (Microfluidizer). HPH is commonly used industrially for the production of sub-micron emulsions or nanoemulsions, although its greatest disadvantage is that it is inefficient as it causes droplets to re-collide during processing with a chance of coalescence (Jafari *et al.*, 2008). In comparison, the Microfluidizer is more efficient but has a low flowrate and is not easily scalable for industrial production (Gavi *et al.*, 2007). The Microfluidizer is a relatively recent device and the droplet break-up mechanism is not fully understood (Cook and Lagace,

1985). This current gap in knowledge has led to the need for a better understanding of how both high pressure devices produce nanoemulsions.

1.1.3 Additional application for nanoemulsions

The primary motivation for this thesis is to promote opportunities for reducing obesity, through developing lower fat foods that can be consumed in place of the higher fat alternative. A popular method of reducing the calorie content in emulsion based foods is to replace the fat present with polysaccharide particles which are processed to have similar mechanical and lubricative properties to the fat it replaces. This has been shown to be possible (REFs), however, the main complaint is that these polysaccharide particles (or fluid gels) taste bland. It is proposed that inclusion of oil within these particles may overcome this complaint. Investigating this with nanoemulsions will promote the chance of trapped the oil within the gel (due to the smaller size) and also allow the product to have all the additional advantages that nanoemulsions pertain: longer stability, faster delivery of vitamins and minerals and enhanced creaminess.

1.2 Aims and objectives

The work in this thesis aims to develop the understanding of high pressure devices to optimise the efficiency of the emulsification devices for the future. The primary aim is to understand droplet break-up within the turbulent inertial and turbulent viscous regimes for both devices.

Turbulent inertial regime is valid when the droplets are broken by velocity fluctuations in flow, and would typically be expected in water continuous and sunflower oil dispersed

emulsions. The literature relating to turbulent inertial flow is incomplete with a low understanding of the Microfluidizer compared to a slightly more developed literature base for the valve homogeniser. Initially, the emulsification in the Microfluidizer needs to be experimentally tested and compared to a computational model to learn more about the flow within the geometry. Once the flow in the Microfluidizer is better understood the aim is to compare the processing of the two devices for changes in phase viscosities and emulsifier type to indicate droplet break-up and in-processing coalescence (sometimes referred to as re-coalescence). This work is presented in Chapter 3.

Turbulent viscous flow is present when droplet deformation and break-up is induced by viscous stresses and inertial effects can be neglected. This is may occur when sunflower oil is the continuous phase and water is dispersed (W/O emulsions). The production of sunflower oil continuous nanoemulsions (or similar oils) is very novel and has not been published before. Thus, there is low understanding on the emulsion formation. Initially this work will probe the influence of energy dissipation (pressure) and residence time (passes) on the emulsions droplet size and distribution. Following this, the formation of a stable interface with low interfacial tension will be investigated, as this is an important variable in forming emulsions in turbulent viscous flow (Walstra, 2003). A secondary aim is to show that it is possible to produce a W/O nanoemulsion that has to potential to behave as an oil mimetic, with different attributes to the micron sized W/O emulsion already on the market; Flora Cuisine.

Nanoemulsions are claimed to enhance flavour release (de Roos, 2003), however this has not been fully investigated. Therefore the final key objective is to understand how volatile release

changes between nano-sized droplets compared to larger droplet sizes for O/W emulsions. Flavour release should be considered from both the continuous and dispersed phase for different oil phase fractions and a range of droplet sizes.

The aim of the final chapter is to incorporate oil within fluid gel particles to develop a fluid gel fat mimetic that contains small amounts of oil to maintain the flavour of the full fat alternative. This has not been studied before and therefore the initial task is to test if oil can be incorporated within the gelling dispersed phase whilst monitoring oil inclusion efficiency and the resulting fluid gel properties. If oil inclusion is possible the influence of emulsifier type (used to stabilise the oil droplets) on the gel properties should be investigated.

The work in this thesis is not restricted to the food industry as nanoemulsions are produced using high pressure devices in several industries.

1.3 Thesis layout

This thesis follows an alternative thesis format, which compared to the conventional format, allows work to be presented similar to the corresponding peer reviewed published papers. Each of the main results chapters includes: an introduction, materials and methods, results and discussion, conclusions and further work.

The motivation and outline of this thesis is introduced in this chapter; **Chapter 1**. This is followed by **Chapter 2** which is split into two parts, **Chapter 2A** focusses on the supporting literature relevant to all the results chapters. **Chapter 2B** is a paper entitled ‘Emulsification:

Mechanistic Understanding', this was a peer-reviewed published paper that included work published within this thesis.

The results chapters, **Chapter 3** to **Chapter 6**, are each presented in a similar layout to peer-reviewed papers and therefore include a material and methods section within the main results chapters. This thesis format, over the conventional form is shorter in length because the literature review is less.

Chapter 3 explores the droplet break-up of O/W nanoemulsions in high pressure devices. This is followed by **Chapter 4** which covers the production of W/O nanoemulsions.

Chapter 5 investigates the claim that nanoemulsions have faster flavour release in O/W nanoemulsions, with emphasis on the relationship between flavour release with different droplet sizes and oil phase volumes.

Chapter 6 investigates a novel application for nanoemulsion technology; the incorporation of nanoemulsions within fluid gel particles.

The final chapter, **Chapter 7**, concludes the work completed in this thesis, the major implications of the work and summarises areas for future research or development.

1.4 Publications and presentations

The results throughout this thesis have been published as follows:

Peer reviewed publications

- Lee, L. and Norton, I. (2013). "Comparing droplet breakup for a high-pressure valve homogeniser and a Microfluidizer for the potential production of food-grade nanoemulsions." Journal of Food Engineering **114**(2): 158-163.
    - This work is discussed in Chapter 3
- Lee, L., Niknafs, N., Hancocks, R. and Norton, I. (2013). "Emulsification: Mechanistic Understanding." Trends in Food Science & Technology **31**(1): 72-78.
    - This work is discussed in Chapter 2B
- Lee, L., Hancocks, R., Noble, I. and Norton, I. (2014). "Production of water-in-oil nanoemulsions using high pressure homogenisation: A study on droplet break-up." Journal of Food Engineering **131**: 33-37.
    - This work is discussed in Chapter 4

The following papers are being prepared for submission:

- Lee, L., Yang, N., Norton, J. and Fisk, I. (2014). "Flavour release from nanoemulsions through static headspace analysis and in-*vivo* analysis: impact of aroma compound physiochemical properties, oil fractions and droplet sizes."
    - This work is discussed in Chapter 5
- Lee, L., Hancocks, R. and Norton, I. (2014). "Functional κ-carrageenan fluid gels with the inclusion of nanoemulsion droplets to enhance flavour and structural properties."
    - This work is discussed in Chapter 6

The figures and tables from this thesis that have already been published are listed below. It should be noted that the discussion within this thesis is very similar to the discussion published in these papers:

- Comparing droplet breakup for a high-pressure valve homogeniser and a Microfluidizer for the potential production of food-grade nanoemulsions.
    - *Figure* 3.4, *Figure* 3.5, *Figure* 3.6, *Figure* 3.7, *Figure* 3.12, *Figure* 3.16, *Figure* 3.18, *Figure* 3.19 & *Figure* 3.20
- Production of water-in-oil nanoemulsions using high pressure homogenisation: A study on droplet break-up.
    - *Figure* 4.2, *Figure* 4.3, *Figure* 4.4, *Figure* 4.5, *Figure* 4.7 & *Figure* 4.9

Oral Presentations

- Lee, L. and Norton, I. (2012). Processing Nanoemulsions. Oral presentation at the Royal Society of Chemistry Mixing conference, Birmingham, UK (March 2012).
- Lee, L., Hancocks, R., Noble, I. and Norton, I. (2012). A comparison of nano-emulsion formation from a high-pressure valve homogenizer and a Microfluidizer. Oral presentation at the XVIth International Congress on Rheology in Lisbon, Portugal (August 2012).
- Lee, L., Hancocks, R., Noble, I. and Norton, I. (2013). Food grade water-in-oil nanoemulsions from a high-pressure valve homogenizer and a Microfluidizer. Oral presentation at the 104th American Oils in Montreal, Canada (April 2013).
- Lee, L., Hancocks, R., Noble, I. and Norton, I. (2013). Food grade W/O nanoemulsions from a high-pressure valve homogenizer and a Microfluidizer. Food Structure and Functionality Conference – 15 years later, Poland. (June 2013)
- Lee, L., Hancocks, R., Noble, I. and Norton, I. (2014). Functional fluid gels with the inclusion of nanoemulsion droplets to enhance flavour and structural properties. Oral

presentation at the 12th International Hydrocolloids Conference in Taipei, Taiwan (May 2014).

Poster Presentations

- Lee, L., Douaire, M. and Norton I. (2012). "Comparison of high-pressure valve homogeniser and Microfluidizer for nano-emulsion formation for the production of food-grade nanoemulsions." Poster presentation at the International Symposium of Food Structure and Rheology, Zurich, Switzerland (April 2012).
- Lee, L. Hancocks, R., Noble, I. and Norton, I. (2013). "Production of nanoemulsions from high pressure homogenisation." Poster presentation at the IChemE Early Careers Event, Nottingham, UK (September 2013).

CHAPTER 2A: LITERATURE REVIEW

2.1 Introduction to the literature review

The aim of this chapter is to introduce supporting literature relevant to the results presented in the chapters that follow.

2.2 Introduction to emulsions

An emulsion is a mixture of two immiscible fluids, typically oil and water, with one phase dispersed within another. For an O/W emulsion the oil is dispersed within a water continuous phase, and for a W/O emulsion these phases are the reverse. The size of the dispersed phase varies between 0.1 to 100 μm (McClements, 2011). This work considers the lower end of this range which is often referred to as a nanoemulsion. The size of a nanoemulsion is debated and some define it as having droplet diameters of 50 – 100 nm (Solans *et al.*, 2005), with others extending the upper limit to 200 nm (McClements, 2011). Emulsifiers are added to the system to reduce the interfacial tension between the oil and water phases and thereby reduce emulsion destabilisation.

Emulsion behaviour is dependent on a variety of factors:

- **Type of emulsion (W/O or O/W)**

  Primarily the emulsion behaviour is dependent on the continuous phase of the emulsion, with the differences exaggerated as the dispersed phase volume decreases. The best examples to demonstrate the difference is to consider how the two emulsions behave under gravity.

Gravity separation occurs when the dispersed phase density is different from the continuous phase density and it causes the dispersed phase to either cream or sediment according to the density differences. This can lead to complete phase separation of the emulsion. The separation velocity in a dilute emulsion is described by Stokes Law (Binks, 1998), this is derived by ignoring the inertia effects of the Navier-Stokes equation which is valid for when the co-efficient of drag is below 24 divided by the Reynolds number (Yang *et al.*, 2015):

$$\boldsymbol{v_s = \frac{2r^2(\rho_c - \rho_d)g}{9\eta_c}} \qquad \textbf{Equation 2-1}$$

Where, v_s is the velocity of the dispersed phase droplet relative to the continuous phase (m s^{-1}), r is the radius of the droplet (m), ρ_c is density of continuous phase (kg m^{-3}), ρ_d is density of the dispersed phase (kg m^{-3}), g is gravity (m s^{-2}), η_c is the continuous phase viscosity (Pa s). A positive value indicates creaming of the dispersed phase.

Within oil dispersed emulsions, the dispersed phase density is lower than the continuous phase density and thus the direction of the separation velocity is upwards and the emulsions cream. For nanoemulsions, Brownian motion acts on the length scale of the droplets and it is claimed that O/W nanoemulsions do not cream because Brownian motion acts as the dominant force on this length scale and the density force is negligible. Phase separation is therefore very slow, on the order of several years, if it occurs at all (Walstra and Smulders, 1998).

- **Oil-water interface**

Emulsion formation and stability is strongly dependent on the emulsifier types used, interfacial area of the emulsion droplets and emulsifier coverage at the interface. Coalescence, droplet merging, is dependent on the aforementioned variables and occurs in three stages (shown in Figure 2.1). Firstly the droplets approach each other, the film between the droplets drain and if it drains completely it is likely that the two (or more) droplets will coalesce.

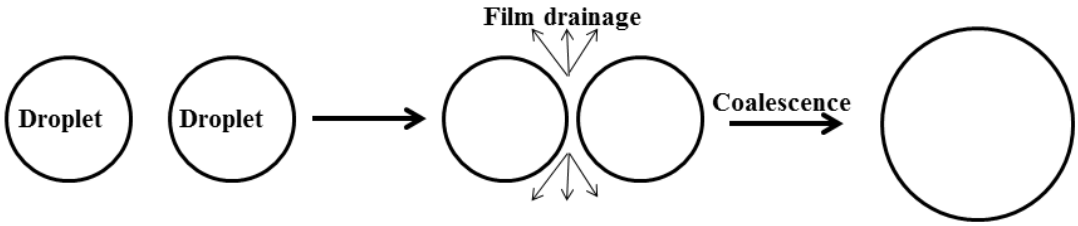

Figure 2.1: Diagram demonstrating film drainage and coalescence

There are other factors that can increase the chance of coalescence. Firstly, if the droplet interface is stretched the emulsifier concentration around the interface can reduce and cause areas of the interface to have insufficient emulsifier present, thus the droplet is more vulnerable to coalescence (Feigl *et al.*, 2007). Additionally, Kabalnov (1998) stated that gaps in emulsifier coverage (or holes) can spontaneously form in the interface from thermal motion. Similarly, if this occurs the droplets are more vulnerable to coalescing after film drainage.

- **Properties of both the phases**

Physical properties of the phases will influence the break-up regimes and physical properties of the resulting emulsion these could include viscosity, mass density, dielectric constant, ionic strength and solubility of the relative phases (Walstra, 2005). The latter is particularly important when considering the production of nanoemulsions

as was shown by Wooster *et al.* (2008). They demonstrated that smaller droplet sizes were produced when the solubility between the two phases was closer together. However the rate of Ostwald ripening increased with the increased solubility and the nanoemulsion was less stable.

- **Dispersed phase volume fraction**

  The volume fraction of droplets influences the droplet interactions during flow and consequently the rheology of the emulsion. For dispersed phase volumes of 70% or higher the droplets have a larger interactions as they have to deformation one another to pack, this produces a higher viscosity (Walstra, 2005). When the dispersed phase volume is 10% or less the effects of coalescence are minimised as the droplets have low interactions during flow (Tcholakova *et al.*, 2004).

- **Size distribution of the droplets**

  In general, the smaller the droplet size the more stable the emulsion to coalescence. However, if the distribution of droplets is large the emulsion will be more prone to emulsion destabilisation via another phenomenon: Ostwald ripening. The mechanism of Ostwald ripening is shown in Figure 2.2 and is the growth of larger droplets at the expense of smaller ones due to mass transport of soluble dispersed material through the continuous phase. Ostwald ripening is particularly an issue if the dispersed phase is partially soluble within the continuous phase. Unlike the other main instability mechanisms, Ostwald ripening is relatively insensitive to oil volume fraction or rheology of the continuous phase. The thermodynamic driving force for Ostwald ripening is the increasing chemical potential of a dispersed phase component with decreasing droplet size. This leads to a greater tendency for dissolution from smaller

droplets than from bigger ones (Dickinson, 2009). Ostwald ripening is identifiable as the emulsion distribution is bi-modal.

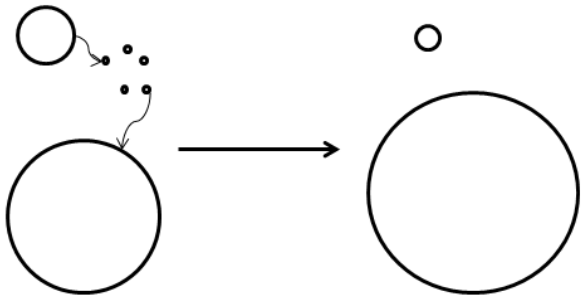

Figure 2.2: Schematic representation of Ostwald ripening

A theoretical expression was developed by Lifshitz, Slesov and Wagner (LSW theory) to describe the parameters that influence Ostwald ripening rate, ω, (Lifshitz; and Slyozov, 1961):

$$\omega = (r)^3 - (r_0)^3 = \frac{8\sigma_{OW} c_\infty v^2 D}{9R_g T} t \qquad \textbf{Equation 2-2}$$

Where r and r_0 are the average radii of the droplets (m) and c_∞ is the solubility of the droplet in the continuous phase (mol/m^3), v is the molar volume of the particle material (m^3/mol), D is the diffusion co-efficient (m^2/s), R_g is the ideal gas constant (J/mol.K), T is temperature (K) and t is time (s).

The predicted Ostwald ripening rate of an emulsion can be calculated and compared to the emulsion destabilising rate to determine if the emulsion coarsening is attributable to Ostwald ripening.

2.2.1 Emulsifiers

Emulsifiers are added into emulsions to reduce the interfacial tension between the oil and water phases. They reduce the amount of energy required to produce an emulsion and then

prolong the stability of the emulsion by reducing coalescence via a series of different mechanisms. Interfacial tension is the contractive force per unit length, acting in the interface and parallel to it (Vliet, 2000). Addition of an emulsifier disrupts the contracting forces and reduces the interfacial tension.

An emulsifier is a molecule that is partially soluble in both the aqueous and oil phases and will position at the oil-water interface to reduce interfacial tension and droplet coalescence. Over the years there have been many theories proposed to quantify HLB more accurately, Griffin (1949) proposed one of the first and characterises the emulsifier using the hydrophilic and lipophilic balance (HLB) of an emulsifier:

$$HLB = 7 + \sum(hydrophilic\ group\ numbers) - \sum(lipophilic\ group\ numbers)$$

Equation 2-3

When the value is below 7 the emulsifier is more lipophilic and will more readily dissolve in the oil phase and is likely to stabilise W/O emulsions. Above 7 the emulsifier is more hydrophilic and will stabilise the reverse emulsion.

More recent modifications to the HLB calculation have accounted for the molecular weights of the head group as a percentage of the entire molecule (divided by 5 to provide a scale from 1 – 20), another useful build on the original HLB calculation was to consider hydration changes through temperature (Balson, 1999). This detail is not considered in this thesis.

When emulsifiers are dissolved into solution, at low concentrations the molecules arrange at the interface or exist as monomers within the continuous phase. At a critical concentration of

emulsifier, aggregates or micelles form through interactions with the part of the emulsifier that is insoluble within the continuous phase (Birdi, 1977). The most common conformation for micelles is spherical in shape with the part of the emulsifier that is insoluble with the continuous phase is arranged in the centre of the structure minimising contact with the continuous phase.

There are several types of emulsifiers which stabilise the interface in different ways:

- Non-ionic (For example Tweens and PGPR) – non-ionic emulsifiers create steric hindrance which act to reduce film drainage for coalescence by preventing the droplets from approaching each other (Walstra, 2003).

  Tween 20, or polyoxyethylene (20) sorbitan monolaurate, is one of the most commonly used emulsifiers in industry; its molecular structure is shown below. The lipophilic part of the molecule is the hydrocarbon chain and the hydrophilic part is the polyoxyethylene part where the electronegative oxygen atoms make it polar.

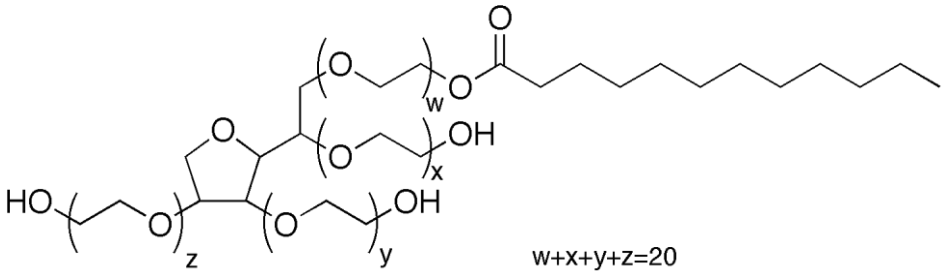

Figure 2.3: Molecular structure of Tween 20 or Polyoxyethylene (20) sorbitan monolaurate

- Ionic emulsifiers

  These emulsifiers are charged and stabilise against coalescence by adsorbing into the oil-water interface and electrostatically repelling neighbouring droplets, thus reducing the chance of coalescence or Ostwald ripening. Sodium dodecyl sulphate (SDS) is an

example of an anionic emulsifier that is commonly used as a model emulsifier for understanding food systems, despite not being safe to consume.

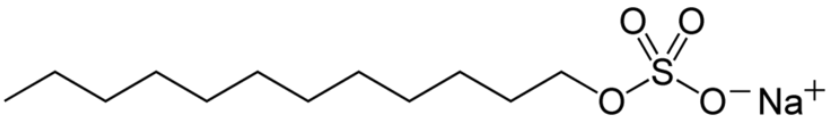

Figure 2.4: Molecular structure of SDS

- Polymeric

  The linear protein, sodium caseinate, or globular protein, β-lactoglobulin, are classic examples of proteins used in the food industry (Qian and McClements, 2011). Proteins have regions of positive and negative charge (in certain pH ranges proteins can be amophoteric) and therefore they provide some localised electrostatic repulsion. Furthermore, proteins are polymeric molecules and this means the time for adsorption and reorganisation at the interface is longer than low molecular weight emulsifiers however once adsorbed they stabilise against coalescence more effectively (Lee *et al.*, 2013, O'Sullivan *et al.*, 2014).

2.2.2 Light scattering of emulsions

Emulsions are commonly manufactured to be translucent by matching the refractive index of the continuous phase to that of the dispersed phase. However, it is often claimed that nanoemulsions become translucent below a certain droplet size (Solans *et al.*, 2005, McClements, 2011), this is due to a different mechanism. As the droplets become smaller, light is scattered less and therefore the emulsion appears more translucent, this occurs around 20 nm (Sun *et al.*, 2005). Additionally, the optical properties of emulsions also change

according to the size of the emulsion droplets and their distribution with respect to the wavelength of visible light (400 – 700 nm) (Höhler *et al.*, 2014). Assuming a monomodal distribution the expected scattering of light according to the droplets for a given droplet size is (Walstra, 2005):

- 20 nm droplets appear grey or almost translucent
- 200 nm droplets appear bluish
- 2 um droplets show as white
- 20 um or larger appear less white

Niknafs *et al.* (2011) exploited the relationship between light scattering and droplet size to measure emulsion droplet size change during processing. This technique was useful in showing the equilibrium between break-up and coalescence for different emulsifier concentrations and types. It was shown that Tween 20 adsorbs quickly to the interface but can be removed from the interface relatively easily thus exhibiting a higher rate of coalescence.

2.2.3 Emulsion formation

During emulsion formation the dispersed phase is broken up via an input of mechanical energy. This is done by deforming and breaking up the droplets, the emulsifier must then adsorb and stabilise the interface to reduce the chance of coalescence if the droplet collides with another. This section will consider the flow regimes for emulsification to create droplet deformation and break-up. Coalescence will not be discussed in this section and will be discussed more specifically with reference to high pressure homogenisation in sections 2.2.4.1 & 2.2.4.2.

2.2.3.1 Flow regimes for emulsification

The break-up of droplets during emulsification is highly dependent on the type of flow, this can be identified using the Reynolds number (Reynolds, 1883); a dimensionless number that describes the ratio of inertial forces ($U\rho_c$) to viscous forces (η_c/L). Reynolds number may be defined as:

$$Re = \frac{\rho_c L U}{\eta_c}$$

Where ρ is the density of the fluid (kg/m^3), η_c is the dynamic viscosity of the continuous phase (Pa.s), L is the characteristic length (m), and U is the velocity of the flow (m/s).

There are two types of flow, laminar and turbulent. Laminar flow, or viscous flows, is flow along constant streamlines in the direction of flow. It occurs when the effects of fluid viscosity are balanced by those arising from fluid inertia or pressure gradients (Dowling, 2012). As the value of the Reynolds number increases instabilities in the flow occur, or velocity fluctuations. The point at which these instabilities occur is known as the critical Reynolds number past which the flow regime is no longer laminar. The flow regime between laminar and turbulent is known as the transitional region. The Reynolds number at which these flows occur are different according to the geometry of the vessel. For flow within a cylindrical pipe laminar flow will occur below a Re value of 2000 and turbulent flow occurs above 3000. Turbulent flow is highly chaotic and exhibits high velocity fluctuations where eddies are present. An eddy is explained to be an unstable turbulent motion localised over a certain length scale.

2.2.3.2 Droplet deformation with viscosity ratio

Droplet deformation for break-up is often modelled in terms of a single droplet, and as the droplet deforms the deformation, D, is characterised by considering the width, W, and the breadth, B of the deforming droplet.

$$D = \frac{W - B}{W + B}$$ **Equation 2-4**

Figure 2.5: Diagram to demonstrate width and breadth of droplet deformation

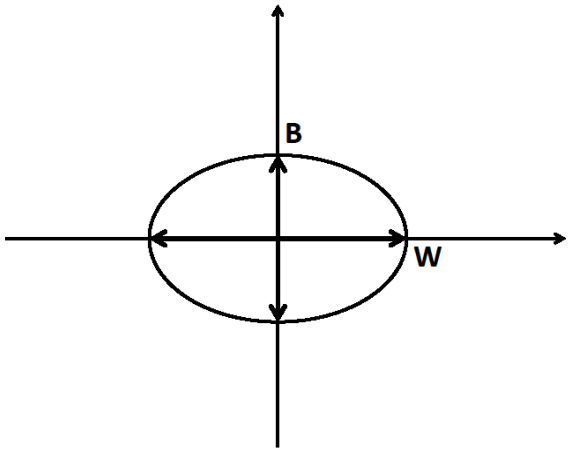

Taylor discussed the effect of viscosity ratio in terms of the Capillary number and slightly altered this to consider a function of viscosity ratio (Taylor, 1935) (Equation 2-5). The Capillary number is a dimensionless number that is a ratio of inertial forces (external stresses) to viscous forces necessary to deform a droplet to the point of breaking. The capillary number describes the maximum stable drop size in laminar flow (Equation 2-6). Turbulent droplet break-up is described by the Weber number and this is the ratio of inertial forces to internal pressure (or Laplace pressure) (Equation 2-7).

$$f(\eta_{ratio}) = \frac{19\eta_{ratio} + 16}{16\eta_{ratio} + 16}$$ **Equation 2-5**

Where, η_{ratio} is the viscosity ratio of dispersed phase viscosity over continuous phase viscosity.

$$Ca = \frac{\dot{\gamma} r \eta_d f(\eta_{ratio})}{\sigma_{OW}} \qquad \textbf{Equation 2-6}$$

Where, $\dot{\gamma}$ is shear rate, r is droplet radius, η_d dispersed phase viscosity, f(η_{ratio}) is the function of viscosity ratio and σ_{OW} is the interfacial tension between oil and water.

$$We = \frac{\nabla v \eta_c d}{2\sigma_{OW}} \qquad \textbf{Equation 2-7}$$

Where ∇v is the velocity gradient (m/s), η_c is the continuous viscosity (Pa/s) and d is the droplet diameter (m).

These correlations are derived from single droplets or ideal flows and when applied to non-ideal emulsification systems these equations may no longer be reliable for the predicting unknown parameters, for example minimum droplet sizes achievable (Stegeman *et al.*, 2002).

2.2.3.3 Droplet break-up in laminar flow

Laminar flow, or viscous flows, is flow along constant streamlines in the direction of flow. Droplet break-up in this flow can either be from simple shear or extensional flow. Simple shear creates droplet rotation followed by deformation within and this is a function of viscosity ratio, see the figure below.

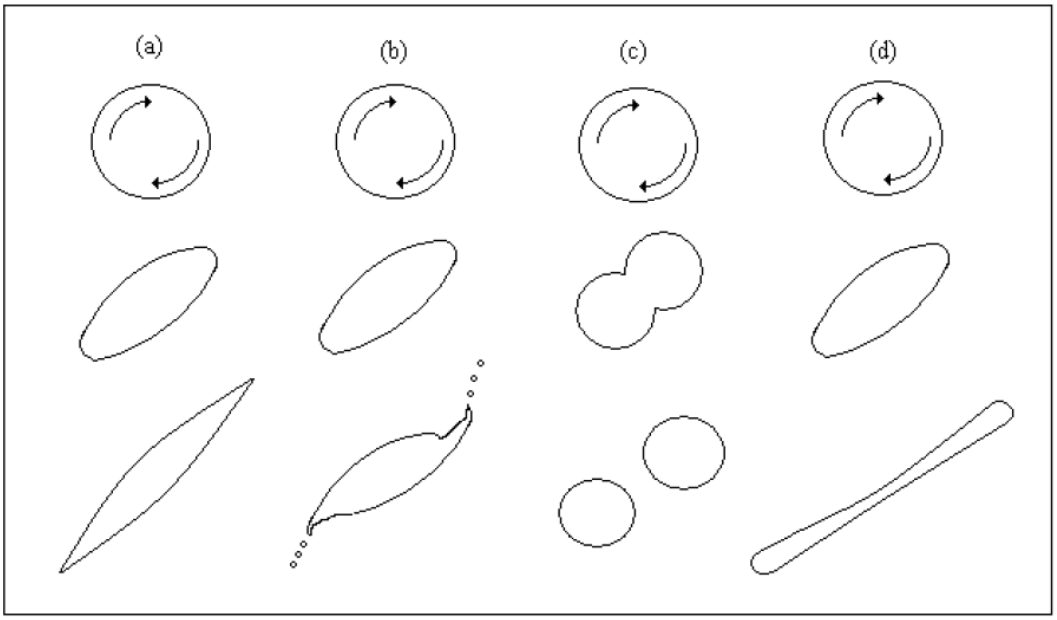

Figure 2.6: Schematic diagram of droplet deformation and break-up under simple shear for emulsions with viscosity ratios a) < 0.05 b) 0.05 – 0.2 c) 1 – 3.5 and d) > 3.5 (Henry, 2007, McClements, 2004)

At the lowest viscosity ratio, the droplet is deformed but not broken as the continuous phase is too viscous compared to the dispersed phase to cause break-up. As the ratio increases the droplets break-up via tip streaming, or droplet splitting. Finally, at the highest viscosity ratios the droplet is stretched but does not break as the energy in the continuous phase does not transfer quickly enough to break the highly viscous dispersed phase.

In extensional flow, or elongation, the droplet is stretched and Rayleigh instabilities create droplet break-up. Figure 2.7 demonstrates how Grace (1982) tested droplet break-up in extensional flow.

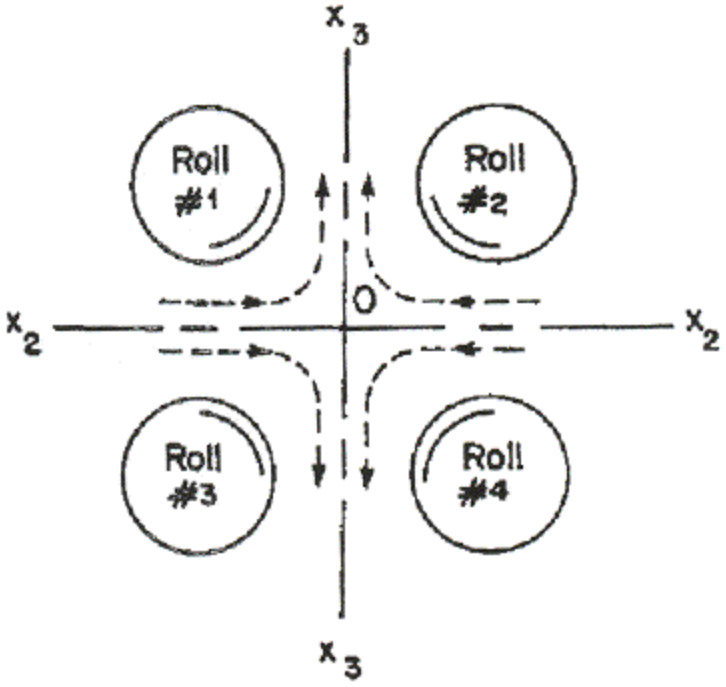

Figure 2.7: Irrotational shear field, or extensional flow, created by a four roll device (Grace, 1982)

Using four roller mills the droplet break-up in extensional flow was investigated. The flow along the $x_2 - x_2$ axis is compressional and then extensional along the $x_3 - x_3$ axis. It was shown that droplet break-up in extensional flow is independent of viscosity ratio (Grace, 1982). In the same study, equations to correlate the capillary forces (viscous / interfacial forces) to the viscosity ratio for rotational (simple shear) and irrotational (extensional) shear flow were presented. This is shown in Figure 2.8.

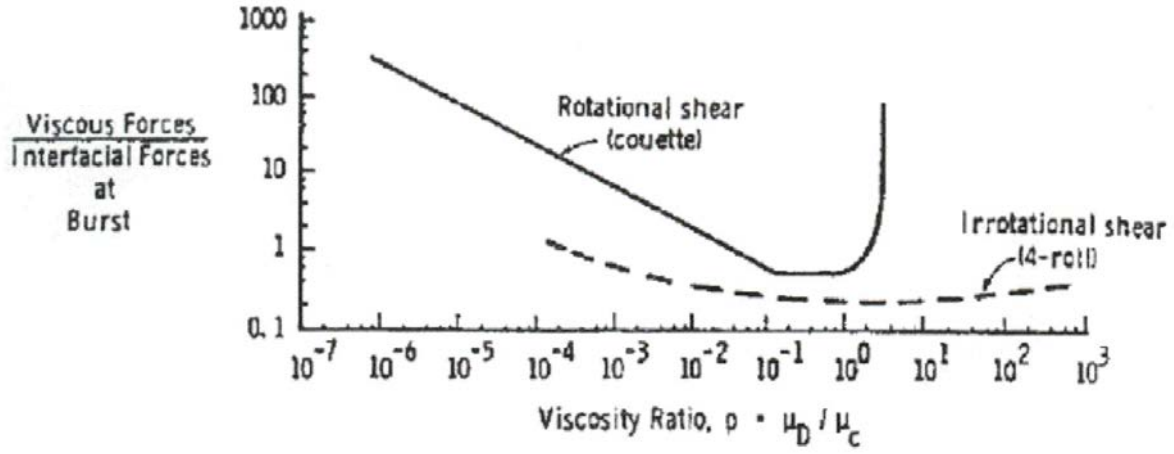

Figure 2.8: Comparison of effect of viscosity ratio on critical shear in rotational (simple shear) and irrotational (extensional) shear fields (Grace, 1982)

Stegeman *et al.* (2002) criticised the validity of the work, emphasising that in practice the droplet sizes are often smaller than the capillary forces predict as the devices causing droplet break-up are not solely from one droplet break-up mechanism.

2.2.3.4 Droplet break-up in turbulent flow

Droplet break-up in turbulent flow relates to the energy in the flow and how this dissipates. Kolmogorov theory of energy dissipation proposes a mechanism for energy dissipation and droplet break-up.

Kolmogorov's theory describes how energy is transferred from larger to smaller eddies in turbulent flow (Kolmogorov, 1949). Large eddies are unstable within the flow and break-up and form smaller eddies, this process of eddy break-up continues and the energy of each eddy is transferred to their daughter eddies. This is known as the energy cascade, and continues until the size of the eddy is small enough that it is stable. At that point molecular viscosity is effective in dissipating the kinetic energy as heat. Kolmogorov's hypothesis of local isotropy

states that at sufficiently high Reynolds numbers, the small-scale turbulent motions are statistically isotropic for all systems. Whereas the large scale turbulence is anisotropic and is a function of the emulsification method. Therefore the rate of energy dissipation, ε (W/kg), for any system is determined by the largest eddies and the kinematic viscosity, ν (m^2s^{-1}), of the system.

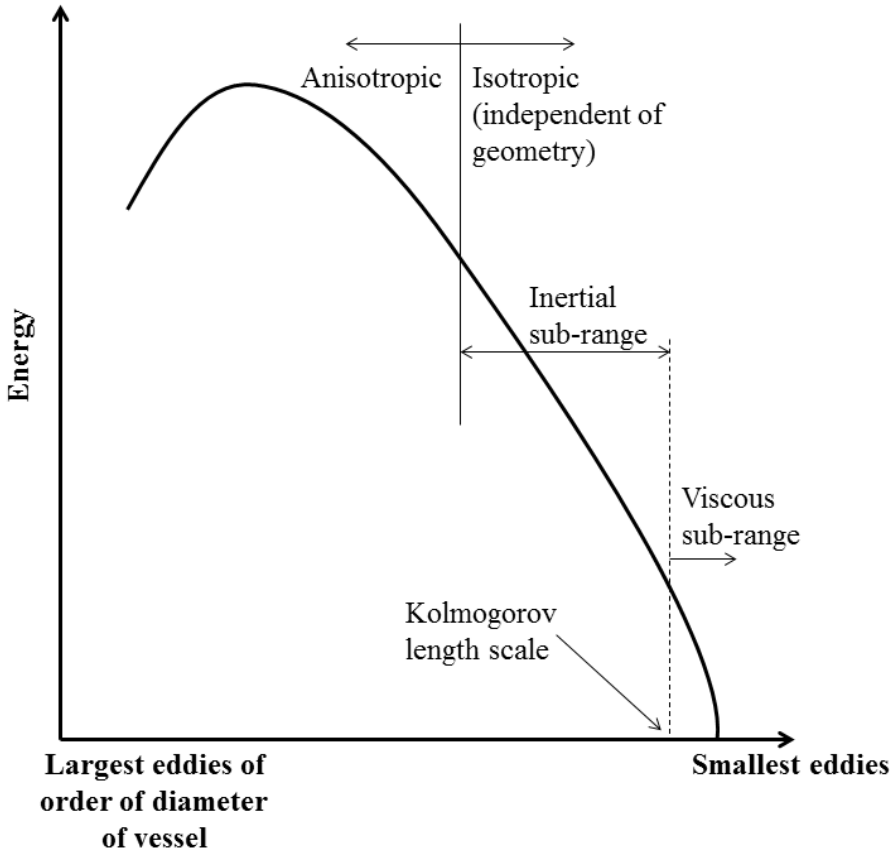

Figure 2.9: Energy spectrum as described by Kolmogorov (Kolmogorov, 1949)

Kolmogorov identified three equations to characterise the turbulent microscales of length (λ_K), velocity (u_η) and time (τ_η), all indicative of the smallest eddies present in the flow:

$$\lambda_K = \left(\frac{\nu^3}{\varepsilon}\right)^{1/4}$$ **Equation 2-8**

$$u_\eta = (\varepsilon\nu)^{1/4}$$ **Equation 2-9**

$$\tau_\eta = \left(\frac{\nu}{\varepsilon}\right)^{1/2}$$ **Equation 2-10**

There are two regimes within turbulent flow: turbulent inertial and turbulent viscous. In turbulent inertial the droplet break-up is equivalent to the size of the Kolmogorov length scale, see above for equation. When the droplets are significantly smaller than this length scale the droplet break-up regime is said to be turbulent viscous and the mechanism of droplet break-up has been proposed to be similar to that of simple shear in laminar flow (Walstra, 1998).

Walstra (2005) also proposed equations to describe the external stress acting on a droplet for each turbulent regime, the approximate droplet size and the time for droplet deformation. These equations are generic and therefore should be used to understand the variables that control droplet break-up rather than as precise equations. Table 2-1 lists these.

Table 2-1: Turbulent regimes and their dependence on droplet break-up parameters

	Turbulent viscous	**Turbulent inertial**
External stress acting on droplet	$\varepsilon^{1/2}\eta_c{}^{1/2}$ **Equation 2-11**	$\varepsilon^{2/3}d^{2/3}\rho_c{}^{1/3}$ **Equation 2-12**
Droplet size	$\frac{\sigma_{OW}}{\varepsilon^{1/2}\eta_c{}^{1/2}}$ **Equation 2-13**	$\frac{\sigma_{OW}{}^{3/5}}{\varepsilon^{2/3}\rho_c{}^{1/5}}$ **Equation 2-14**
Time for droplet deformation	$\frac{\eta_d}{\varepsilon^{1/2}\eta_c{}^{1/2}}$ **Equation 2-15**	$\frac{\eta_d}{\varepsilon^{2/3}d^{2/3}\rho_c{}^{1/3}}$ **Equation 2-16**

The equations in Table 2-1 summarise the variables dependent on the droplet deformation and break-up process. Notably, within turbulent viscous flow the stress causing droplet deformation is dependent on both the energy dissipation rate and continuous phase viscosity. In contrast, droplet deformation within turbulent inertial flow is independent of the continuous phase viscosity and more dependent on the size of the droplets present during homogenisation.

2.2.4 Nanoemulsions

Nanoemulsions can be produced using low or high energy techniques. Low energy techniques exploit chemistry to cause phase inversion (Tadros *et al.*, 2004, Solans *et al.*, 2005), whereas

high energy techniques create a large amount of mechanical energy in the system. Then when this dissipates as kinetic energy it creates droplet deformation and break-up (Kolmogorov, 1949, Hinze, 1955). There are two commonly used high pressure devices for producing nanoemulsions: high pressure valve homogeniser and a high pressure impinging jet device (Microfluidizer). These are introduced in the next two sections.

2.2.4.1 Nanoemulsion formation using a high pressure valve homogeniser

A high pressure valve homogeniser (HPH) consists of a piston pump and a narrow gap, where a coarse emulsion is forced into the gap and at the exit turbulence creates droplet break-up and small droplet sizes are formed. Typical operating pressure are up to 150 MPa whereas, pressures as high as 350 MPa have been reported (Floury *et al.*, 2004a).

Tcholakova *et al.* (2004) experimentally studied the influence of emulsifier type, and concentration along with ionic strength of the aqueous solution on the droplet size. It was found that by changing the ionic strength or using SDS induced electrostatic repulsion between the oil droplets and reduced coalescence within the system. Also, when the emulsifier concentration was in excess the droplet sizes fitted well with the Kolmogorov – Hinze theory for turbulent droplet break-up. This work was extended from within the same research group with a series of three papers all published within 2007. Initially the droplet size produced by a high pressure valve homogeniser was studied and was shown to decrease by increasing the energy dissipation rate (predominantly a function of pressure) and reducing the interfacial tension, dispersed phase viscosity and oil phase volume (Vankova *et al.*, 2007a). The droplet size distributions formed in turbulent inertial flow did not depend on the

energy dissipation rate or interfacial tension, but were more influenced by the dispersed phase viscosity. The following papers analysed the droplet breakage rate and showed that droplet break-up was dependent on the Kolmogorov length scale and the efficiency of droplet deformation (Vankova *et al.*, 2007b) and proposed a mechanism for droplet break-up within higher viscosity dispersed phases (see Figure 2.10).

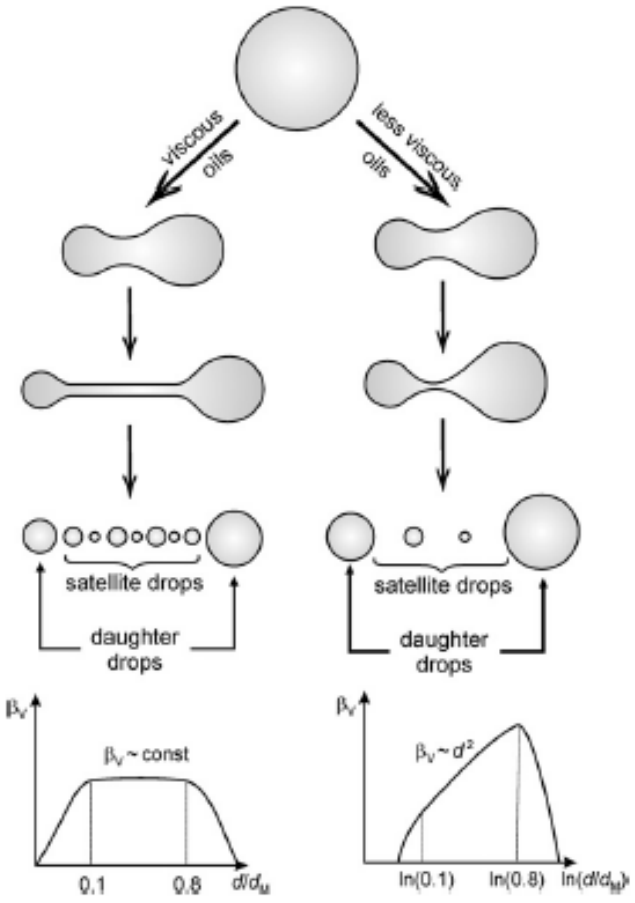

Figure 2.10: Proposed mechanisms for differences in droplet break-up for emulsions droplets with low and high dispersed phase viscosities (Tcholakova *et al.*, 2007).

Figure 2.10 highlights that higher viscosity dispersed phases produced a larger proportion of satellite droplets when the droplets break-up and therefore producing a wider droplet size distribution compared to lower viscosity dispersed phases.

Donsì *et al.* (2011a) designed four different geometries based around a valve homogeniser design. The mean droplet size did not vary between designs and was more dependent on the operating pressure. However, it was observed that some designs caused non-uniform flow regimes which produced a wider distribution of stresses and consequently a higher droplet size span. It was also shown that inducing a series of extensional flow regions after the main turbulent energy had dissipated promoted coalescence as the emulsifier did not have enough time to adsorb and stabilise the interface.

Floury *et al.* (2004a) studied the HPH flow patterns by initially using a RNG k-ε turbulence model to computationally model the flow behaviour through the valve. The computational results were then compared to experimental data. According to the first paper, extensional flow occurs between the valve seat and valve gap. It was shown that the time required to disrupt the droplets, in simple sunflower oil in water emulsions, was much longer than the residence time of the extensional flow. In the follow-up paper, it was suggested that break-up will occur in the highly turbulent region located at the exit of the gap (Floury *et al.*, 2004b). This work highlighted that cavitation is present in the HPH, but it is unclear if cavitation is responsible for droplet break-up as the mechanism for dissipation is similar to turbulent inertial flow (Walstra, 2005).

The majority of research currently highlighted in this section has related experimental results to theory and suggested the likely flow patterns responsible for the observed emulsion characteristics. Innings and Trägårdh (2007) developed a technique for measuring the flow fields by building a translucent acrylic HPH, scaled up from a lab scale HPH (whilst maintaining the relevant dimensionless numbers), and monitored the hydrodynamics using particle image velocimetry (PIV). The study confirmed that entry into the valve gap creates extensional flow, and highlighted complete turbulence suppression within the gap followed by a highly turbulent and a directionally unstable turbulent jet at the exit of the gap. Under similar flow conditions the jet may be located centrally at the exit from the gap or attach to either of the walls. Interestingly, the droplet size produced did not depend on the position of the jet.

2.2.4.2 Nanoemulsion formation using a high pressure impinging jet device (Microfluidizer)

A Microfluidizer operates to a similar pressure to a HPH (150 MPa) via an air-driven piston pump, and droplet break-up occurs from high turbulence and shear created by the collision of two impinging jets oriented 180^{o} to each other (Cook and Lagace, 1985, Siddiqui *et al.*, 2009). In order to determine the droplet break-up mechanism it is important to understand the geometry of the device and the factors that affect energy dissipation including the volume over which the energy dissipates.

Henry (2007) studied the droplet size change and in-processing coalescence behaviour in the Microfluidizer for a wide variety of different emulsifier types non-ionic emulsifiers (Tweens, Brij 96, and a selection of sucrose esters), phospholipids (phosphatidylcholine and

phosphatidylglycerol) and proteins (whey protein concentrate and β-lactoglobulin). There was slight changes in droplet size with different emulsifier types used. Henry *et al.* (2009) developed a new technique for measuring coalescence by using a hydrophobic dye in half of the oil droplets and then determining how the dye distribution changed after processing through the Microfluidizer. Coalescence in emulsions stabilised by non-ionic emulsifiers was shown to be reduced to zero once 2 wt.% emulsifier was used, which corresponded to the smallest droplet size produced. The following publication from this team further investigated the coalescence behaviour of phospholipid and protein stabilised emulsions (Henry *et al.*, 2010). Similarly, when the minimum droplet size was observed coalescence reduced to zero. The stability of the resulting decane-in-water emulsions were monitored with respect to the LSW equation for Ostwald ripening. The emulsions stabilised by phospholipids initially produced a larger droplet size, likely because they usually stabilise W/O emulsions, however, the emulsion did not ripen. In contrast, the emulsions stabilised by whey and β-lactoglobulin destabilised at a rate 10 times faster than would be predicted by the LSW equation.

Jafari *et al.* (2007a) studied the Microfluidizer to understand how to produce nanoemulsions with a narrow droplet size distribution. For proteins and Tween 20 emulsions the Sauter-mean diameter was 150 nm with a span of 1.1 (droplet size at 90^{th} percentile minus droplet size at the 10^{th} divided by the droplet size at the 50^{th}). However, the smallest droplet size distribution was formed when a modified starch was used to stabilise the droplets although the droplet size was larger (600 nm). This research also showed that between 40 – 60 MPa and 2 passes through the device was the optimum homogenising conditions to produce a narrow droplet size distribution.

Wooster *et al.* (2008) furthered this work by investigating the physical properties of the dispersed phase oil and demonstrated that a minimum in droplet size can be achieved by reducing the dispersed phase to continuous phase viscosity ratio. The average droplet size of 40 nm was achieved by using SDS to stabilise the droplets and a high molecular weight PEG to thicken the continuous phase. Additionally, a low viscosity oil was used to minimise the force required to break the droplets. When longer chain triglycerides are used in the dispersed phase the emulsion also resists Ostwald ripening and is stable for over 3 months.

Qian and McClements (2011) showed that the droplet size of octadecane-in-water emulsions is dependent on the emulsifier type with SDS producing the smallest emulsions followed by Tween 20, β-lactoglobulin and sodium caseinate, respectively. This contradicts the results found by (Henry, 2007). The main difference between the results is the dispersed phase viscosity, with Henry (2007) using a low viscosity oil (decane ~1mPa s) compared to a higher viscosity oil (corn oil ~30 mPa s) used by Qian and McClements (2011). Qian and McClements (2011) further tested the continuous and dispersed phase viscosities by modifying them to test a range of viscosity ratios. The lowest droplet size was observed with SDS at the smallest viscosity ratio. However, the other emulsifiers were less dependent on viscosity ratio.

2.2.5 Water-in-oil emulsions

In many oil continuous emulsions, stability is either provided via a formation of a continuous phase network (*i.e* cross-linked paraffin (Hodge and Rousseau, 2003)), or by using interfacially active materials such as lipid particles and/or emulsifiers (Ghosh and Rousseau, 2011). A common emulsifier used to stabilise water-in-oil emulsions is polyglycerol

polyricinoleate (PGPR), it is a polymeric molecule which adsorbs into the water-oil interface and produces a high elastic interface (Wilde *et al.*, 2004). The molecular structure of PGPR is shown in Figure 2.11.

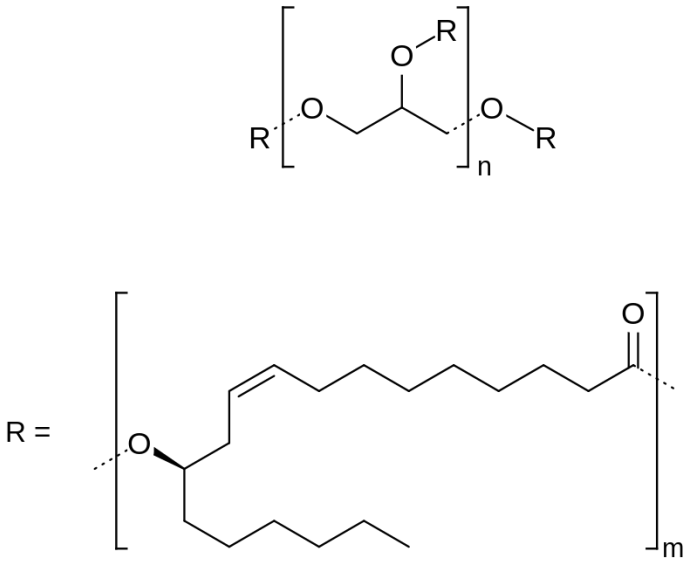

Figure 2.11: Molecular structure of polyglycerol polyricinoleate (PGPR), where the top structure is the polyglycerol backbone and R is the polyricinoleate

PGPR has an overall neutral charge, although, the lone pair of electrons on the oxygen atoms would be expected to contribute to dipole moments (Shaw, 1991). Adsorption of dipolar molecules at an interface will not contribute to a net surface charge, but the presence of a layer of orientated dipolar molecules at the interface may make a significant contribution to the nature of the electrical double layer (Shaw, 1991).

Marze (2009) studied the relaxation processes of PGPR at the interface. When the interfacial coverage of PGPR approaches complete coating the adsorption of PGPR into the interface ceases to be a diffusion controlled mechanism and becomes dependent on the molecular rearrangements at the interface. With addition of salt this rearrangement allows for tighter packing at the interface (Márquez *et al.*, 2010).

Interfacial rheology, or dynamic interfacial tension, can be used to study the deformation and flow of thin films of materials at liquid-liquid interfaces, more specifically the oil-water interface (Richards, 2014). It is measured by oscillating a droplet at a certain frequency and the contributions of storage and loss modulus are measured and this indicates the relaxation characteristics of the interface. This is useful for understanding the behaviour of PGPR at the interface with different electrolytes.

Electrolytes are either kosmotropes (structure makers) or chaotropes (structure breakers) and are named according to their ability to structure water. Small ions (cosmotropes) due to their high charge density cause strong electrostatic ordering of nearby water molecules (Kumar and Venkatesu, 2014). The water structuring ability of ions reduces approximately with a reduction in charge density and Gibbs free energy of hydration. This aligns with the Hoffmeister series for salts, Table 2-2, which was initially identified for the ions salting out power.

Table 2-2: Table summarising the Hofmeister series

Cations: $NH_4^+ > K^+ > Na^+ > Li^+ > Mg^{2+} > Ca^{2+} > CH_6N_3^+$	
Anions: $SO_4^{2-} > HPO_4^{2-} >$ acetate > citrate > $Cl^- > NO_3^- > ClO_3^- > I^- > ClO_4^- > SCN^-$	
Low end of series	**High end of series**
Higher interfacial tension	Reduces interfacial tension
Decreases solubility of hydrocarbons / oils	Increases solubility of hydrocarbons / oils
High salting out power (aggregates)	High salting in power (solubilises)

Márquez *et al.* (2010) made W/O emulsions stabilised by several concentrations of PGPR and investigated the influence of adding electrolyte on the stability and interfacial properties of these emulsions. A series of chlorides were tested (sodium, magnesium, calcium and potassium), calcium lactate and calcium carbonate. The lowest elastic modulus was produced with calcium chloride, and this corresponds to the highest Hofmeister number of the salts tested. Bohinc *et al.* (2001) had previously related the thickness of the electrical double layer to be the smallest for this ion compared to the others used. Increasing both the emulsifier concentration and/or salt concentration increased the stability, decreased the interfacial elasticity and allowed higher quantities of dispersed phase to be stabilised within the emulsion (Márquez *et al.*, 2010). The enhanced stability was attributed to an increase in repulsive forces between droplets from the higher density of emulsifier. Pawlik *et al.* (2010) measured the interfacial viscosity and elasticity for calcium chloride and suggested that it was likely that the addition of salt strengthens the interactions between the emulsifiers at the interface.

It was highlighted by Márquez *et al.* (2010) that impurities in the oil used can interfere with the packing of PGPR at the interface, for example oleic acids, monoolein and inherent emulsifiers. Similarly, competitive adsorption of other oil soluble emulsifiers at the interface is known to reduce stability, whereas, if a water soluble emulsifier is used (SDS) the stability is enhanced (Wilde *et al.*, 2004).

Márquez *et al.* (2010) were not the first researchers to observe that salt allows a higher volume of internal phase to be stabilised, Aronson and Petko (1993) had previously used salt in conjunction with a mixed emulsifier system and produced an emulsion with 95% water in mineral oil.

2.3 Flavour release

2.3.1 Flavour detection and measurement

Flavour, or aroma, release from food emulsions in the mouth is a complicated process (Taylor and Roozen, 1996). Flavours are detected by the tastebuds on the tongue's surface although it is mostly associated with aroma detection by the olfaction system (Taylor and Roozen, 1996). This comprises of an external nose and inner nasal cavity. The inner nasal cavity consists of two chambers divided by a septum, and three bones that are long and narrow which direct the flow of the air in and out past the olfactory region where the flavour volatile is detected by the olfactory receptors and an electrical signal is sent to the brain which perceives the smell (Sankaran *et al.*, 2012).

During eating, volatile flavours are released via the nose from the mouth (termed retronasal olfaction). The flavour is detected as the air is expired through the nose and out past the olfactory region. Upon swallowing, the volatile release is more intense as more air is expired through the nose. Since flavour release is such a complex process it makes designing a measurement technique to accurately represent flavour release through time very difficult. Several flavour release techniques have been used previously including measuring the brain's response to flavour by an electroencephalograph (Lorig, 2000), using trained sensory panels (Guinard *et al.*, 2002) or by measuring the release during oral processing either via gas chromatography or mass spectrometry. Sensory panels are advantageous as they can identify flavour combinations through descriptions such as 'earthy'. They can indicate flavour thresholds, where above this flavour concentration the human nose can detect it. In addition, the panel can easily highlight the intensity and length of time that the flavour is detected for. However, sensory panels are costly, have large variability in results and are therefore less reliable. Mass spectrometry techniques are typically the most reliable technique (Langridge, 2004) as it has less bias between participants and the flavour release is measured via detection of volatile release before, during and after oral processing.

2.3.2 Measurement of aroma release

Mass spectroscopy equipment can be used to measure and understand different flavour release mechanisms from an emulsion. The two common methods are:

- Headspace measurements

  This is the equivalent to sniffing food. The food sample is placed in a glass bottle and is left to equilibrate (Sulmont *et al.*, 2002), then the air above the sample (i.e. the headspace) is measured. There are two methods of measuring the headspace; static or

dynamic. Under static conditions a small aliquot of air is sampled and measured, whereas, under dynamic conditions an inert gas is blown over the sample which incorporates more volatile for measurement. The dynamic headspace measurement is more close to real-life sniffing of food.

- In-*vivo* measurements

  In-*vivo* testing measures flavour release from the sample during oral processing. This is measured from the air expelled from the nose throughout consumption.

PTR (proton transfer reaction) and APCI (Atmospheric Pressure Chemical Ionisation) are the most common method of mass spectroscopy used to detect aroma intensities. APCI-MS will be discussed further here, it is a 'soft' technique that rarely breaks down the molecular structures of the compounds being measured, thus producing mass to charge (m/z) ratios either one above or one below the molecular weight expected. PTR creates molecular cleavages (bonds breaking to produce smaller fragments of the original molecule) and is a useful technique if the flavour volatiles have a similar molecular weight.

APCI-MS is a chemical ionization method, therefore, initially the reactant ion is formed, and this is from water (see equation below). Within emulsions, water is always readily available and so is a suitable choice. Once ionised, the charge can be transferred to the volatiles in the sample stream.

$$H_20 + H^+ \rightarrow H_3O^+$$ **Equation 2-17**

$$H_3O^+ + R \rightarrow H_2O + RH^+$$ **Equation 2-18**

where R is the volatile

After ionisation, the sample enters the quadropole in the mass spectrometer, where the sample is oscillated via an electrostatic field. The amplitude of oscillation is dependent on the m/z of the individual components. In addition to measuring the known flavour volatiles in a sample it is also useful to measure acetone. Acetone is naturally present in the breath and appears in peaks corresponding to when the lungs exhale (Langridge, 2004), this useful as the volatile release can be tracked relative to breath patterns.

The human nose can detect limonene at 1.2 ppm (Pradrayuttawat *et al.*, 1997) whereas the APCI-MS measures flavour compounds down to 10 ppbv (parts per billion per volume) and this is beyond what the human nose can detect for many flavour volatiles (Linforth and Taylor, 2000). Since the sensitivity is greater than the human nose it is an appropriate technique as it should measure at least the quantity that a human would detect.

2.3.3 Flavour release from emulsions

The food matrix is known to affect the delivery profile and the overall perception of the retronasal aroma and therefore the flavour release mechanisms are different depending on whether the food is an emulsion or a gelled system, for example (Taylor and Linforth, 2001). Doyen *et al.* (2001) studied flavour release in emulsions and the influence of sample dilution with saliva on the hydrophilic flavour release and observed that upon dilution the volatile release increases. Carey *et al.* (2002) showed that the influence of hydrophobicity of the volatile and oil concentration on aroma release was important in cloud emulsions (i.e. emulsions containing 0.1 – 0.3% lipid). Additional data presented in this work suggested that the chain length of lipid, lipid particle size and emulsifier type did not significantly affect the partitioning of aroma into the emulsion's headspace. This work was extended by Meynier *et*

al. (2005) who studied the influence of droplet size distribution on hydrophilic flavour partitioning and showed that the distribution was not as important as the formation of an interfacial area; they showed that below 0.5 μm the partition co-efficient drastically reduced and continuous phase flavour detection was increased in the headspace.

Linforth *et al.* (2010) have collated data totalling 345 values from several studies tested by their research group over the years to determine the effect of fat on in-*vivo* flavour release and generate a predictive model for adjusting flavour compound concentrations. This shows how flavour release changes with product reformulations i.e. lower fat contents.

Paraskevopoulou *et al.* (2009) monitored the flavour partitioning of mastic gum oil volatiles in alcohol emulsions with varying droplet size (including 150 nm), emulsifier type and oil fraction. Sodium caseinate reduced the hydrophobic volatile partitioning into the headspace to the greatest extent due to the thickness of emulsifier at the interface and whey protein isolate to the least. As the droplet size decreased down to 150 nm with sodium caseinate emulsions the volatile measured in the headspace increased and this was explained to be because as the droplet size decreased the emulsifier coverage and interfacial layer reduced thus allowing more flavour transfer. However, the author did not acknowledge that an increase in total droplet surface area should theoretically also increase the rate of hydrophobic volatile transfer out of the dispersed phase (Cussler, 2009), see equation below.

$$\begin{pmatrix} rate\ of\ mass \\ transferred \end{pmatrix} = \begin{pmatrix} mass\ transfer \\ coefficient \end{pmatrix} \begin{pmatrix} interfacial \\ area \end{pmatrix} \begin{pmatrix} concentration \\ difference \end{pmatrix} \qquad \textbf{Equation 2-19}$$

Therefore these results match one of the hypotheses being tested in this work: flavour release from the dispersed phase is faster for smaller droplet sizes as the surface area for mass transfer of the flavour is increased.

Harrison *et al.* (1997) proposed theories for mass transfer of aroma compounds between the phases in an emulsion into the air by predicting partition coefficients based on the molecular hydrophobicity and lipid/oil fraction. Using a similar technique the impact of physiochemical properties of ethyl butyrate (hydrophilic) and limonene (hydrophobic) on mass transfer through the emulsion phases were predicted.

In this work the two aroma compounds selected were ethyl butyrate (hydrophilic) and limonene (hydrophobic). These aromas were selected as they are easy to distinguish in the mass spectrometer and are commonly used in flavour release experiments due to their simple structures that minimally interact with other components in the emulsion (Langridge, 2004).

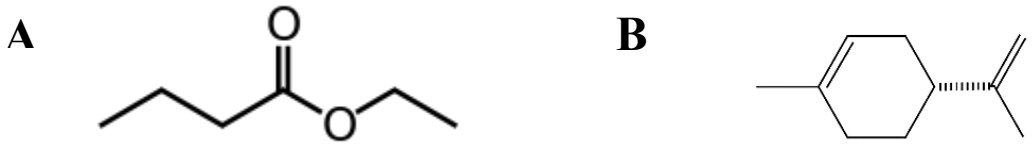

Figure 2.12: Molecular structures of the flavour volatiles A) ethyl butyrate (water soluble) B) limonene (oil soluble) (Tisserand and Young, 2014)

The extent to which the aroma compounds will transfer between the phases can be predicted by considering their respective mass transfer coefficients at the air-water, oil-water and oil-air interfaces (K_{AW}, K_{OW} and K_{OA} respectively). These are shown in Table 2-3. In addition to these coefficients a mass transfer coefficient between the air and emulsion, K_{AE}, has been calculated according to the following equation (Harrison *et al.*, 1997):

$$K_{AE} = \frac{K_{AW}}{\emptyset\,(K_{OW} - 1) + 1}$$ **Equation 2-20**

Where Ø is the oil fraction in the emulsion

Table 2-3: Physical parameters for ethyl butyrate and limonene estimated from EPI Suite[4.1]: Kaw – air-water partition coefficient; Kow – oil-water partition coefficient, Koa – oil-air partition coefficient and Kaw – air-emulsion partition coefficient calculated from Equation 2-20.

Compounds	K_{AW} (a)	K_{OW} (b)	K_{OA} (c)	K_{AE} (d, 10%)	K_{AE} (d, 30%)
Ethyl Butyrate	0.69	71	4365	8.61E-02	3.13E-02
Limonene	15.54	67608	18197	2.30E-03	7.66E-04

(a) K_{AW} (Air/Water) was estimated from the Henry's Law constant - bond contrition at 25 ◦C by *HenryWin v3.20*
(b) K_{OW} (Octanol/Water) was estimated through *KowWin v1.68*
(c) K_{OA} (Octanol/Air) was estimated through *KoaWin v1.10*
(d) K_{AE} (Air/Emulsion) was calculated from Equation 2-20, 10% and 30% is the oil fraction Ø.

The results in Table 2-3 can be used to indicate where the aroma compounds will reside within the emulsion. For example, once limonene has transferred out of the oil phase, its rate of mass transfer to the air phase is much faster (K_{AW} = 15.54), thus the limiting step is transferring across the oil-water interface. It is relevant to consider this for the in-*vivo* results, where the conditions are more dynamic than the headspace, and the release of limonene through the oil-water interface may be more likely. For ethyl butyrate the mass transfer for release is only from the aqueous phase to the air and thus the release should be higher, although to correct for this the concentration of continuous phase aroma used was reduced (see 5.2.2 for emulsion preparation). This was calculated using the equation developed by Linforth *et al.* (2010).

2.4 Nanoemulsions within fluid gels

2.4.1 Polysaccharide structures

Polysaccharides are extracted from a variety of sources including seaweeds, plants, bacteria, fungi, insects, crustacea, animals and even humans (Prajapati *et al.*, 2014). The term polysaccharide covers a wide large range of carbohydrate polymers with either single repeating carbohydrate units (e.g. cellulose and starch) or two or more repeating units (e.g. agar, alginate and carrageenan). The polymers can be linear or highly branched and consequently produce a variety of different properties. This is why they find their common use as viscosity modifiers in food.

The polysaccharide used within this work is carrageenan, a linear sulphated polysaccharide with two repeating units. It is naturally derived from red seaweeds and there are three main types of carrageenans each differing by the extent of sulphation. The repeating alternating polyanionic units are shown in Figure 2.13.

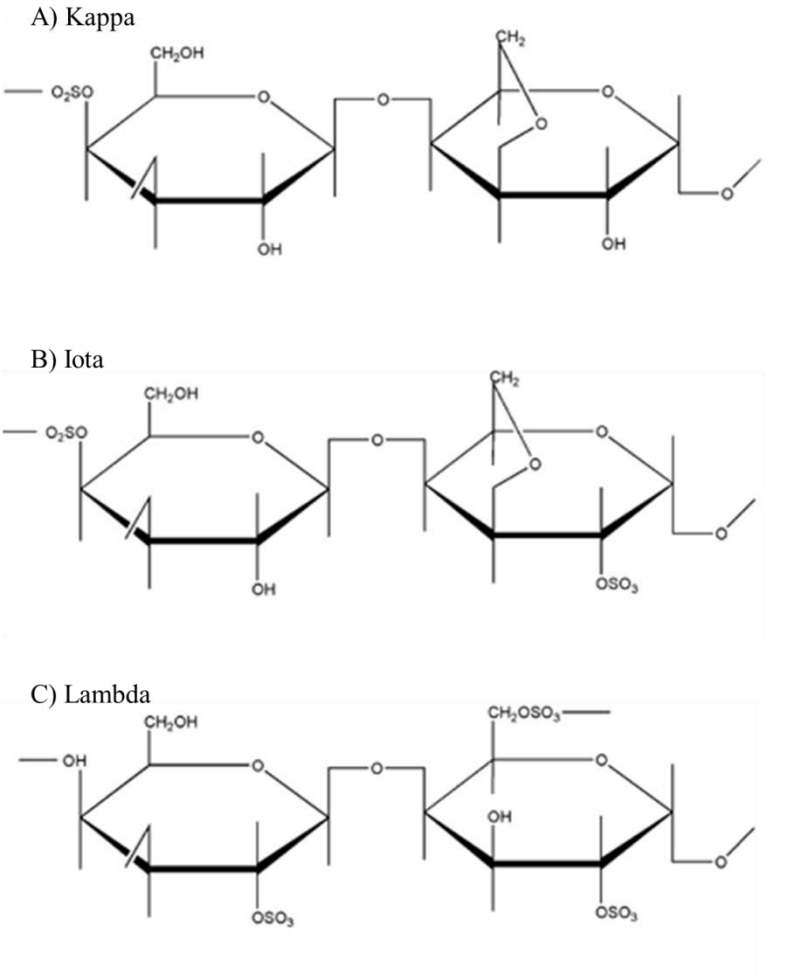

Figure 2.13: Molecular structure of the three main types of carrageenans: A) Kappa, B) Iota and C) Lambda

Iota and lambda carrageenan respectively form a soft gel and does not gel. Whereas, kappa carrageenan, (1→3)-β-D-galactose-4-sulphate-(1→4)-3,6-anhydro-α-D-galactose, gels with addition of salt.

2.4.2 Gelation of κ-carrageenan

The mechanism for gelation of κ-carrageenan (κ-c) has been debated in literature. Originally Anderson *et al.* (1969) proposed double helix gelation, although this study was overlooked and contradicted by Smidsrød *et al.* (1980) and Paoletti *et al.* (1984). These papers considered

the thermodynamics of gelation and suggested single coil ordering with cationic bridging between these coils.

The currently widely accepted model was proposed by Morris *et al.* (1980) and is the domain model, see Figure 2.14.

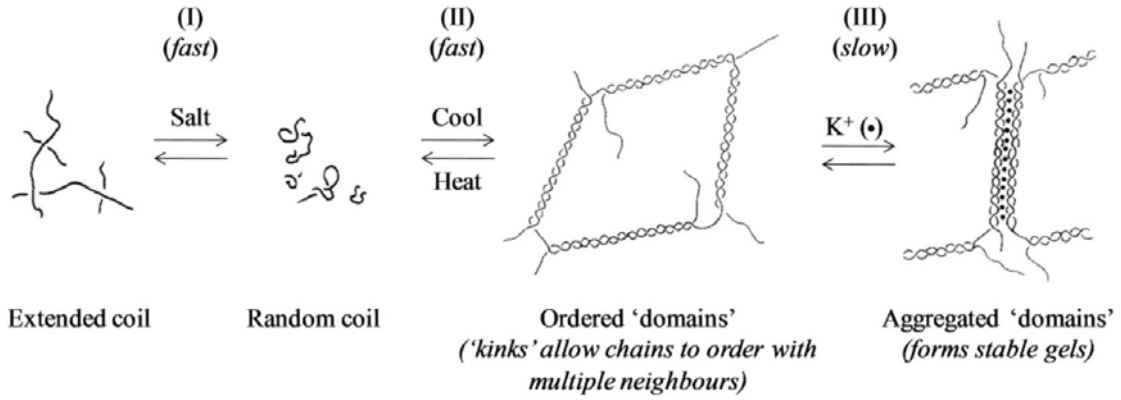

Figure 2.14: The domain model for gelation of κ-carrageenan in presence of potassium ions (Goodall and Norton, 1987, Morris *et al.*, 1980, Garrec, 2013).

According to the model, carrageenan exists as a coil in the hot polysaccharide solution and upon cooling these coils order into helices (step II: coil-helix transition) which then aggregate via cation bridging between the sulphate groups of the carrageenan (step III: helix-helix aggregation). The kinetics of each step was further investigated by Goodall and Norton (1987) where the conformation ordering of the coils into helices was shown to take between milliseconds and minutes. This was followed by a much slower process whereby the helices undergo slow lateral association into a thermodynamically more stable aggregated structure (Goodall and Norton, 1987).

The double helix conformational ordering and aggregation was further evidenced by optical rotation (Bryce *et al.*, 1982) and small angle x-ray scattering (Yuguchi *et al.*, 2002).

2.4.2.1 Influence of salt concentration on gel properties

The rate of conformational ordering and aggregation is increased by increasing the ionic strength and thereby screening interchain repulsions (Goodall and Norton, 1987). This is known as the salt screening effect and the extent of the screening can be manipulated to produce different properties. Increasing the salt concentration therefore increases the temperature of onset of gelation, and the resulting gel is stronger from the increased interchain aggregation (Morris *et al.*, 1980, Goodall and Norton, 1987).

The addition of salt causes a gelling/melting hysteresis where higher temperatures are required to disrupt the more aggregated structure and this effect is exaggerated when larger concentrations of salt are added (due to higher aggregation).

2.4.2.2 Influence of sodium caseinate on gel properties

Oakenfull *et al.* (1999) showed that adding similar quantities of sodium caseinate into κ-carrageenan gels (0.2 wt.%) did not change the onset or enthalpy of gelation but did increase the energy required for re-melting (Nono *et al.*, 2011). The storage modulus of the gel is increased (Hemar *et al.*, 2002) and is thought to be due to the interactions between the polymers; with the positive regions on the sodium caseinate interacting with the sulphate groups on the carrageenan (Ribeiro *et al.*, 2004).

2.4.3 Sheared gelation for production of fluid gels

Fluid gels are produced by cooling a hot gel solution through its gelation point whilst shearing and confining the gelation to particulates (Brown *et al.*, 1995). It is important to note the difference in production between a fluid gel formed from shear throughout gelation compared to a shear gel which is a quiescently formed gel that is broken up with mechanical energy during shearing. Figure 2.15 shows photos of A) a fluid gel and B) a fluid gel with oil included (fluid gel emulsion). κ-carrageenan was used as the polysaccharide in this work as the fluid gel particles are most closely matched to oil droplets (Garrec, 2013).

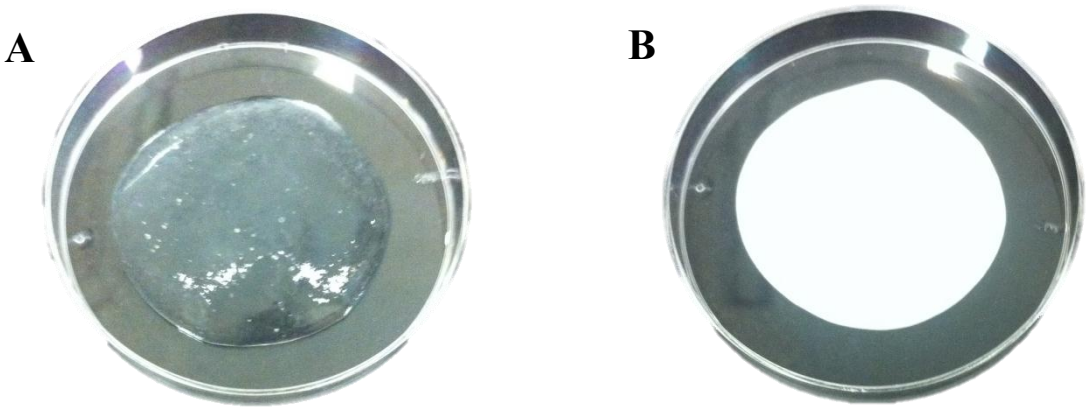

Figure 2.15: Photographs of fluid gels without oil (left) and with 10% oil (right). The gels were produced using 1.1 wt.% κ-carrageenan of the continuous phase and 0.2 wt.% KCl overall and the emulsifier used to stabilize the oil is Tween 20. For more information on how these were produced see section 6.2 Materials and Methods.

Fluid gels were initially developed by Unilever to transport a quiescent gel formulation more easily. The aim was to transport the fluid gel and once it arrived at the desired destination the thermo-reversible properties of the polysaccharide gel would be exploited by re-melting and then cooling quiescently the fluid gel to produce a quiescent gel (Brown *et al.*, 1995, Norton *et al.*, 1999). Fluid gels were developed further by the food industry as a fat or oil mimetic, with the aim of partially replacing the full fat food stuffs with a fluid gel. The fluid gel should

exhibit similar rheological, lubricative and flavour properties with a significantly lower calorific value due to the fibrous nature of the polysaccharides used.

Figure 2.16 demonstrates the range of properties that can be achieved from varying the concentration of polysaccharide used in fluid gel formation: pourable, spoonable to spreadable (Norton *et al.*, 2006). Whilst this work looked at agar, there have been multiple studies looking at the rheology of κ-carrageenan fluid gels where the concentration of salt used is also manipulated to control the stiffness of the gel particles (Garrec *et al.*, 2013, Garrec, 2013). Fluid gel particles behave as 'hairy particles' since the shear applied during production interferes with the molecular ordering process compared to quiescent gel formation (Chan *et al.*, 1988). This produces incomplete helix formation and these coils interfere at the surface of the fluid gel particles thus contributing to a higher elastic modulus (Garrec and Norton, 2012b, Garrec *et al.*, 2013).

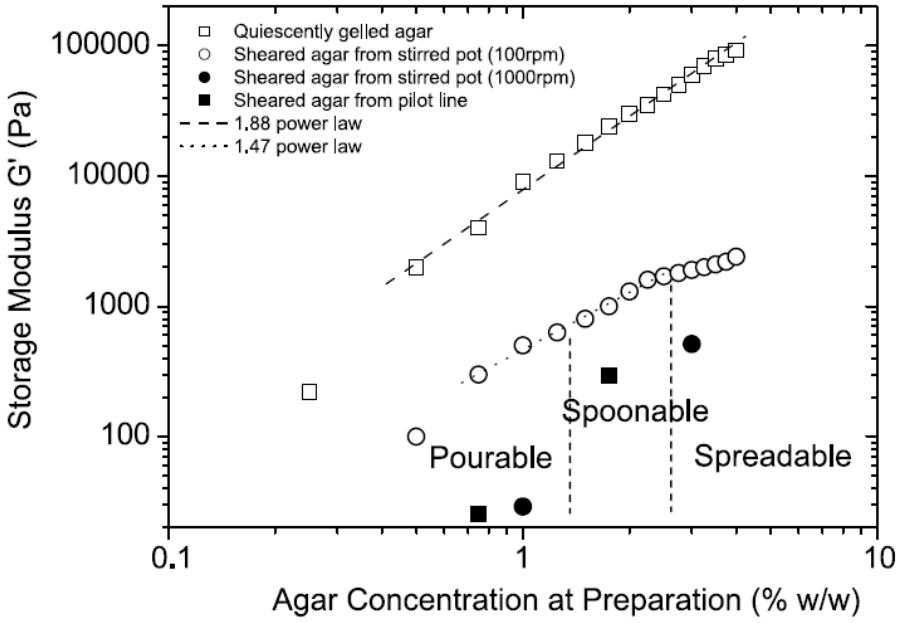

Figure 2.16: Relationship between concentration of agar and the storage modulus for quiescently gelled agar compared to an agar fluid gel. The properties pourable, spoonable and spreadable emphasises the range of properties that fluid gels cover (Norton *et al.*, 2006).

There have been a few studies that have identified in-processing gel structural changes during fluid gel production. Chan *et al.* (1988) studied the development of gel domains by using light scattering. It was shown that if shear is high it distorts gelation and the growth of the domains which leads to the production of anisotropic domains. This is known as the phase separation of gel to produce fluid gel particles. When fluid gels are produced on a rheometer the viscosity increase is in one step and therefore does not show the ordering and aggregative steps to be separate (Gabriele *et al.*, 2009). For continuous production of fluid gels a jacketed pin stirrer is used. The flow dynamics and shear rates of this device were studied by Gabriele (2011). A non-gelling fluid (glycerol) was compared to a 2 wt.% agar gel solution. Glycerol showed a uniform map of shear rate throughout the height of the pin stirrer. Whereas with agar, due to the phase change of the polysaccharide solution the viscosity increase led to a

significant decrease in shear rate between the bottom and the top of the pin stirrer. Despite this, the transition between polysaccharide solution and fluid gel was gradual.

κ-carrageenan fluid gel particle sizes range from approximately 5 µm in size up to large aggregated structures of 100 µm or larger. The particle size can be manipulated either by controlling the shear or cooling rates of the process (Gabriele *et al.*, 2009) and is strongly dependent on the ratio of shear to quiescent cooling (Garrec and Norton, 2012b). The micrographs below show the small spherical fluid gel particles achieved at high shear rates compared to the aggregates that are formed at lower shear rates. Garrec and Norton (2012b) demonstrated that if 98% of the molecular ordering has occurred during shearing the final bridges that are formed during the quiescent cooling step can be broken when the sample is sheared again.

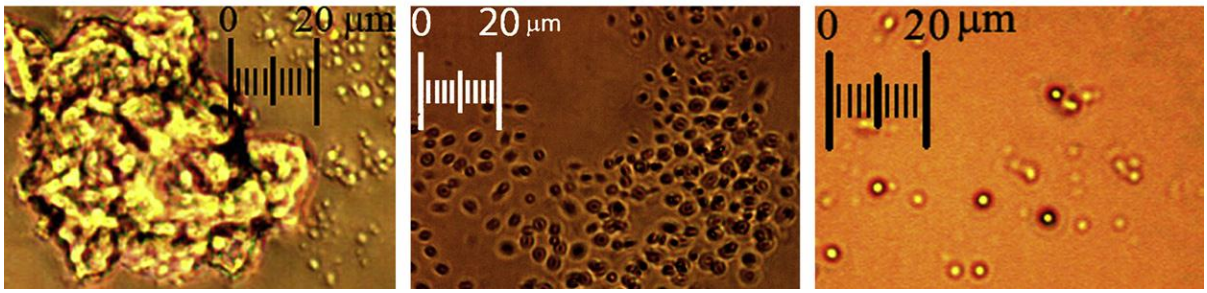

Figure 2.17: Micrographs of diluted fluid gel particles produced under different shear rates 0.5 s^{-1} (left), 1 s^{-1} (middle) and 5 s^{-1} (right) (Gabriele *et al.*, 2009).

Following on from the microstructural studies for the bulk properties of fluid gels, tribology has been used to simulate sensory response. Tribology measures the lubrication of fluid gels between the tongue and the palate within the mouth. More specifically this method relates the

thickness, stability and texture of fluid gels to perceived creaminess for mimicking fat (Garrec and Norton, 2012a, Mills and Norton, 2013, Fernández Farrés *et al.*, 2014).

2.4.4 Oil inclusion in gel systems

This literature survey has highlighted that there have been several studies on understanding kinetics of κ-c gelation and investigating the production of fluid gels with rheological properties similar to fat. To date, the research has focussed on the fluid gel only system, with minimal work on incorporating oil into the gel particulates during sheared cooling.

There has been some research focussed on encapsulating oil within biopolymer structures, for example, entrapping oil within protein-polysaccharide complexes (Matalanis and McClements, 2012) or encapsulating liposomes within a gel (Vollhardt *et al.*, 2002). However, the work by Brown *et al.* (1999) is more similar to the work carried out in this thesis. They developed a biopolymer fluid gel which was then used to suspend a second phase between the gel particulates. This work was later extended and a method was patented for producing a fluid gel with a second phase (ethylene glycol distearate) trapped within the first phase to deliver slowed release within shampooing of the second phase (Brown *et al.*, 1999).

The research in this chapter is different from this as the trapped phase is oil for the application of fat mimetic. The fluid gels with oil produced in this work will be referred to as fluid gel emulsions.

CHAPTER 2B: EMULSIFICATION: MECHANISTIC UNDERSTANDING

This final part of the literature review chapter includes a peer-reviewed paper published in Trends in Food Science & Technology during 2013, entitled 'Emulsification: Mechanistic Understanding'. The lead author was Laura Lee (current thesis author), with collaborating authors: Nima Niknafs, Robin Hancocks and Ian Norton. The paper reviewed the leading research in droplet break-up during emulsification carried out in Ian Norton's research group.

Abstract

This paper reviews current work from our group on the mechanism of droplet break-up and coalescence. In order to do this a reflectance technique was used to measure the rate of coalescence for different emulsifier types and concentrations. It was shown that droplet coalescence in flow cannot be stopped by emulsifiers and the coalescence rate was unaffected by emulsifier type or concentration. However, addition of a high concentration of Pickering particles suppressed coalescence in flow, which can be explained by the associated high adsorption energy. If the interface is only partially covered by particles, this can result in phase inversion. These results were compared for several emulsification techniques: high pressure valve homogenisation, microfluidization and membrane emulsification. In contrast to previous studies it has been shown that membranes produce droplets smaller than the pore size, and this is only possible if the emulsifier has a fast adsorption rate.

Introduction

Emulsions are found both in industrial and domestic environments. An emulsion is a mixture of immiscible liquids, usually oil and water, where one is dispersed within the other as droplets. The most common method of emulsification is from an input of mechanical energy to the system that creates droplet deformation and break-up to produce smaller droplets (Binks, 1998). Smaller droplets have many advantages, for example they are more stable to creaming, provide faster mass transfer for release of flavour molecules, and cause reduced scattering of light and as a result the emulsion can become translucent, typically at droplet diameters below 50 nm (McClements, 2011).

The mechanism by which the droplets are formed and broken by the different processing methods is a continuing area of interest (Walstra, 2005). Emulsification depends mainly on emulsifier type and concentration used, relative viscosities of dispersed/continuous phases and the hydrodynamic conditions of the mixing device. In laminar flow, droplets are deformed and broken by simple shear flow or elongational flow, in either case resulting in droplet break up from extension, and tip streaming or trailing (Windhab *et al.*, 2005). When the flow regime is turbulent droplet break-up is either from cavitation or shear. Droplet break-up from shear is described by the Kolmogorov-Hinze theory (Kolmogorov, 1949, Hinze, 1955). Two types of droplet break-up are identified: turbulent inertial and turbulent viscous (Walstra and Smulders, 1998). Turbulent inertial break-up is when the droplet deformation is caused by the smallest scale eddies in the system and therefore droplets are of the same order of magnitude to the eddy size. In turbulent viscous break-up regime, droplet sizes are reduced below the size of the smallest eddies in the system from the shearing forces created within the eddies. Droplet deformation and break-up in turbulent viscous flow is mechanistically similar to

laminar (Walstra, 2003), and typically occurs between viscosity ratios of 0.1 – 5 (dispersed viscosity/continuous viscosity) (Walstra, 2005).

Droplet break-up occurs in several stages, droplet deformation and break-up followed by stabilisation from adsorption of emulsifiers to the newly produced interface. If the interface is not stabilised before another droplet collides with it the droplets may coalesce and form one larger droplet.

The resistance to droplet deformation is from the internal pressure of the droplet (ΔP), defined by the Laplace equation:

$$\Delta P = 2\sigma_{OW} / R \qquad \textbf{Equation 2-21}$$

This demonstrated that the internal pressure increases with an increase in interfacial tension (σ_{OW}) and a decrease in droplet radius (R). As such the production of smaller droplets requires a higher amount of energy to create droplet deformation and break-up. According to the Laplace equation a silicone oil droplet of 100 nm radius with Tween 20 (γ ~7mN/m) would have an internal pressure of 0.15 MPa. To produce emulsion droplets in this size range various high energy processing techniques have been employed. The most common high pressure devices used are: high pressure valve homogenisation and high pressure impinging jet devices (e.g. Microfluidizer). High pressure valve homogenisers use a piston pump to force a premixed coarse emulsion through a specially designed valve containing a gap of approximately 10 μm under high pressure (Innings and Trägårdh, 2007, Håkansson *et al.*, 2011). The flow regime within the valve gap is laminar elongational flow and this transforms into turbulent at the exit of the valve gap (Tcholakova *et al.*, 2004). Several passes through the machine may be required in order to reach small droplet sizes. Another high pressure method

of producing nano-sized droplets is to use a Microfluidizer. The Microfluidizer splits the coarse emulsion flow into two and redirects it to a chamber which allows the streams to impinge at approximately 180^{o} (Cook and Lagace, 1985). The impact of the two high velocity and high pressure streams creates a region of high turbulence and shear for droplet disruption. At the exit of the chamber the fluid is subjected to elongational flow and this is thought to allow for emulsifier adsorption at the newly formed interfaces and thus minimising coalescence (Henry *et al.*, 2009). The mechanism for droplet break-up in a Microfluidizer has limited information since the internal dimensions of the chamber are unknown, however, previous work has shown that droplet size is a function of pressure and passes through the chamber (Jafari *et al.*, 2007b), dispersed to continuous phase viscosity ratio (Qian and McClements, 2011, Wooster *et al.*, 2008), emulsifier type and concentration (Henry *et al.*, 2010).

A new method for emulsification is membrane emulsification (Joscelyne and Trägårdh, 2000) where droplets are formed differently, with each droplet produced singly at the surface of a micro-porous membrane. Changing the forces that affect the formation of droplets (shear, trans-membrane pressure, interfacial tension and buoyancy) results in different mechanisms of droplet detachment from the membrane surface.

Emulsification mechanism

A reflectance technique was developed and used to determine the mechanisms controlling droplet size evolution in real-time during emulsification. The technique has previously been described by (Niknafs *et al.*, 2011), and is based on the dependency of light reflectance of an emulsion with its droplet size and dispersed phase volume fraction. The technique benefits

from its non-invasive nature and has been shown to be sufficiently accurate for investigation of emulsification.

Droplet coalescence was investigated in a jacketed glass vessel maintained at 25°C. A Chroma meter (Konica Minolta, Japan) was positioned underneath the vessel, where the reflectance of the system was measured at 30 sec intervals. All chemicals were obtained from Sigma Aldrich (USA), and water was double distilled de-ionised. Initially oil in water emulsions were produced using a mixer (at natural pH and room temperature of 25° C), with varied oil phase volumes and type and concentration of emulsifier, and then transferred to the mixing vessel. By carefully adjusting the processing conditions (in this case the rate of rotation of the mixing impeller, and therefore the shear experienced by the emulsion), it is possible to investigate the droplet coalescence mechanisms individually as was previously shown (Howarth, 1964, Wright and Ramkrishna, 1994). Processing began at a constant impeller speed of 1600 rpm (1^{st} processing step); the very early stages of this step are dominated by droplet break-up events. After two hours of processing, the impeller speed was taken down to 800 rpm (2^{nd} processing step), which creates an environment where coalescence dominates (Niknafs *et al.*, 2011). Processing during this second step was also allowed to take place for two hours and measurements were obtained throughout this time.

The experimental set-up allows both the break-up and coalescence of droplets to be monitored separately as a function of emulsifier type, concentration and dispersed phase volume and infer rates of coalescence. For further confidence these experiments would have to be repeated with more time points. Figure 2.18 shows data collected for 10%, 20% and 50% dispersed phase volume.

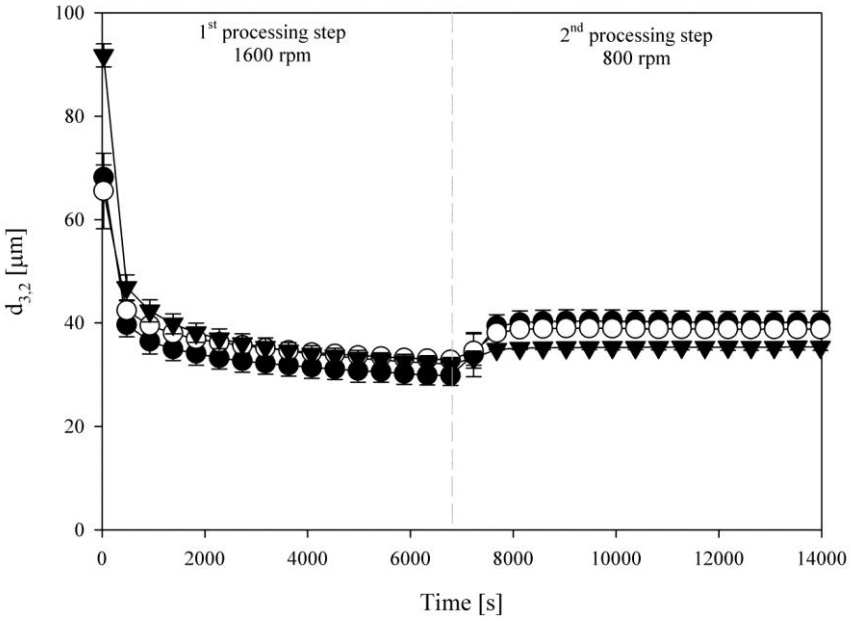

Figure 2.18: Droplet size evolution data obtained from emulsification experiments in the presence of 1% Tween 20 containing 10% (●), 20% (○) and 50% (▼) of the dispersed phase volume fraction of rapeseed oil.

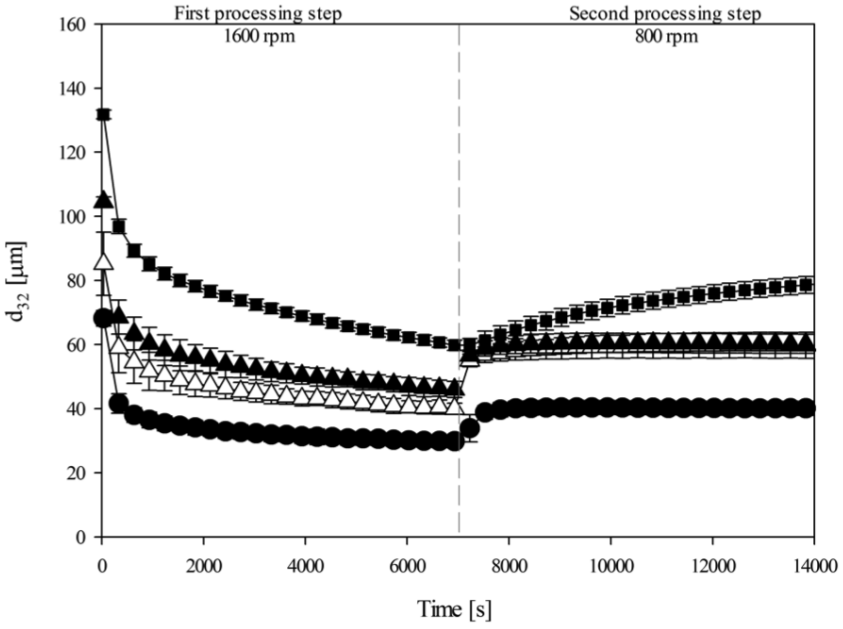

Figure 2.19: Droplet size evolution data obtained from emulsification experiments with no emulsifier (■), 1% sodium caseinate (Δ), 1% whey protein isolate (▲) and 1% Tween 20 (●) with 10% dispersed phase volume fraction of rapeseed oil.

As can be seen from Figure 2.18 the droplet break-up and coalescence rates (as defined by (Niknafs *et al.*, 2011)) are the same for all dispersed phase volumes.

Figure 2.19 shows Tween 20 at 1% has reduced the coalescence rate and caused smaller droplets, when compared to the data with no emulsifier. However the emulsifier is not stopping coalescence in shear. This observation can be explained by the force at which droplets collide being equal in either case (i.e. independent of emulsifier) so that film drainage rate is limiting coalescence rather than the time of contact. The different emulsifiers were tested to determine if the rate of break-up and film drainage is influenced by emulsifier choice.

The gradient of the curve shows droplet break-up (negative gradient) and coalescence (positive gradient) rates for different emulsifiers. The largest rate of droplet break-up was observed for Tween 20, this is expected as it adsorbs faster to the interface and therefore stabilises newly formed droplets more quickly than the protein emulsifiers, which adsorb more slowly due to readjustment of their molecular configurations at the interface (Dickinson *et al.*, 1994). Once the processing rate is slowed the coalescence rate is the same for all emulsifiers. This shows that the rate of desorption from the interface in flow is the same for all emulsifier types and that the film drainage rate is the rate limiting step, rather than emulsifier effects.

If the mechanism proposed so far is correct then particles should stop coalescence as under quiescent conditions it is known that once adsorbed on the interface, desorption requires a

high amount of energy, about 1000 kT (Binks and Fletcher, 2001). This was tested using 0.02% and 1% silica particles.

It was found that at the low concentration of silica particles coalescence was not suppressed. This is likely to be due to the low concentration so there is only partial coverage of the interface. The emulsion that contained 1% Tween 20 with 1% silica particles showed that droplet coalescence is completely suppressed. In this case the concentration of silica particles is much higher and as a result the droplet interfaces are covered by silica particles. This is in contrast with the case in Figure 2.19 where the presence of 1% Tween 20 alone showed that the rate of droplet coalescence was only slowed down and not stopped.

This result is using silica particles which are model particles with a given wetting angle suitable for stabilising O/W emulsions. Whereas, in practice presence of particles does not always suppress coalescence in flow, particularly if the wetting angle of the particles would preferentially promote stabilisation of W/O emulsions. An example of this is during the production of low fat spreads, the emulsion is known to phase invert in the presence of particles. If particles stop droplet coalescence in flow how does this occur? The role of the fat crystals has been studied and shows that in flow as the crystals are formed during cooling, inversion occurs once crystals are present (Norton *et al.*, 2009, Frasch-Melnik *et al.*, 2010). These studies indicate that by causing partial coverage of the interface with solid particles film drainage can occur in flow and therefore induce coalescence leading to phase inversion. This is achieved by controlling the tripalmitin concentration and cooling rate in the process to give partial coverage of solid particles at the interface, thus increasing the rigidity of the interface. Therefore the droplet/droplet interaction in flow becomes more hard-sphere/hard-

sphere, which reduces film drainage rates and increases coalescence (Pelan *et al.*, 1997). However, if the solid particle concentration is increased to the point where the concentration of particles covers the entire interface the droplet coalescence will be suppressed and phase inversion does not occur.

High pressure homogenisation techniques

There is growing interest in the use of smaller oil droplets in food products. This is as they give more efficient use of materials or better delivery systems and if the droplets produced are small enough they allow oil to be added without scattering of light. So as the knowledge of droplet break-up and coalescence is developed how can we use this to produce smaller droplets? There are a growing number of publications in this area. Jafari (2007b) used a Microfluidizer at relatively low operating pressures, 40 – 60 MPa, to produce emulsions with narrow droplet size distributions. A similar study on a high pressure valve homogeniser (HPH) showed the same trends (Håkansson *et al.*, 2011), whole investigations on relative phase viscosities showed that by reducing the difference in dispersed and continuous phase viscosities led to smaller droplet sizes (Wooster *et al.*, 2008, Qian and McClements, 2011).

In order to test some of these conclusions we have produced oil-in-water emulsions with 10 wt.% silicone oil (viscosity 0.05 Pa s), and distilled deionised water containing 3 wt.% Tween 20 as the continuous phase. The relatively low dispersed phase volume fraction and high emulsifier concentration were selected to increase break-up efficiency and reduce coalescence in the process. The change in viscosity ratio was achieved by modifying the aqueous phase viscosities of the system using glycerol between 0 – 50wt.% (it is known that the use of

glycerol changes the interfacial tension however this is reported as having only a minor effect (Qian and McClements, 2011))(Figure 2.20).

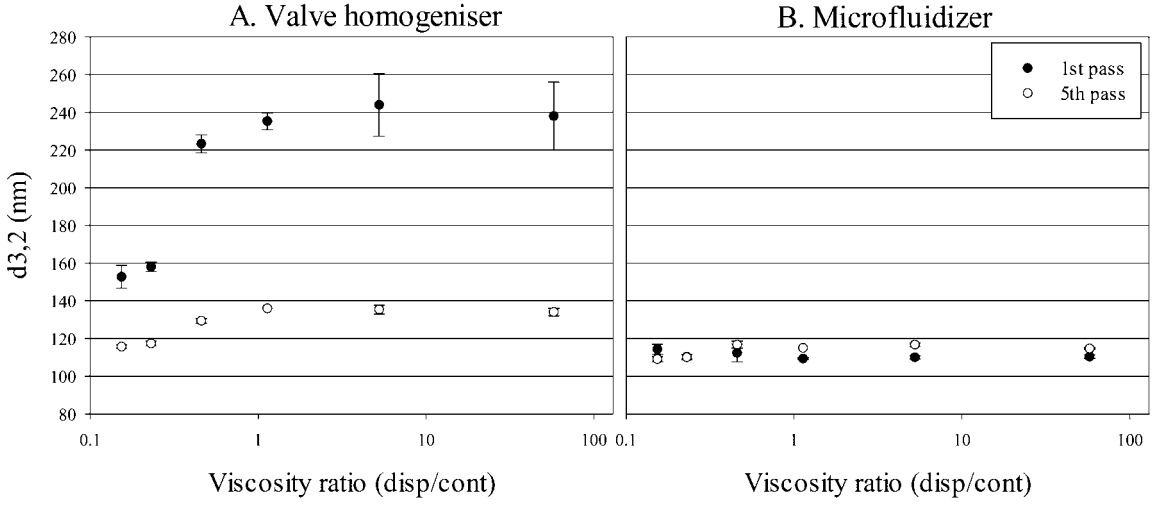

Figure 2.20: Effect of change in viscosity ratio on the first pass (●) and fifth pass (○) at 150 MPa for the high pressure valve homogeniser (A) and Microfluidizer (B) on the mean droplet diameter in 10 wt.% silicone oil (0.05 Pa s) in water emulsions containing 3wt.% Tween 20 and glycerol (variable from 0 – 80 wt.%)

As can be seen from Figure 2.20 the Microfluidizer produces much smaller droplets. This is a consequence of the difference in geometry so that within the Microfluidizer chamber the emulsifier has enough time to adsorb and cover the droplet interface as it is formed. On increasing the number of passes the two devices produce droplets of comparable sizes. As the two geometries are different and thus the energy dissipation rates are different the fact that the droplet sizes after several passes are the same once the emulsifier has been given time to adsorb to the interface implies that the droplet size is controlled by the chemistry of the emulsifier not the process. It is hypothesised that the HPH requires several passes to get to the final droplet size because there is a dynamic equilibrium between droplet break-up and coalescence, the more passes leads to a higher overall residence time leading to a shift in the

equilibrium towards droplet break-up. In future studies we will investigate this and also compare overall droplet size distributions to fully understand the mechanism.

Figure 2.20 shows that by increasing the viscosity ratio (reducing the continuous phase viscosity), the droplet size increases, this is particularly evident for the HPH. This dependency can be explained by droplet deformation and breakup mechanisms. As the continuous phase viscosity increases, coalescence is reduced thus producing a smaller droplet size.

In the Microfluidizer there is not much difference in the droplet size. The presence of elongational flow after the jets impinge is hypothesised to be responsible for the observed behaviour. The independency of viscosity on elongational flow has been previously observed by (Walstra and Smulders, 1998, Grace, 1982).

It has been reported that the smallest droplet size in simple shear flow is produced for a viscosity ratio of 1, it was reported that droplet deformation and break-up in turbulent viscous flow can be equated to that seen in simple shear flow and therefore it would be expected that a minimum in droplet size should be observed at 1 (Walstra and Smulders, 1998). The normal viscosity range associated with turbulent viscous flow is between 0.01 and 5 (Walstra, 2005) Figure 2.20 shows that there is no minimum observed within this range. The overall trend observed for both devices is that by decreasing the viscosity ratio, the droplet sizes reduce. This is very different to previously published data using a colloid mill (Walstra and Smulders, 1998). Although more work is required this data suggests that the physical chemistry at the interface is an important consideration and we cannot simply consider the physical aspects of the problem.

Membrane emulsification

Previous sections have shown that by using conventional emulsification techniques there are two phenomena that need to be considered: the break-up of droplets and subsequent stabilisation of the newly formed interfaces to prevent coalescence. Membrane emulsification can be considered as a droplet production method. It produces droplets singly at a desired size by using pressure to force the fluid through a membrane with uniform pores, into the flowing continuous phase (Joscelyne and Trägårdh, 2000, Nakashima *et al.*, 1991). The purpose of the cross-flowing continuous phase is to provide a detaching force to break the forming droplet from the pore, and also to transport formed droplets away from the membrane reducing the chances of coalescence after droplet production. This technique offers advantages over high-energy emulsification because during processing there is limited coalescence and therefore it uses emulsifiers efficiently, and the final emulsion has a narrow droplet size distribution and potentially longer shelf life.

The cross-flow membrane emulsification system used here contained a 10 mm outside diameter membrane tube. Air pressure was used to force a dispersed phase of sunflower oil through the pores into a continuous phase of deionised distilled water and emulsifier. The continuous phase was re-circulated over the outside surface of the membrane at varied speeds using a pump. The pressure across the membrane (trans-membrane pressure) was carefully controlled using a digital regulator, and the absolute pressure was monitored at the inlet and outlet of the continuous phase to the membrane module, so the actual trans-membrane pressure could be found. The continuous phase pump was calibrated to give an accurate linear velocity of the continuous phase across the membrane surface. All chemicals were purchased

from Sigma Aldrich (USA) and the continuous phase was made using double distilled de-ionised water. The continuous phase was made up with a percentage by weight of the emulsifier, and was at natural pH and room temperature (25° C).

Experiments were performed to produce oil in water emulsions to 1% dispersed phase volume, using a shirasu porous glass membrane of 1 μm mean pore diameter. The type and concentration of emulsifier was varied, and the results are shown in Figure 2.21.

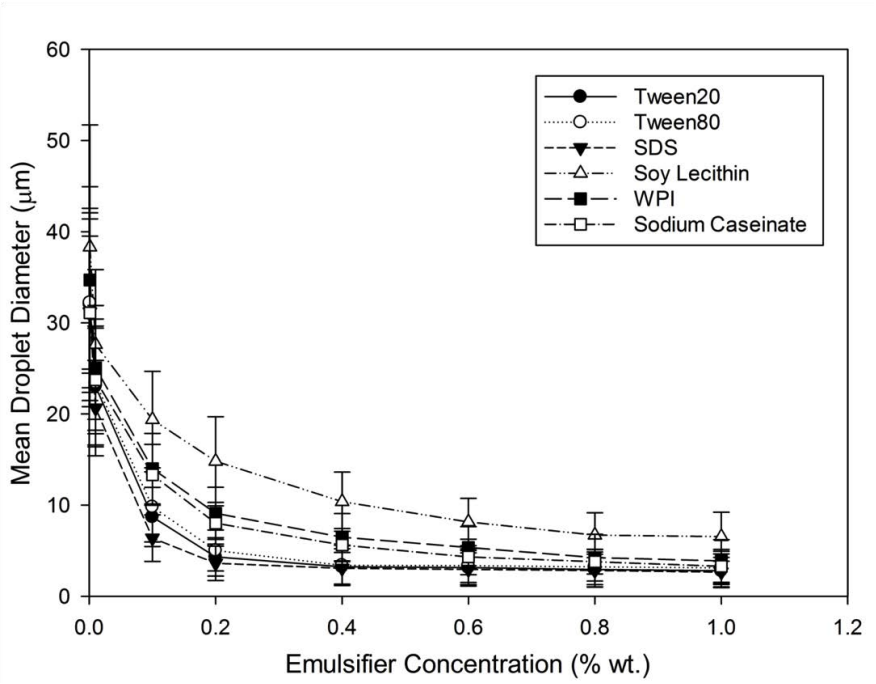

Figure 2.21: Emulsions were produced using the 1 μm pore diameter SPG membrane with different concentrations of different emulsifiers; Tween 20 (●), Tween 80 (○), SDS (▼), Soy Lecithin (△), WPI (■) and Sodium Caseinate (□). The emulsions were made at 0.6 ms^{-1} cross-flow velocity and 10 kPa trans-membrane pressure. 1% dispersed phase volume was reached for each emulsion.

As can be seen in Figure 2.21 the droplet size obtained decreases as the emulsifier concentration increases. As this is now a droplet formation process rather than a droplet

break-up this implies that the speed with which an emulsifier reduces interfacial tension is important. As can be seen the different emulsifiers have different effects; the SDS, Tween 20 and Tween 80 produce similar droplet sizes. The SDS induces an electrostatic repulsive force (Tcholakova *et al.*, 2004) between droplets, and this reduces droplet coalescence, therefore, if droplet coalescence were present we would expect to see a larger difference between the emulsion droplet size produced. An explanation for this observation is that the droplets are not subjected to a high-energy environment as with the high pressure emulsification methods, therefore the collision energy will be low. As can be seen from Figure 2.21 the protein produces the same size droplets as Tween and SDS once the concentration is high enough. This is expected as full interfacial coverage can occur in the process for higher concentrations. However, the results are quite different from those observed from mechanical emulsification processes. The data obtained with soy lecithin are quite different. Lecithin forms vesicles within the continuous phase (Pan *et al.*, 2002), which must dissociate before the emulsifier can absorb to the forming interfaces, and so the interfacial tension is reduced yet more slowly and therefore the largest droplets are produced when using lecithin.

The mechanism of droplet formation and detachment from an individual pore can be considered as a consequence of four forces acting on the forming droplet (Schröder *et al.*, 1998): inertia of the fluid as caused by the cross-flow membrane pressure, the interfacial tension, cross-flow shearing forces from the continuous phase and the buoyancy force of the dispersed phase. Thus the size of a droplet for a given pore depends on which force is dominant, and the droplet size changes depending on the regime.

To illustrate the effects of the forces mentioned above, experiments were performed changing the cross-flow velocity and the trans-membrane pressure. These operating conditions change the shear rate and the inertial forces governing droplet detachment respectively. The results of these experiments are shown in Figure 2.22.

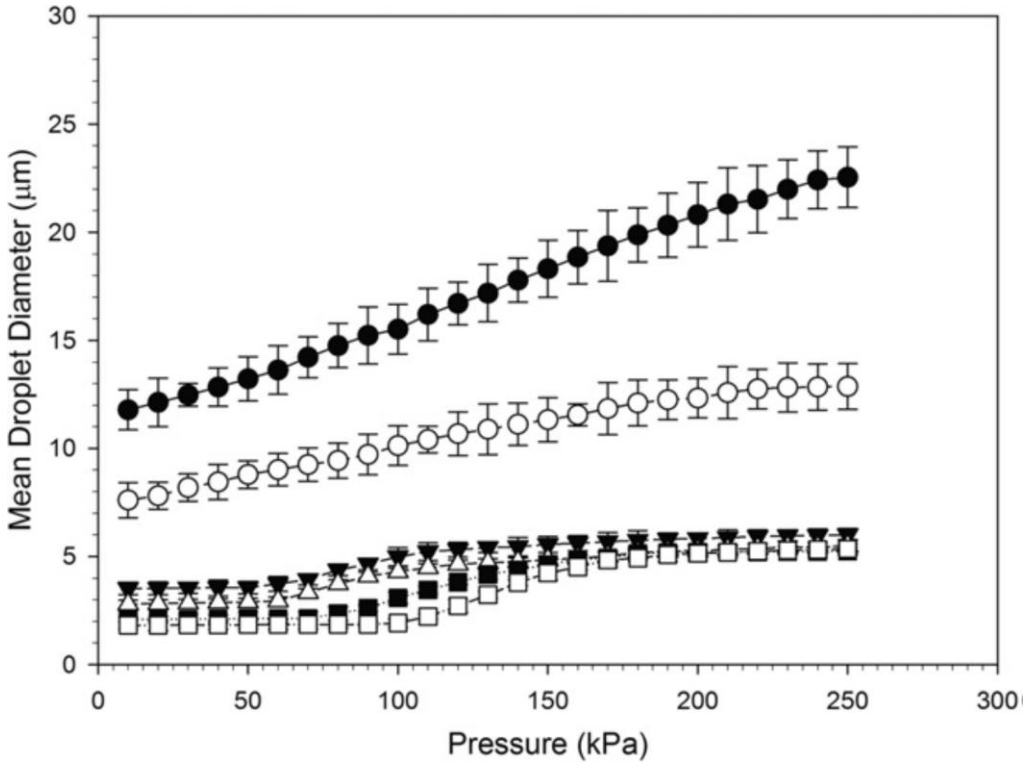

Figure 2.22: The effects of trans-membrane pressure on the droplet sizes produced at different linear cross-flow velocities (0.165 ms^{-1} (●), 0.275 ms^{-1} (○), 0.550 ms^{-1} (▼), 0.600 ms^{-1} (△), 0.850 ms^{-1} (■) and 1.1 ms^{-1} (□). The emulsions were 1% phase volume with 1% Tween 20 emulsifier, made using the 1 μm pore diameter SPG membrane.

As can be seen at lower pressures and higher cross flow velocity the shear breaks droplets from the surface quickly, leading to the smallest droplets, which can be smaller than the pore size but as mentioned before the surface chemistry and rate of surface coverage need to be carefully controlled. At medium pressures and high cross flow velocity, droplets grow at the

pores fast enough to reach a size where the interfacial tension is enough to pinch the neck of the forming droplet causing detachment before the shearing force can detach the droplet. At higher pressures and high cross flow velocity, the pressure causes the dispersed phase to flow from the pores as streams, which then breakup into droplets due to Rayleigh instabilities.

Nano-sized droplets have been produced with the same membrane system; these required high cross-flow shear along with higher applied pressure to overcome the higher capillary pressure of a small pore size membrane. Thus under these conditions the mechanistic chemical engineering aspects dominate (Hancocks *et al.*, 2012).

Conclusions

A reflectance technique was used to study the mechanism of break-up and coalescence during processing. It was found that coalescence in flow cannot be stopped by emulsifiers and the rate of coalescence was the same for all emulsifiers used. The only way to stop coalescence in flow was using a high concentration of Pickering particles to allow for full interfacial coverage. If the interface is only partially covered by particles, it cannot be stabilised against coalescence and this can result in phase inversion.

The study on emulsion production from membranes showed that droplets smaller than the pore size can be produced. This is only possible using a high cross-flow velocity, small pore size and a trans-membrane pressure just above the critical droplet formation pressure.

CHAPTER 3: PRODUCTION OF OIL IN WATER (O/W) NANOEMULSIONS USING HIGH PRESSURE

3.1 Introduction

Nano-sized or sub-micron droplets are increasingly becoming more common in emulsion based products. This has led to the industrial need for a better understanding of how droplet break-up is caused using high pressure devices.

This chapter focusses on the production of oil in water (O/W) nanoemulsions from a high pressure valve homogeniser (HPH) and a Microfluidizer. The influence of pressure and number of passes (residence time in the region of peak energy dissipation) on the emulsion droplet size and droplet size distribution is tested. To verify the regime of turbulence present and its role in droplet break-up within the Microfluidizer, the device's fluid dynamics were computationally modelled. The emulsification performances were further tested by comparing the influence of oil dispersed phase to aqueous continuous phase viscosity ratios and emulsifier types.

3.2 Materials and methods

3.2.1 Materials

Silicone oil with viscosities of 0.01, 0.05 and 0.1 Pa s (product numbers 378321, 378356 & 378364 respectively), Tween 20 (P7949) sodium caseinate (C8654), and glycerol (G7757) were purchased from Sigma Aldrich (UK). SDS (S/5200/53) was purchased from Fischer

Scientific (Loughborough, UK). Double distilled water was used for the preparation of all solutions.

3.2.2 Emulsion preparation

Oil-in-water emulsions were produced by homogenising 10 wt.% silicone oil with 90 wt.% aqueous phase (3 wt.% Tween 20 and 0 – 80 wt.% glycerol). The low weight per cent of oil was selected to minimise effects of droplet collision and the mass of the emulsifier was tested to be in excess for the smallest emulsion produced in this paper.

A coarse emulsion was prepared by using a Silverson mixer at 5000 rpm for 60 s at room temperature. Prior to this work the effect of the coarse emulsion droplet size (5 – 30 μm) was tested and was shown to have no effect on the droplet size after high pressure emulsification. Nanoemulsions were produced by passing the coarse emulsion through an air-driven Microfluidizer or a valve homogeniser for up to 15 passes through the machines at an operating pressure of 50 – 150 MPa. See below for details of the devices.

For each data point presented within this thesis, three separate emulsions were produced: weighed, prepared and measured. The errors bars are plus or minus one standard deviation.

3.2.2.1 High pressure valve homogeniser

A high pressure valve homogeniser (NS1001L PANDA), manufactured by GEA Niro Soavi was used to produce the nanoemulsions studied in this work. Its maximum operating pressure is 150 MPa. A schematic of the valve is shown in Figure 3.1.

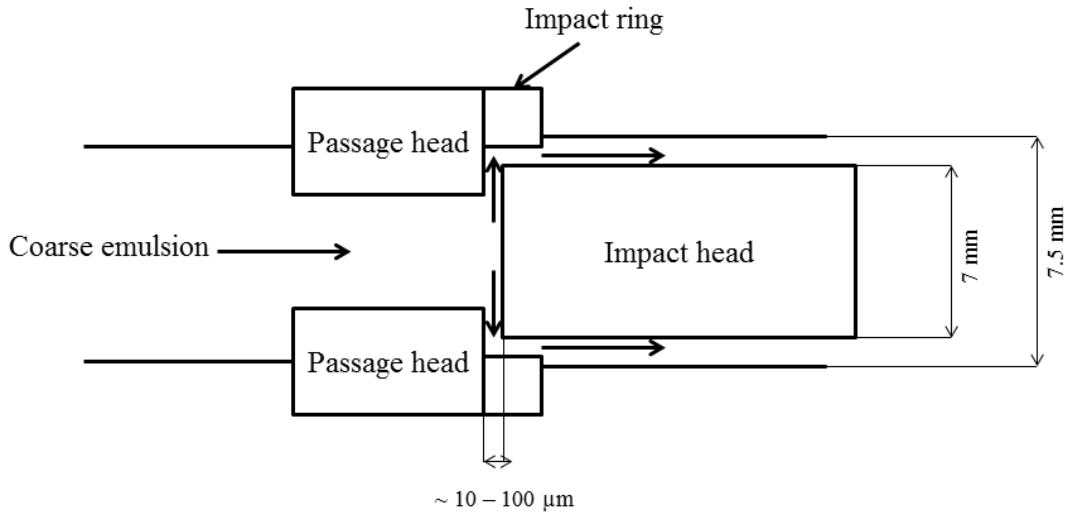

Figure 3.1: Valve homogenizer dimensions. Note that the impact head is cylindrical.

The coarse emulsion is fed into the machine where the pressure of the fluid is increased via a piston pump operated by a motor. The fluid passes through the valve seat and is forced through the valve gap between the impact head and the passage head (Figure 3.1). At the exit from the valve gap the dimensions are much larger and the pressure energy dissipates causing turbulence and droplet break-up. The fluid then exits the HPH and is collected for either testing or passing through the device again. The emulsions can be passed through the device an unlimited number of times although each pass increases the temperature of the fluid due to viscous energy dissipation.

3.2.2.2 Microfluidizer

The Microfluidizer M110S, manufactured by Microfluidics Corp, Newton, MA, was used to produce the nanoemulsions. Its operating pressure ranges from ~ 20 – 150 MPa and runs by an air driven piston pump. A schematic diagram of the impact chamber is shown in Figure 3.2 and the flowrates and velocities at given pressures are in Table 3-1.

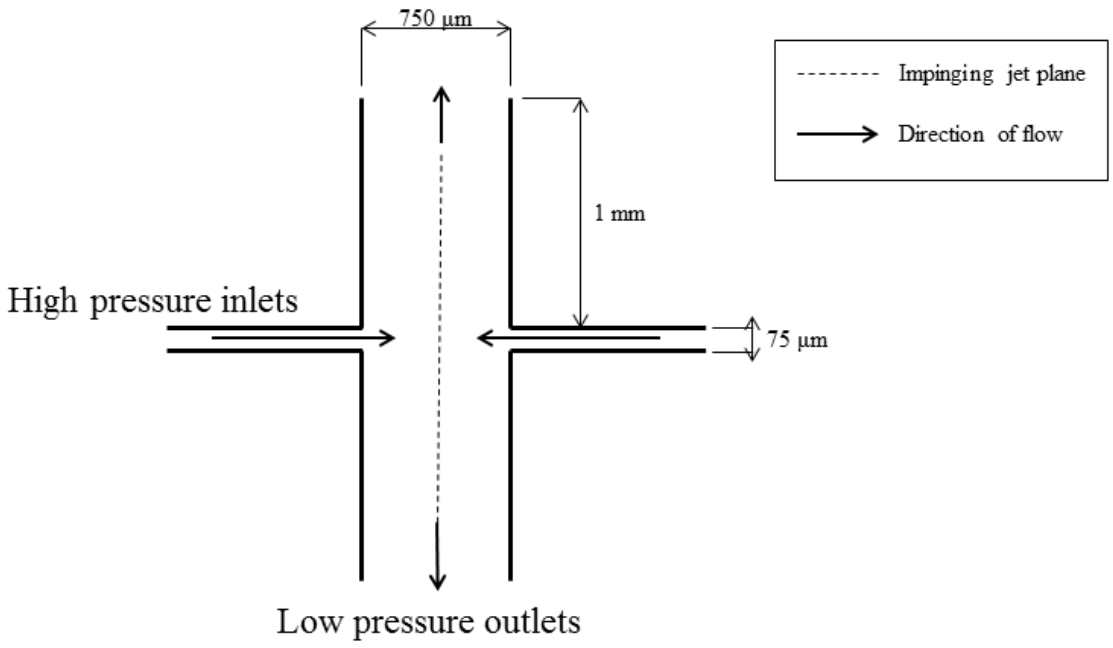

Figure 3.2: Microfluidizer dimensions estimated from conversations with manufacturers at purchase and from the patent (Cook and Lagace, 1985) (diagram not to scale).

Table 3-1: Average flowrates in the Microfluidizer for water at pressures 50, 100 and 150 MPa measured experimentally.

Pressure (MPa)	Average flowrate (m^3/s)	Velocity of inlet (m/s)
50	3.97E-06	449
100	5.36E-06	606
150	5.99E-06	677

The coarse emulsion is fed into the machine via a hopper and flows through the piston pump which increases the pressure of the fluid before it enters the chamber. Droplet break-up within the 'Y type' chamber (described by the manufacturer as the 'Y' type) occurs from the pressure energy dissipating as the jets, oriented 180° to each other, enter the chamber and

impinge. This creates high turbulence, jet velocities (Table 3-1) and shear values from the collision and efficient droplet break-up. Subsequent to exiting the chamber the fluid's temperature is reduced via a cooling tube submerged in equal proportions of ice and water. The Microfluidizer has a capability to operate continuously without the fluid being removed and re-feed back into the hopper; however, this option was not used.

3.2.3 Emulsion characterisation

3.2.3.1 Particle size measurements

The particle size distribution and volume to surface weighted mean droplet diameter, $d_{3,2}$, was measured by a Malvern Mastersizer MS2000 (Malvern, UK) with a Hydro SM manual small volume sample dispersion unit attached. The sample was diluted with double distilled water (RI=1.33) to 2% laser intensity (measured by the Mastersizer) to reduce effects from multiple scattering. The measured diffraction is then translated by the Malvern software into a droplet size distribution by using Mie theory (Hodkinson and Greenleaves, 1963). The software was configured to measure three repeats on each sample. For the nanoemulsions tested within this chapter it was common to see that each of the repeats run on an individual sample were identical.

For the smallest emulsions the size was verified against a dynamic laser system: high performance particle sizer, HPPS 5001 (Malvern, UK) (see 4.2.3.1 for more details for this method). Droplet size measurements were taken immediately after production of the emulsions.

The refractive index of the oils was measured using a Rudolph research refractometer J357 (New Jersey, USA).

3.2.3.2 Viscosity measurements

Viscosity measurements of the aqueous and oil phases were performed using a dynamic shear rheometer with cup and vane geometry (cup diameter 25 mm, with vane width 23 mm and clearance of 10 mm) with a Bohlin Gemini Nano Rheometer (Malvern, UK), and viscosities were taken at 100 s^{-1}. All measurements were performed at 25^{0}C.

3.2.4 Computational fluid dynamics

3.2.4.1 Literature review relevant to selecting CFD method

Computational fluid dynamics (CFD) is used to simulate flows within emulsification devices to predict emulsion formation. It is a relatively inexpensive technique to predict the most efficient geometry/dimensions for the device (Gavi *et al.*, 2007). There are several types of turbulent models that can be used to model turbulence, the model selection depends on the information that is required. For example large eddy simulation models the large scale eddies in the system, whereas a k-ε turbulence model simulates the turbulent kinetic energy and energy dissipation through to the turbulent length scales, and most importantly for this work the Kolmogorov length scale.

There have been no studies on modelling the Microfluidizer geometry however there have been several research groups that have modelled the valve homogeniser. Table 4-1 summarises the model details.

Table 3-2: Previous models of high pressure valve homogenisers

Reference	Turbulence model	Geometry	Number of cells in mesh	Phases	Wall treatment
(Stevenson and Chen, 1997)	Standard k-ε	2D	20,000	1	WF*
(Floury *et al.*, 2004a)	RNG k-ε	2D	350,000	1	LReF**
(Kelly and Muske, 2004)	Realizable k-ε	2D	65,000	1	*Unclear from reference*
(Casoli *et al.*, 2010)	Standard k-ε	2D	350,000	1	LReF
(Håkansson *et al.*, 2012a)	Standard k-ε & realizable k-ε	2D	278,000	1	WF

*WF – wall function

**LReF – low Reynolds number formulation

The valve homogeniser has smaller dimensions in the gap compared to the Microfluidizer, this why several researchers chose to use a low Reynolds number formulation wall treatment. This is not necessary for the Microfluidizer, as the flow in the inlet jets is turbulent. The most common turbulent model selected is the standard k-ε. Håkansson *et al.* (2012a) modelled both the standard k-ε against the realizable k-ε model and stated that whilst the results were similar the realizable model could be considered more suitable as the Navier-Stokes equation within

the model has been modified to better predict the extensional flow and high shear that is viewed within the valve geometry.

The Microfluidizer is expected to have extensional flow subsequent to the jets impinging and therefore the realizable turbulent k-ε model is selected in preference to the standard model.

3.2.4.2 CFD method

Model selection

A realizable k-ε turbulent model will be used to model a one phase incompressible fluid, water, through the Microfluidizer geometry. Flow, velocity and pressure are obtained within the model by solving mass and momentum conservation laws, e.g. Navier Stokes.

Boundary conditions

The Microfluidizer geometry is symmetrical around the impinging plane, therefore, only half of the geometry was modelled. Figure 3.2 shows a representation of the geometry that was modelled and the boundary conditions that were selected. A constant velocity magnitude was selected at the inlet, this was chosen as the velocity was known at this point (see Table 3-1). The walls of the pipe into the chamber were modelled with enhanced wall treatment as the flow at these walls is of interest. Whereas the walls in the main chamber were selected to have a standard wall function as it would be computationally more demanding to model this to the higher resolution too, especially as the behaviour of the fluid at these walls is less interesting.

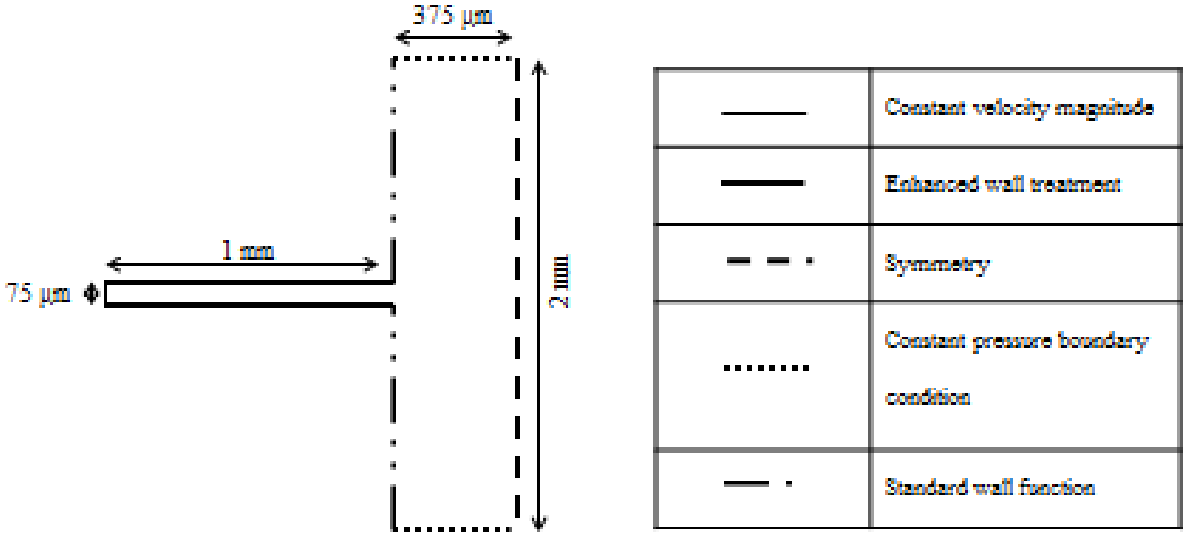

Figure 3.3: Boundary conditions and dimensions used within the model, Microfluidizer dimensions estimated from conversations with manufacturers at purchase and from the patent (Cook and Lagace, 1985) (diagram not to scale).

Mesh

A 2D unstructured 'square' mesh was created using ICEM (ANSYS, Canonsburg, PA, USA). The mesh efficiency was automatically refined to 80% efficiency. Additionally, the mesh was manually refined at the smaller dimensions, more specifically the walls of the inlet pipes. The final number of cells in the mesh was 150,000 cells.

In addition, the first mesh element on the inlet pipe was positioned relatively far from the wall, as this gives more accurate results when used in conjunction with the wall functions within ANSYS.

Mesh independence was not checked, the author assumed that it was reliable as the number of cells was in the same region as the previous models used for the valve homogeniser (see Table 3-2), and the Microfluidizer should be less sensitive on the smaller dimensions than the valve homogeniser.

Convergence

The calculations were performed until all residuals had levelled out (gradient of zero). Convergence was double checked by running the model for further iterations to check that the results did not change.

Modelling software

The modelling software used was Fluent 12.0 (ANSYS, Canonsburg, PA, USA).

Relevance of results

The results are from initial CFD simulations and were only run to complement the experimental work within this thesis.

3.3 Results and discussion

3.3.1 Comparison of high pressure devices for effect of pass number and pressures

In order to compare the emulsification efficiency of both devices a series of oil-in-water emulsions were produced with 10 wt.% silicone oil (viscosity 0.05 Pa s), and 3 wt.% Tween 20 of the continuous phase. Silicone oil was selected in preference to the industrially used sunflower oil as it has a similar viscosity and interfacial tension, however, it has less inherent emulsifier and therefore should exhibit less variation between the results. The low volume fraction of oil was selected to minimise the effects of coalescence from droplet collision and an excess of emulsifier was selected to minimise any effects from emulsifier depletion. Initially these emulsions were passed through the high pressure devices at 50, 100 and 150 MPa for 1 – 5 passes and the droplet sizes and distributions of the emulsions produced were measured (Figure 3.4 - Figure 3.7).

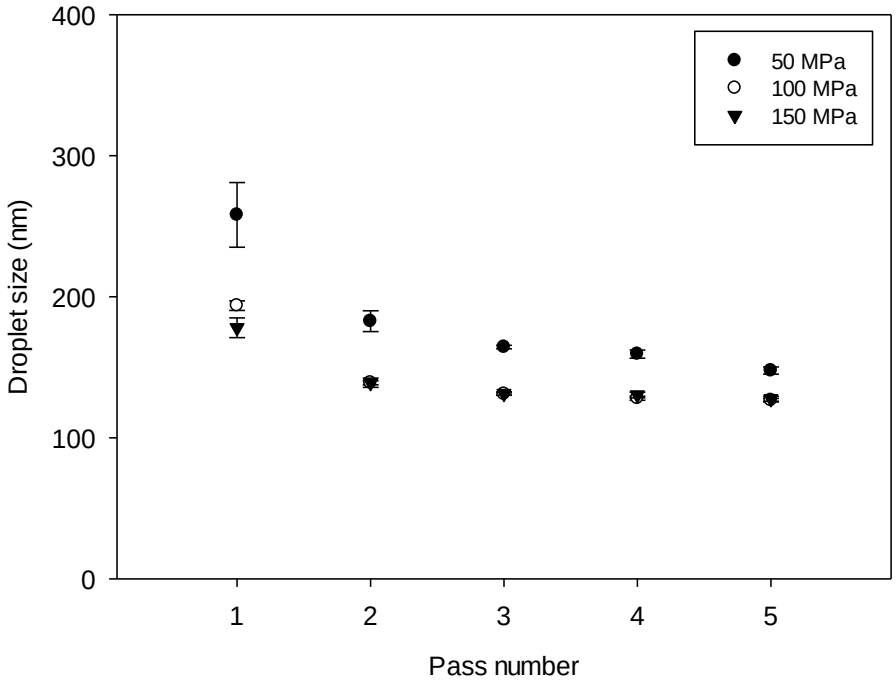

Figure 3.4: Effect of pass number and pressure on 10 wt.% silicone oil (0.05 Pa s) in water emulsion droplet size with 3 wt.% Tween 20 in a valve homogeniser.

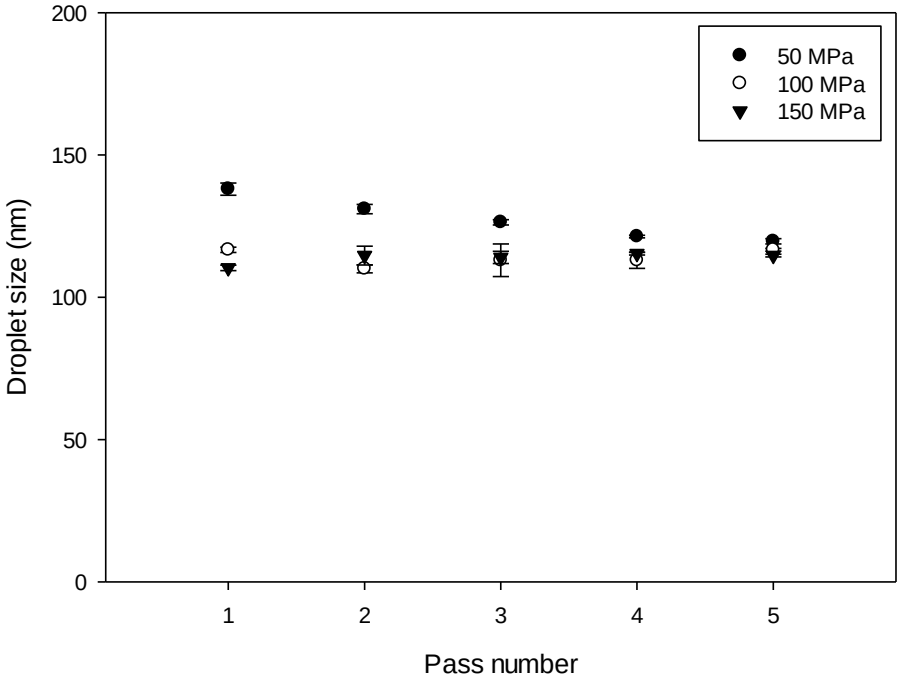

Figure 3.5: Effect of pass number and pressure on 10 wt.% silicone oil (0.05 Pa s) in water emulsion droplet size with 3 wt.% Tween 20 in a Microfluidizer.

As can be seen from Figure 3.4 and Figure 3.5, increasing the pressure of homogenisation in both cases resulted in smaller droplet sizes. This is in agreement with previous studies (Leong *et al.*, 2009, Qian and McClements, 2011, Donsì *et al.*, 2011b, Heffernan *et al.*, 2009).

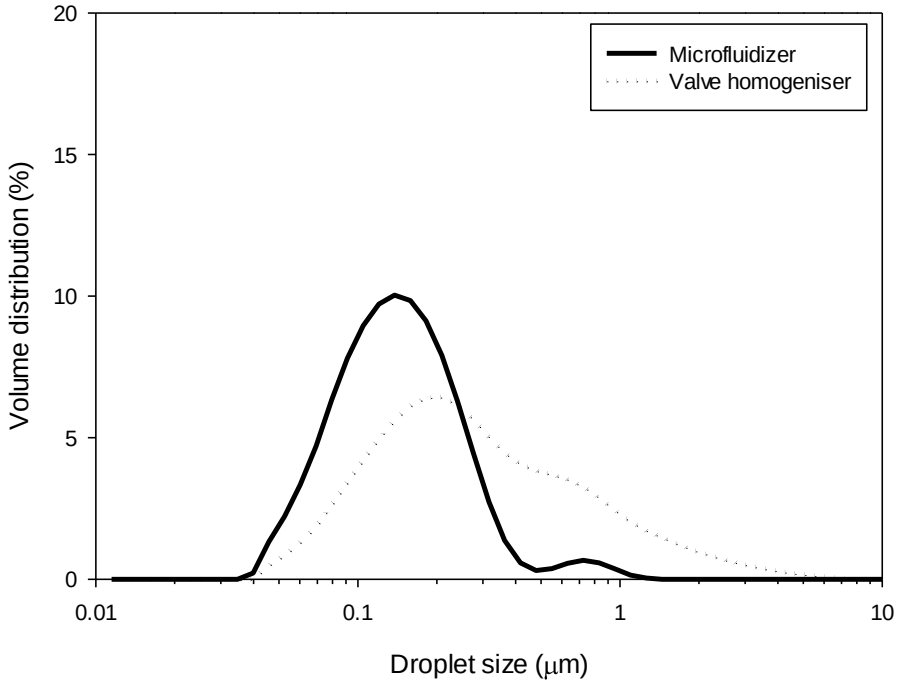

Figure 3.6: Droplet size distribution for silicone oil in water emulsions with 3 wt.% Tween 20 from the first pass in the Microfluidizer and HPH at an operating pressure of 150 MPa

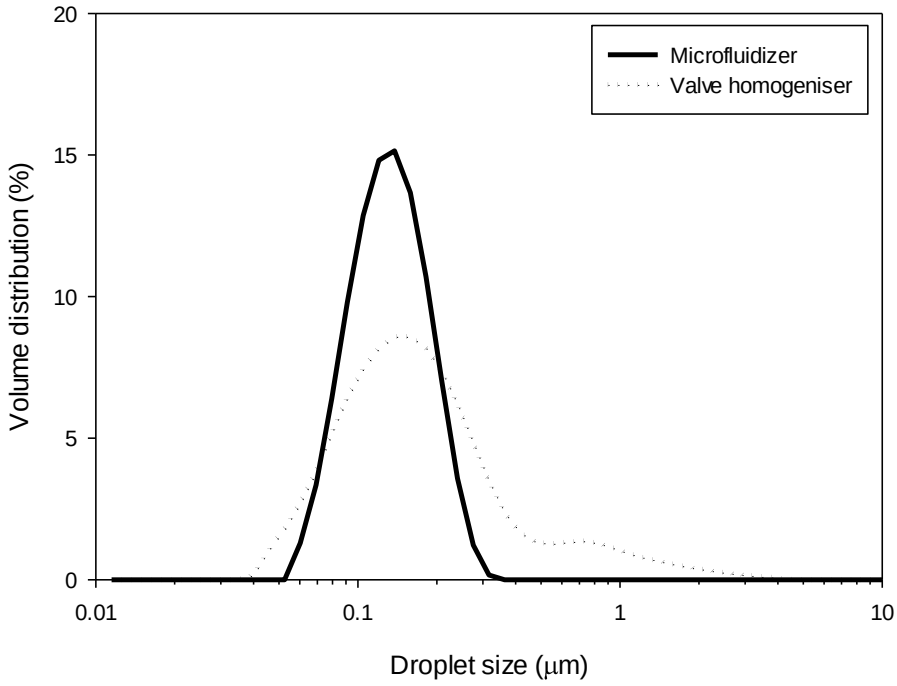

Figure 3.7: Droplet size distribution for silicone oil in water emulsions with 3 wt.% Tween 20 from the fifth pass in the Microfluidizer and HPH at an operating pressure of 150 MPa

From Figure 3.5 it can be seen that in the Microfluidizer the minimum droplet size is achieved after one pass with pressure drops of 100 and 150 MPa, whereas, in the HPH (Figure 3.4) the final droplet size is not observed until the 4^{th} or 5^{th} pass, and for the lowest pressure drop (50 MPa) the results suggest that further passes may have reduced the droplet size further. This difference in droplet size reduction is a consequence of the different geometries. The Microfluidizer creates a tight distribution of shearing forces around the maximum force as the jets impinge (Cook and Lagace, 1985), whereas the HPH creates a wider distribution of forces. Thus, in the Microfluidizer the majority of the coarse emulsion entering the device experiences the highest shear forces and breaks up, and is stabilised by emulsifier, during the first pass, see Figure 3.6. It is hypothesised that after the jets impinge there is extensional flow which increases the time for emulsifier adsorption. The second peak shown around 750 nm is

likely to indicate the presence of coalescence or a bypassing of flow around the area of peak energy dissipation. The latter option is more likely since coalescence in the Microfluidizer was shown by (Henry *et al.*, 2009) to be minimised for oil in water emulsions when excess emulsifier is present and is further evidenced to be bypassing flow as after the fifth pass (Figure 3.7) the distribution is monomodal with a span of 0.9.

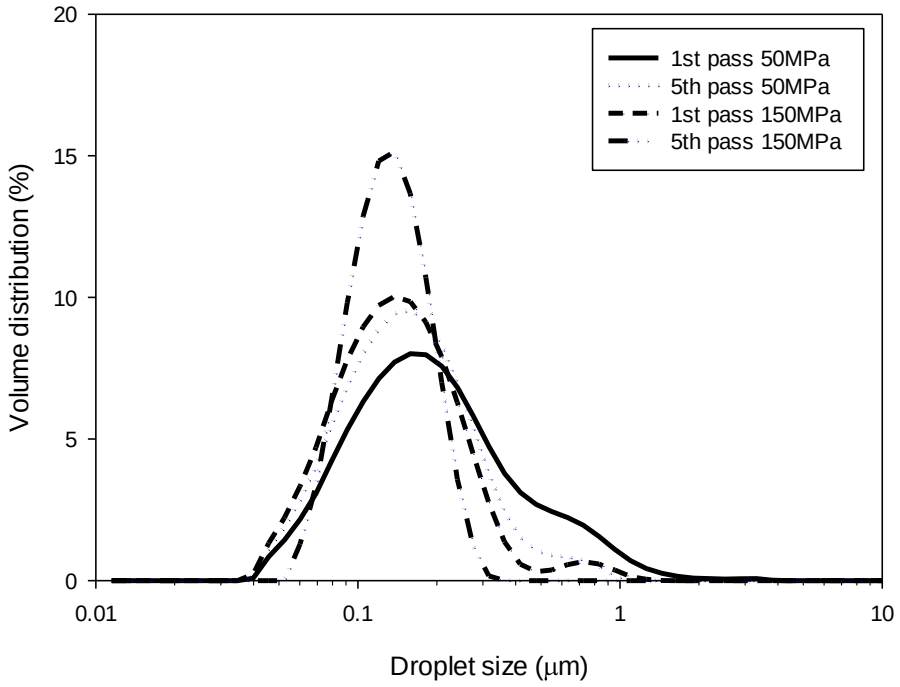

Figure 3.8: Droplet size distribution for silicone oil in water emulsions with 3 wt.% Tween 20 from the first pass and fifth pass in the Microfluidizer at an operating pressure of 50 and 150 MPa

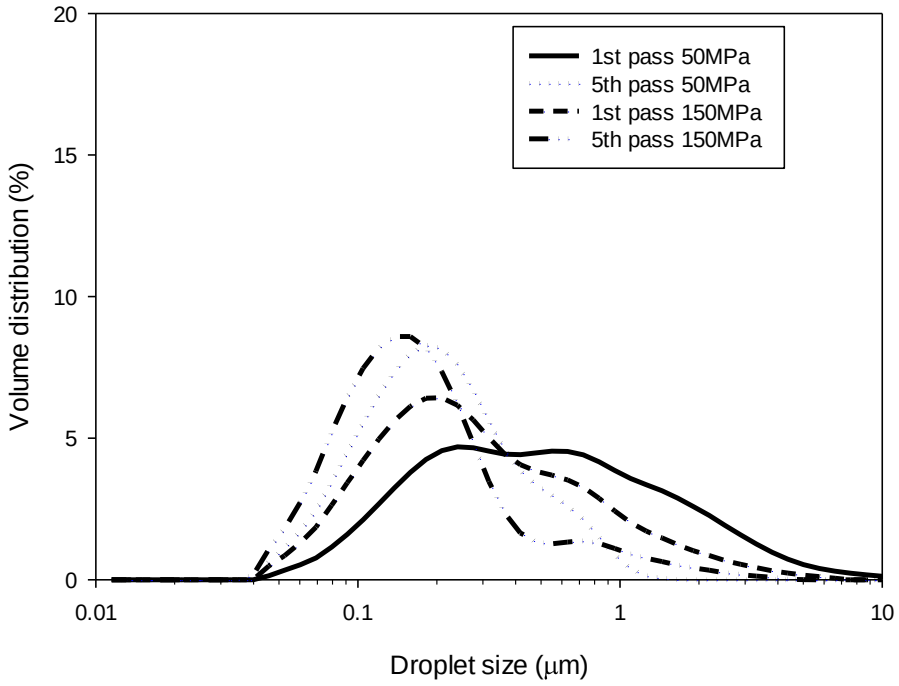

Figure 3.9: Droplet size distribution for silicone oil in water emulsions with 3 wt.% Tween 20 from the first pass and fifth pass in the valve homogeniser at an operating pressure of 50 and 150 MPa

Figure 3.8 shows the influence of changing the operating pressure of the Microfluidizer on the droplet size distributions produced. After the first pass at the lower pressure the second peak is larger than at the higher pressure. To consider why this would occur, the way the energy dissipates and the turbulent length scales should be considered. A larger pressure will dissipate more turbulent kinetic energy with a more uniform distribution of shearing forces (Håkansson *et al.*, 2009) the higher pressure will also result in a smaller Kolmogorov length scale. This length scale should correspond to the droplet size of the main peak. The distribution will also be expected to be narrower at the higher pressure since the velocity of the impinging jet is higher creating more uniform deformation stresses through the main area of energy dissipation. The second peak, as previously explained, should indicate the chance of by-passing of flow from the main turbulent area. Within the HPH, (Figure 3.6 & Figure 3.9),

it is less obvious how the distribution of droplet sizes is produced after the first pass since the distribution is significantly broader. As with the Microfluidizer the peak that corresponds to the smallest droplet size should correlate to the Kolmogorov length scale and the tail distribution should indicate a combination of coalescence and bypassing of flow from the main turbulent region (Håkansson *et al.*, 2009).

Håkansson explained the stages of droplet break-up in a valve homogeniser with respect to the distance away from the valve exit in terms of gap height multiples (Håkansson *et al.*, 2009). Within 20 – 40 gap heights, or approximately 20 – 40 μm after the gap, the turbulent intensity is at the highest producing the majority of the droplet deformation and break-up. Subsequent to this the turbulent intensity significantly reduces and droplet break-up ceases and coalescence becomes prevalent. These results are from both experimental and CFD (Håkansson *et al.*, 2009, Håkansson *et al.*, 2011), and correspond well to the droplet size distributions shown in this work.

At lower pressures the tail of the distribution is larger (Figure 3.9), this is because the flow is less turbulent and also the flow is more likely to by-pass the main region of turbulent dissipation (Innings and Trägårdh, 2007). On subsequent passes through the HPH statistically the larger droplets have more chance of travelling through the area of higher shear forces and breaking up. Thus, the average droplet size decreases and the distribution narrows with the increasing number of passes.

Simulating the flow in the valve homogeniser using computational fluid dynamics is relatively new, with the first results from a commercial CFD package being reported in 1997

to model the complete valve (Stevenson and Chen, 1997), however, it has been developed quickly to learn more thoroughly how the geometry creates droplet break-up and coalescence by modelling two phases and refining the current models to consider emulsifier adsorption types and rates (Casoli *et al.*, 2010, Håkansson *et al.*, 2009, Håkansson *et al.*, 2012a, Håkansson *et al.*, 2012b, Håkansson *et al.*, 2013). The technique has been useful for understanding the flow in the valve homogeniser by highlighting the main regions in the valve geometry that will cause droplet break-up and coalescence and indicating the turbulent sub-ranges that create droplet break-up (Håkansson *et al.*, 2009). The results from these CFD simulations agree with the hypothesises highlighted in this section of the chapter: the valve homogeniser creates droplet break-up from the turbulent jet at the exit of the valve gap. As the turbulent intensity of the jet decreases, and thus droplet deformation is reduced to below that creating droplet break-up, the flow is still chaotic and causes droplet collision and coalescence.

Currently, there has been minimal computational work completed on the Microfluidizer. The results in this section of the chapter has indicated that droplet break-up in the Microfluidizer is from turbulence in the impinging jets and that the extensional flow after the jets impinge creates more time for emulsifier adsorption. To further investigate the hypothesis that turbulence is responsible for droplet break-up in the Microfluidizer the fluid dynamics of the chamber were modelled.

3.3.2 Computational fluid dynamics of Microfluidizer chamber

In order to determine the turbulent length scales in the Microfluidizer a turbulence model was set up to simulate one phase (water) flow through the device. It is possible to develop two

phase flow models however one phase flow was selected as it will give a good indication to the turbulence present and location. The turbulence was modelled using a transient 2D k-ε turbulence model (details can be found in section 3.2.4). The results are shown in Figure 3.10 and Figure 3.11.

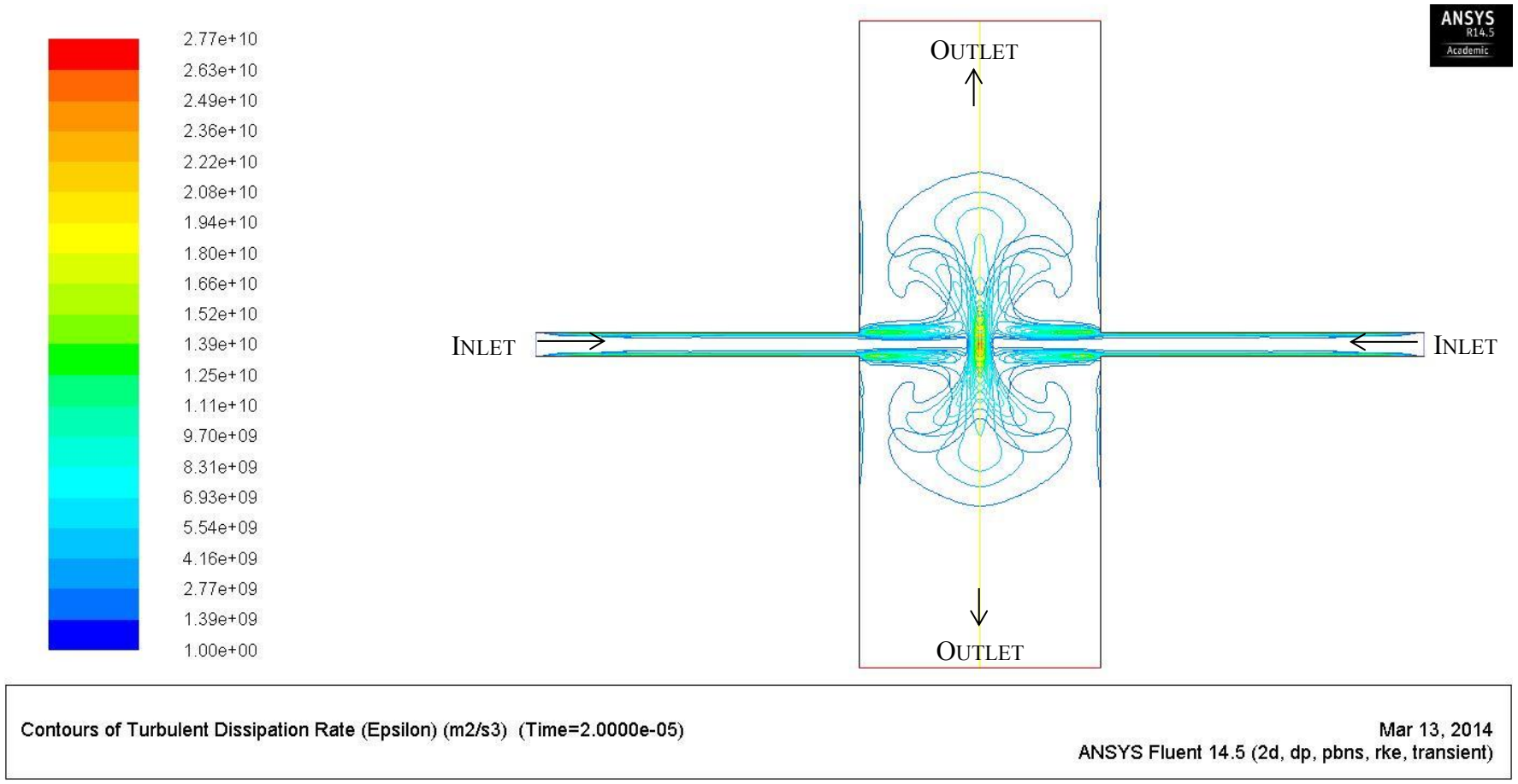

Figure 3.10: Contours of turbulent dissipation energy for a k-epsilon turbulence model with one phase (water) at 50 MPa. The arrows indicate average direction of flow.

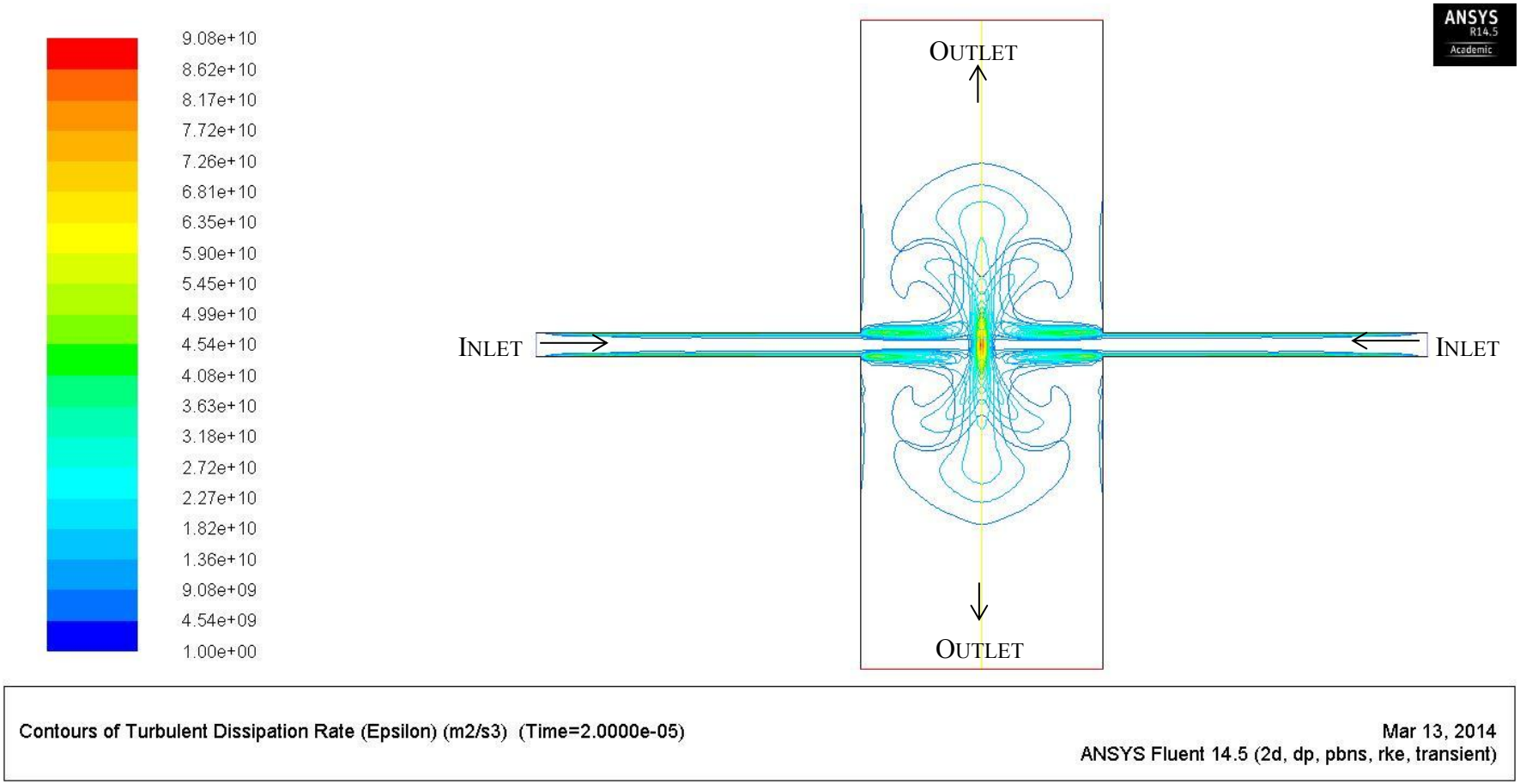

Figure 3.11: Contours of turbulent dissipation energy for a k-epsilon turbulence model with one phase (water) at 150 MPa. The arrows indicate average direction of flow.

Figure 3.10 and Figure 3.11 suggest that for a water continuous system (0.001 Pa.s) the jets will impinge and the centre of the impingement plane experiences the highest rate of energy dissipation. By observing the contour plots it can be seen that the maximum energy dissipation is higher at the higher pressure, thus suggesting that the energy dissipation distribution is both dependent on the geometry and the operating pressure.

It can be seen that as the flow enters the chamber, where the characteristic length increases from 75 μm at the inlet to 750 μm in the chamber, energy dissipates at the outer regions of the jets as the fluid shears the surrounding relatively stagnant areas of fluid. These regions of the jets experience lower energy dissipation and bypass the main region of energy dissipation where the jets impinge. It is therefore likely that this would result in a bi-modal distribution similar to those seen in Figure 3.8. This shearing with stagnant fluid has also been observed in the turbulent jet produced in the valve homogeniser (Innings and Trägårdh, 2007).

Further analyses of the simulation provides data on the peak and mean energy dissipations, these are presented in Table 3-3.

Table 3-3: Energy dissipation rates for different pressures in the Microfluidizer from the k-epsilon model in Fluent using water as the fluid

	Homogenising pressure	
	50 MPa	**150 MPa**
Jet flow rate (m^3/s)	2.03E-06	2.99E-06
Velocity of jet (m/s)*	459	676
Reynolds number of jet (at inlet)	34438	50687
Mean energy dissipation (m^2/s^3)***	1.05E+09	3.01E+09
Peak energy dissipation (m^2/s^3)***	3.02E+10	9.25E+10
Mean Kolmogorov length scale (nm)***	176	135
Minimum Kolmogorov length scale (nm)***	76	58

*this is calculated from the measured flowrate and dimensions of the inlet pipes, see Table 3-1 in Materials and Methods

** Assuming the jet is 75 μm; the diameter of the inlet

***Values obtained from the Fluent simulation

Table 3-4: Main peak heights from silicone oil in water emulsions presented in Figure 3.8 compared to the predicted Kolmogorov length scale from Table 3-3.

Homogenising pressure	**50 MPa**	**150 MPa**
Height of main peak from silicone oil in water emulsions from section 3.3.1	160 nm	140 nm
Mean* Kolmogorov length scale (predicted)	176 nm	135 nm

*Note that the two minimum and mean Kolmogorov length scales were calculated from the peak and mean energy dissipation values.

As expected, Table 3-3 in conjunction with the contour plots, shows that the energy dissipation is larger for the higher pressures and as such the flow is significantly more turbulent in the jet, with a Reynolds number that is 50% larger at the higher pressure.

It was calculated that the mean Kolmogorov length scales for 50 and 150 MPa are 176 nm and 135 nm respectively. Table 3-4 compares this length scale to the peak heights of the silicone oil in water emulsions produced in section 3.3.1. The peak heights were selected in order to account for the droplets that passed through the main region of energy dissipation, and ignore those that by-passed. It is evident that the peak heights and Kolmogorov length scales are similar. This reinforces the hypothesis that the primary mechanism for droplet break-up is inertial turbulence. Another flow type that is likely to be present, subsequent to when the jets impinge, is extensional flow. Since the turbulence is on the similar length scale to the droplet sizes being produced (Table 3-4) it is further suggested here that this extensional flow is unlikely to create droplet break-up however the presence of the flow type increases the time available for the emulsifier to stabilise the newly formed droplets.

The first few sections have considered the droplet break-up in simple oil in water emulsions, where the continuous phase is the viscosity of water. As the viscosity ratio of the emulsion, dispersed/continuous viscosity, is altered it is expected that this will change the rate of droplet deformation and break-up. Therefore the next step is to investigate the effect of changing the viscosity ratio on the droplet break-up mechanisms for both the high pressure devices.

3.3.3 Comparison of viscosity ratio on droplet size for both devices

It has been reported (Wooster *et al.*, 2008, Qian and McClements, 2011) that by decreasing the viscosity ratio (dispersed/continuous) of an emulsion, by increasing the viscosity of the aqueous phase, the droplet size of nanoemulsions reduces. This previous work has been carried out over a limited viscosity ratio and the effect of the added ingredients on the interfacial tension was not considered. In this study we have compared the effect of viscosity ratio on the droplet sizes produced from both the Microfluidizer and the HPH. The viscosity ratio has been varied from 0.1 to 100 by changing the aqueous phase viscosity by adding glycerol from 0 to 80% and by selecting silicone oils with viscosities of 10, 30, 50, 75 and 100 mPa s. Figure 3.12 and Table 3-5 show the droplet sizes produced from the Microfluidizer and valve homogeniser respectively for the three decades of viscosity ratio tested.

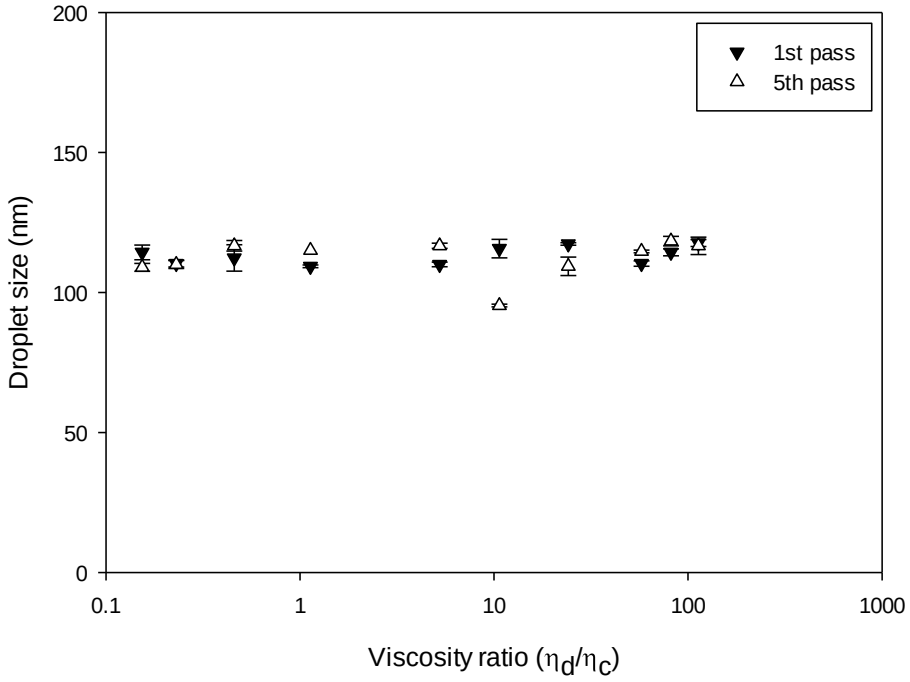

Figure 3.12: Graph showing the change in droplet size for silicone oil (variable viscosity) in water/glycerol (variable viscosity) emulsions with 3 wt.% Tween 20 at 150 MPa in the Microfluidizer

Table 3-5: Table showing the viscosity change and droplet size for silicone oil (variable viscosity) in water/glycerol (variable viscosity) emulsions with 3 wt.% Tween 20 at 150 MPa in the HPH

Continuous Phase viscosity (mPa s)	Dispersed phase viscosity (mPa s)	Viscosity ratio (dispersed / continuous)	1st pass d3,2 (nm)	5th pass d3,2 (nm)
0.00089	**0.10**	113	297 ± 15	156 ± 1
0.00089	**0.073**	81.7	271 ± 29	144 ± 2
0.00089	**0.051**	57.6	202 ± 32	130 ± 4
0.00089	**0.022**	24.2	169 ± 8	122 ± 1
0.00089	**0.0095**	10.7	152 ± 3	115 ± 1
0.0098	0.051	5.25	244 ± 17	135 ± 2
0.045	0.051	1.13	235 ± 4	136 ± 1
0.11	0.051	0.46	223 ± 5	129 ± 1
0.22	0.051	0.23	158 ± 2	117 ± 1
0.33	0.051	0.15	153 ± 6	115 ± 1

The results in Figure 3.12 show that for the three decades of viscosity ratio tested there is minimal droplet size difference, ~110 ± 5nm, thus indicating that the Microfluidizer is independent of viscosity ratio. This would suggest that the time to deform and break the droplets for these viscosities is significantly shorter than the residence time for the majority of

the energy to dissipate. As the viscosity ratio is reduced to between 5 and 0.1 the turbulent break-up mechanism would be expected to change from turbulent inertial to turbulent viscous (Walstra, 2005). Within the turbulent viscous flow the droplet break-up mechanism is the same as that of simple shear flow and the smallest droplet size is produced at viscosity ratio 1. This minimum is not observed here and therefore this indicates that subsequent to droplet break-up there is extensional flow. If extensional flow is present the dependency on viscosity ratio is minimised since the flow type provides more time for emulsifier adsorption (Stegeman, 2002, Stegeman *et al.*, 2002). Within the Microfluidizer this is possible after the jets impinge and exit the chamber.

In contrast to these results the HPH shows a strong dependence of droplet size on viscosity ratio demonstrating a 150 nm difference after the first pass in the emulsions produced between viscosity ratio 100 and 0.1 (Table 3-5). This is due to the time taken to deform the droplets being longer for the higher ratio and therefore the time required to break-up a droplet will increase. If the time to deform the droplets and create droplet break-up is longer than the time for the majority of the energy to dissipate then the droplet size will be dependent on the viscosity of the dispersed phase.

It is also worth noting that between viscosity ratios 10 and 5 there is a rise in droplet size. This highlights that, although it is common to compare droplet size with viscosity ratio, changing the viscosity of both phases changes different emulsion formation mechanisms. Increasing the continuous phase viscosity decreases the chance of re-coalescence in flow. Whereas, reducing the dispersed phase viscosity reduces the time required to deform and break the droplet initially.

In practice, to reduce the viscosity ratio of the system the continuous phase viscosity was increased. As an effect of increasing the viscosity the rate of in-processing coalescence was reduced. Analysis of the droplet size distributions produced will indicate how the droplet break-up mechanism is changed by reducing the viscosity ratio (Figure 3.13 & Figure 3.14) and if the increase in continuous phase viscosity does reduce the second peak at around 700 nm.

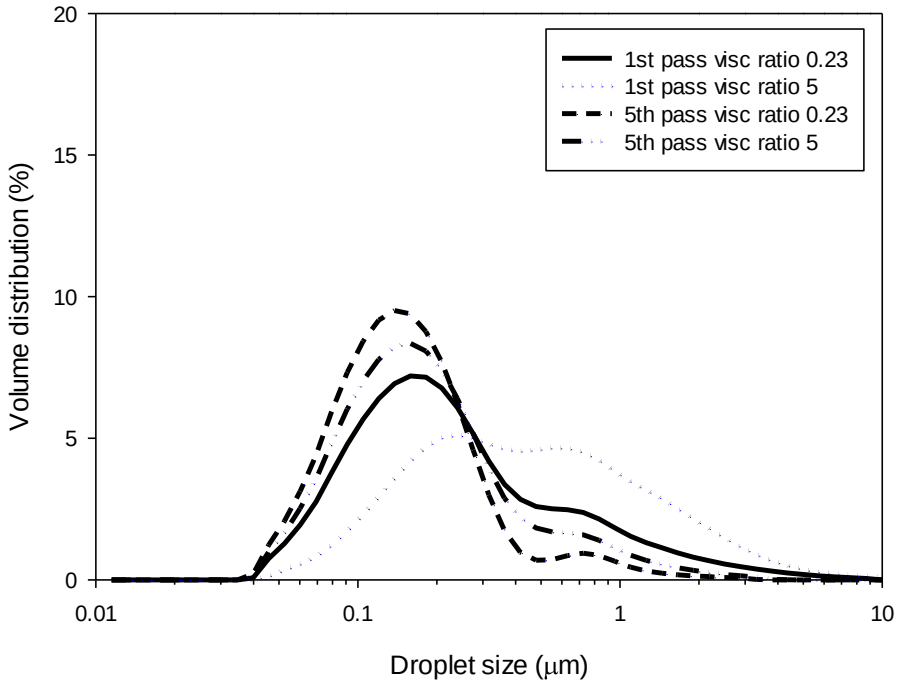

Figure 3.13: Droplet size distributions for two different viscosity ratios of silicone oil (0.05 Pa s) in water/glycerol emulsions with 3 wt.% Tween 20 for the first and fifth pass in the valve homogeniser for an operating pressure of 150 MPa

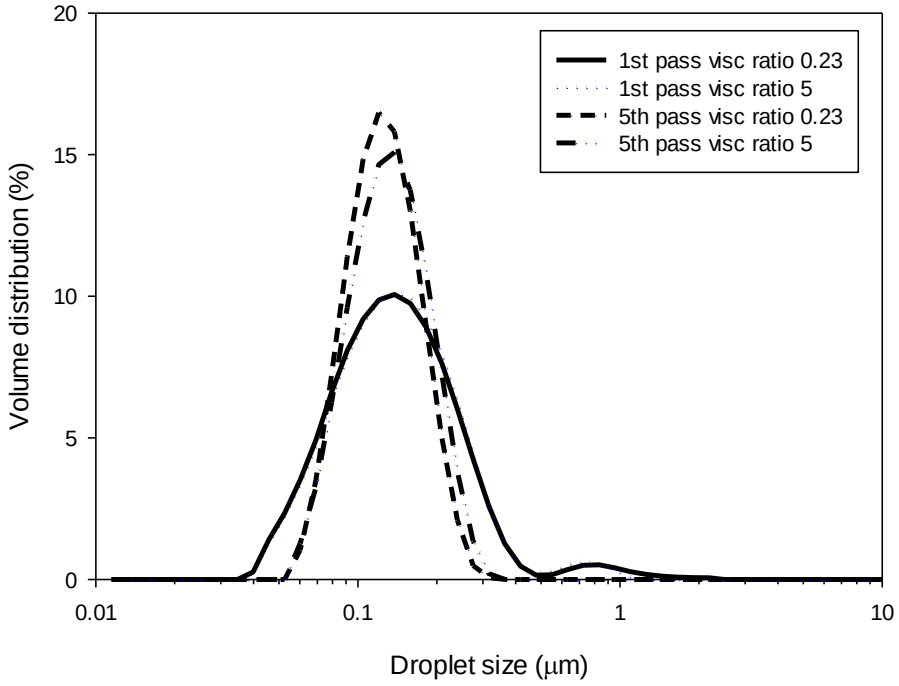

Figure 3.14: Droplet size distributions for two different viscosity ratios of silicone oil (0.05 Pa s) in water/glycerol emulsions with 3 wt.% Tween 20 for the first and fifth pass in the Microfluidizer for an operating pressure of 150 MPa

For both the first and fifth passes in the HPH the droplet size distributions show a bi-modal distribution with the second peak (at 700 nm) from each showing a high volume distribution at the higher viscosity ratio. As previously discussed, this can indicate that there is by-passing of flow around the main turbulent dissipation region or there is in-processing coalescence. Since there is still a difference in droplet size viewed after the fifth pass this could indicate presence of coalescence which is lower for a highly viscous continuous phase (or lower viscosity ratio). These results continue to strengthen the argument that droplet break-up in the valve homogeniser is turbulent and by changing the viscosity ratio of the emulsions either the time required for droplet deformation and break-up has been changed or the time for emulsifier adsorption is different.

The droplet size distributions produced from the Microfluidizer (Figure 3.14) reinforce the hypothesis that droplet size has no dependence on viscosity ratio and the droplet break-up mechanism is the same. These results further develop the hypothesis explained in the previous sections: that the deformation forces created from the jets impinging and the subsequent extensional flow still provides a significantly longer length of time than is required to deform the droplets, break them and then allow emulsifier adsorption.

3.3.4 Effect of emulsifier type on nanoemulsion formation

Three types of emulsifiers: non-ionic emulsifier (Tween 20), low molecular weight anionic emulsifier (SDS) and protein (sodium caseinate) were used at 3 wt.% to produce a series of oil-in-water emulsions with 10 wt.% silicone oil (viscosity 0.05 Pa s). The emulsions were produced on both high pressure devices at 50 and 150 MPa.

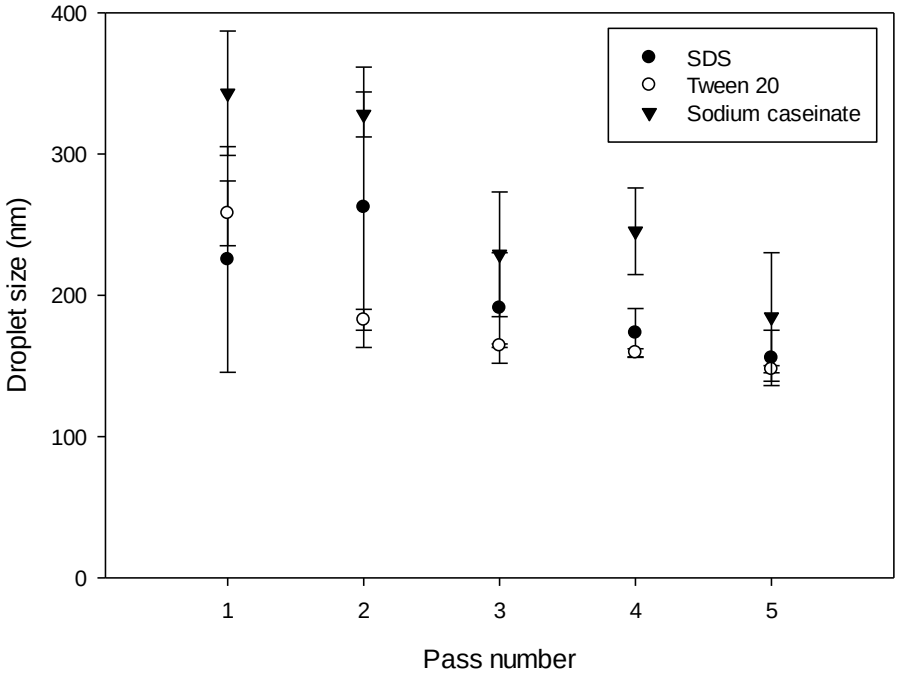

Figure 3.15: Surface weighted mean droplet sizes for 10 wt.% silicone oil (0.05 Pa s) in water emulsions for 3wt.% of the continuous phase in a HPH for the following emulsifiers: SDS, Tween 20, sodium caseinate, at 50 MPa

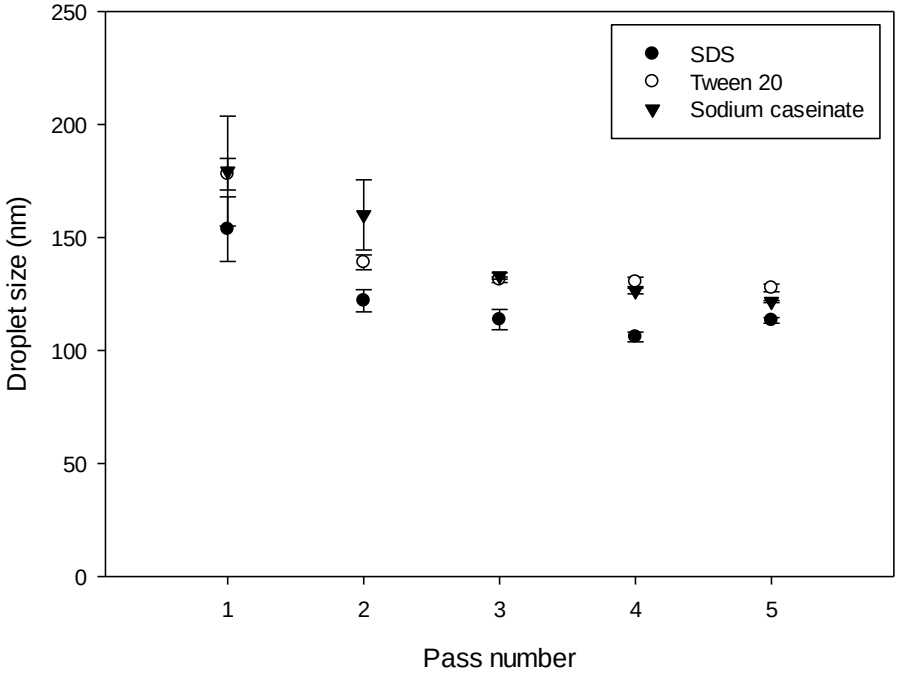

Figure 3.16: Surface weighted mean droplet sizes for 10 wt.% silicone oil (0.05 Pa s) in water emulsions for 3wt.% of the continuous phase in a HPH for the following emulsifiers: SDS, Tween 20, sodium caseinate, at 150 MPa

Figure 3.15 and Figure 3.16 show the droplet sizes produced at 50 and 150 MPa in the HPH. At the lower homogenising pressure the influence of emulsifier type on droplet size is insignificant. However, at the higher pressure the emulsions stabilised with SDS show smaller droplet sizes than Tween 20 and sodium caseinate. SDS is a small anionic emulsifier which when adsorbed onto the interface creates an electrostatic repulsive force between droplets thus reducing the chance of coalescence under the flow conditions (Tcholakova *et al.*, 2004). Therefore this suggests that the use of SDS has reduced coalescence in the HPH at 150 MPa. However, at 50 MPa there is no observed difference in droplet size with emulsifier type thus suggesting there is low coalescence at this pressure. This agrees with Jafari *et al.* (2007a) who reported coalescence to be low below 60 MPa.

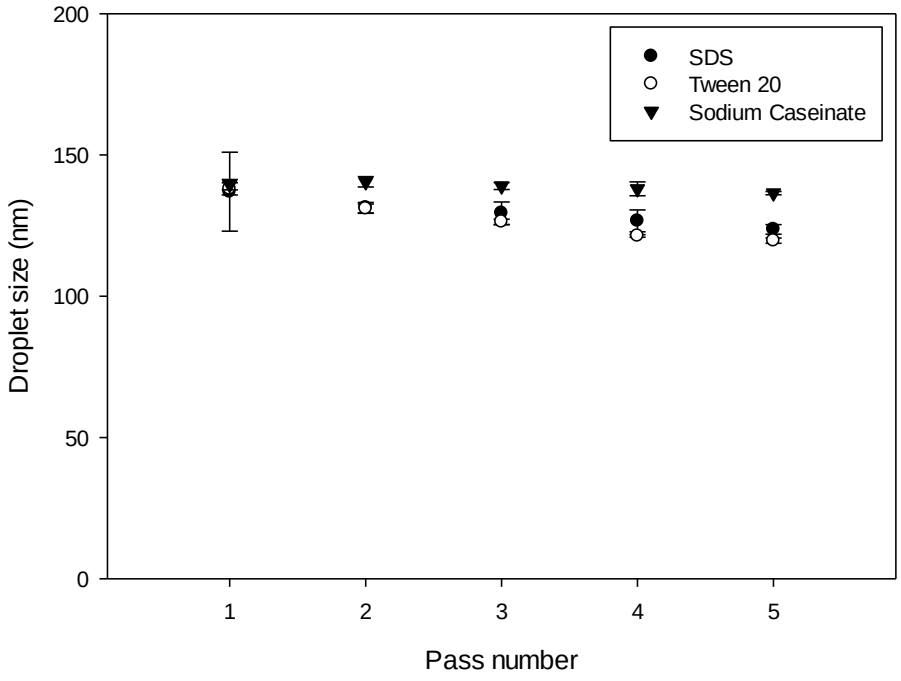

Figure 3.17: Surface weighted mean droplet sizes for 10 wt.% silicone oil (0.05 Pa s) in water emulsions for 3wt.% of the continuous phase in a Microfluidizer for the following emulsifiers: SDS, Tween 20, sodium caseinate, at 50 MPa

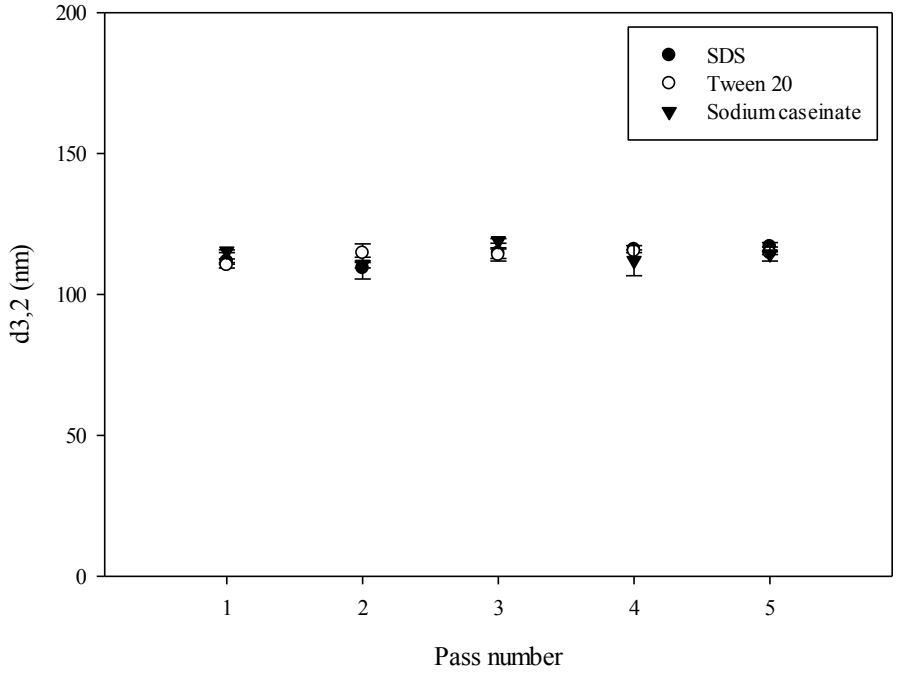

Figure 3.18: Surface weighted mean droplet sizes for 10 wt.% silicone oil (0.05 Pa s) in water emulsions for 3wt.% of the continuous phase in a Microfluidizer for the following emulsifiers: SDS, Tween 20, sodium caseinate, at 150 MPa

For the lower operating pressure in the Microfluidizer (Figure 3.17) the emulsions stabilised with sodium caseinate produced larger droplet sizes, whereas at the higher pressure (Figure 3.18) the Microfluidizer produced a droplet size of 115 ± 5 nm for all three emulsifiers indicating no dependence on emulsifier type. Sodium caseinate is a protein and is the largest emulsifier tested, it is thought that larger molecules take longer to adsorb to the interface and stabilise a droplet (Courthaudon *et al.*, 1991). Larger droplets will be produced when the time for emulsifier adsorption is not long enough to coat and stabilise the droplets before they coalesce. In the Microfluidizer after the jets impinge (and the majority of the turbulent energy has dissipated) the flow is extensional, and at a higher pressure the flow will be extensional for a greater distance, allowing more time for emulsifier adsorption. Therefore at the lower pressure the emulsifier adsorption time is reduced and for the largest emulsifier

(longest emulsifier adsorption time) the time is not long enough to allow emulsifier adsorption and stabilisation before the droplets coalesce. The droplet size distributions of emulsions produced at 150 MPa from both devices are shown in Figure 3.19 to Figure 3.22.

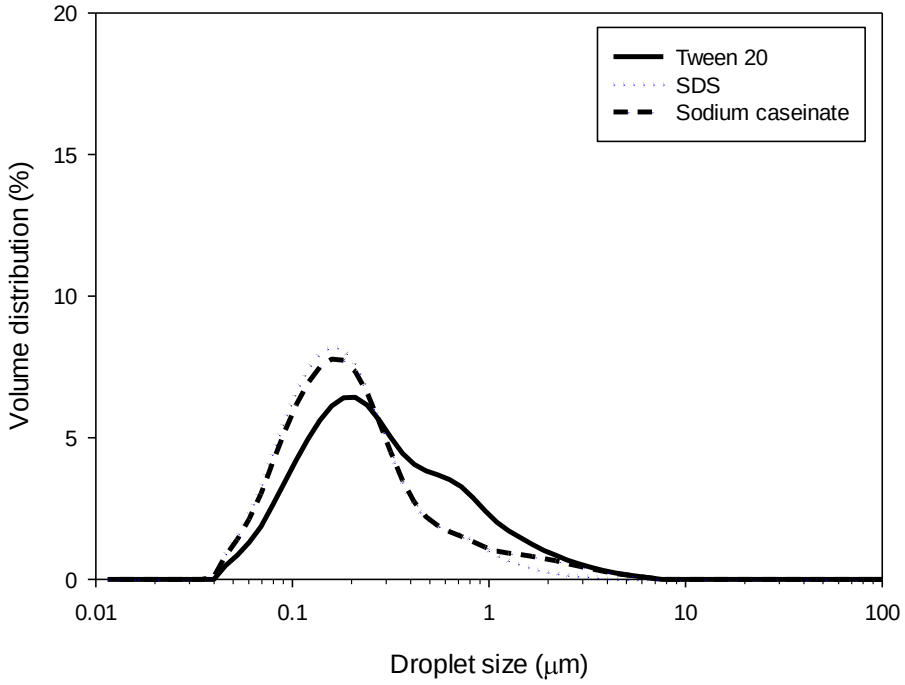

Figure 3.19: Droplet size distribution for silicone oil (0.05 Pa s) in water emulsions with 3 wt.% emulsifier, Tween 20, SDS and sodium caseinate, for the first pass in the valve homogeniser at an operating pressure of 150 MPa

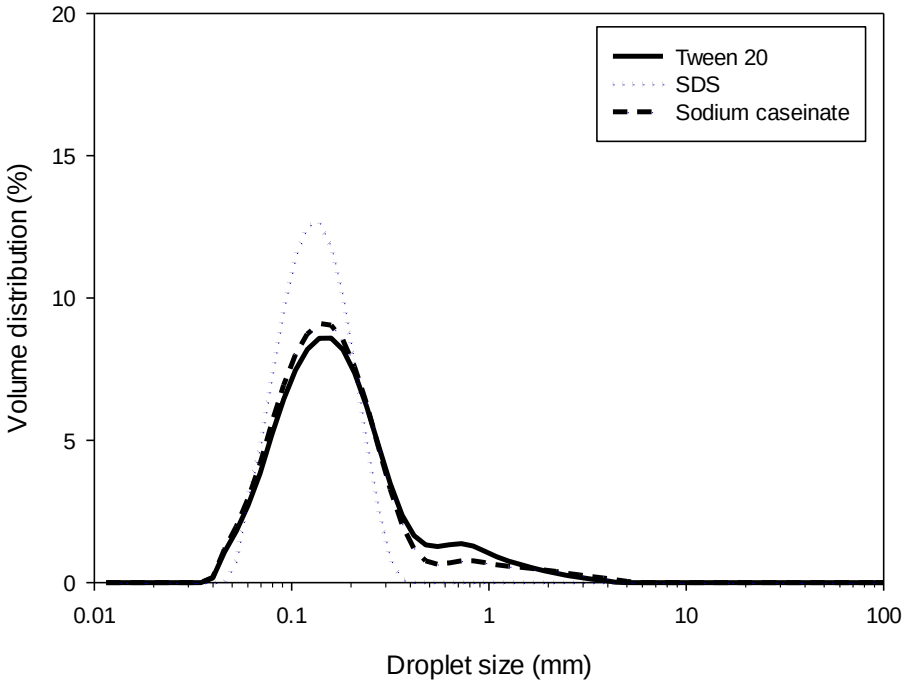

Figure 3.20: Droplet size distribution for silicone oil (0.05 Pa s) in water emulsions with 3 wt.% emulsifier, Tween 20, SDS and sodium caseinate, for the fifth pass in the valve homogeniser at an operating pressure of 150 MPa

For the HPH the droplet size distributions are different with emulsifier type. Figure 3.19 shows that SDS forms a relatively narrow distribution after one pass, and after 5 passes the distribution is mono-modal with a peak at 110 nm (Figure 3.20), the same average droplet size as the Microfluidizer. SDS is anionic, producing an electrostatic repulsive force between droplets which it stabilizes (Tcholakova *et al.*, 2004). Since this force is not present when using a non-ionic emulsifier and is more evident with a protein emulsifier which has regions of positive and negatives charges, the mono-modal peak can be attributed to the reduction in coalescence from this repulsive force.

Figure 3.19 also shows that after the first pass in the HPH Tween 20 has a larger droplet size distribution than sodium caseinate. If a similar droplet break-up mechanism is assumed,

although this may not be strictly true, this indicates a larger proportion of coalescence in the emulsion from lower Tween 20 adsorption. This is not expected as previously it has been reported that the size of an emulsion produced from a HPH is dependent on the time for adsorption of the emulsifier (Donsì *et al.*, 2011b). Since sodium caseinate has a slower adsorption rate compared to Tween 20 the reverse would be expected (Courthaudon *et al.*, 1991). These results can be explained by considering the type of the emulsifier. As the protein is larger than the Tween 20, despite it taking longer to adsorb to the interface once it is coating the droplet it gives more steric hindrance and also electrostatic stabilisation from coalescence. Hence in the turbulent flow as droplets come together the protein slows film drainage and coalescence. Since Tween 20 does not have this mechanism the hypothesis is that it is more likely to be removed from the interface and the droplets will coalesce. Since the droplet break-up and flow theory, developed in previous sections, for the valve homogeniser highlights that coalescence is prevalent in the system. These results further reinforce this theory, and highlight that selection of emulsifier type can reduce coalescence in the system and produce the emulsions more efficiently.

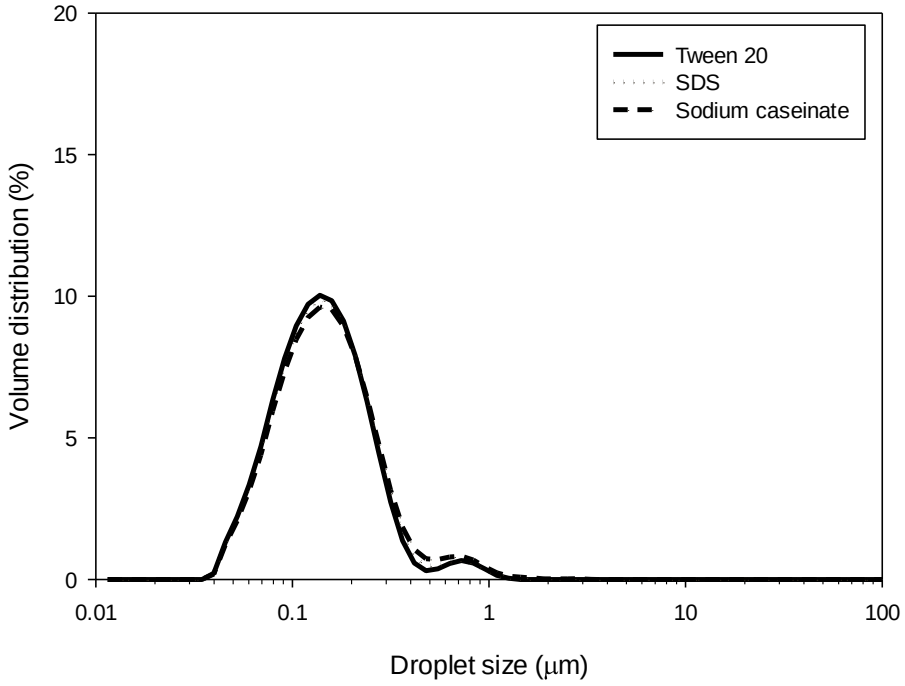

Figure 3.21: Droplet size distribution for silicone oil (0.05 Pa s) in water emulsions with 3 wt.% emulsifier, Tween 20, SDS and sodium caseinate, for the first pass in the Microfluidizer at an operating pressure of 150 MPa

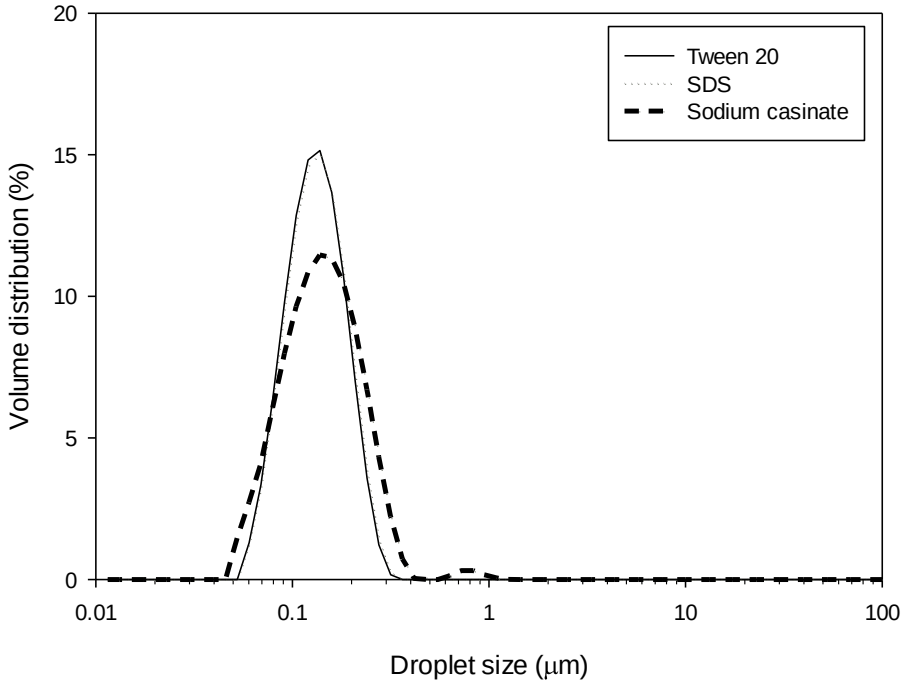

Figure 3.22: Droplet size distribution for silicone oil (0.05 Pa s) in water emulsions with 3 wt.% emulsifier, Tween 20, SDS and sodium caseinate, for the fifth pass in the Microfluidizer at an operating pressure of 150 MPa

The Microfluidizer produces very similar droplet sizes and droplet size distributions (Figure 3.21 & Figure 3.22) after the first pass and the fifth pass for all three emulsifiers. This data suggests that the rate of adsorption and subsequent stabilisation of the interface for these process conditions is not the limiting step in this device. It was observed with sodium caseinate that even after 5 passes a second peak was present at 800 nm. This could be due to protein aggregates and has been seen before with other proteins in high pressure homogenisation (Floury *et al.*, 2000).

The results for the Microfluidizer at 50 and 150 MPa with different emulsifiers have extended the theory of droplet break-up in the device. At the lowest pressure (50 MPa) using the emulsifier with the largest adsorption time (sodium caseinate) a larger droplet size was produced, indicating a dependence on emulsifier type at lower pressures. This is particularly interesting as it indicates that the time required to deform and break a droplet can be reduced to be similar to the emulsifier adsorption time. Since this is possible this is further evidence that the flow type causing break-up is turbulent.

It was shown in sections 3.3.3 and 3.3.4 that the valve homogeniser was dependent on the dispersed phase viscosity and emulsifier type respectively, however, the Microfluidizer was independent of both at 150 MPa but produced a larger droplet size with emulsions stabilised with sodium caseinate at 50 MPa. The aim of this work was to determine if by changing the deformation rate (dispersed phase viscosity) the emulsifier selection may become more important at 150 MPa for the Microfluidizer.

3.4 Chapter conclusions

It has been observed that both devices produce similar final droplet sizes, approximately 100 – 150 nm for pressures 150 MPa – 50 MPa, however the valve homogeniser requires several passes to get to the final droplet size. The differences in droplet size and droplet size distributions are explained by the geometry of the two devices. In the valve homogeniser extensional flow is present in the valve gap followed by a turbulent jet at the exit of the valve, after the peak energy dissipation rate the rate of droplet deformation slows and coalescence is prevalent. This is evident in the droplet size distributions. In contrast the Microfluidizer produces extensional flow from the impinging jet after the main turbulent region leading to less coalescence and longer emulsifier adsorption time. In addition, the impinging jet creates a tight distribution of deformation stresses producing a narrow droplet size distribution. By examining the turbulent forces using CFD it was shown to be likely that the droplet break-up in water continuous systems is due to the turbulent inertial sub-range forces.

Investigations into the influence of viscosity ratio on droplet size showed that the Microfluidizer was independent of viscosity changes (viscosity ratio of between 0.1 and 100 at 150 MPa). The droplet size produced was 115 ± 10 nm for all viscosity ratios. In contrast the HPH showed higher dependency on viscosity ratios. At the exit of the valve gap the energy dissipates via turbulence creating droplet break-up. As the turbulent intensity decreases in distance after the gap the droplet deformation forces are lower and coalescence occurs. For lower viscosity ratios the continuous phase is more viscous and as a consequence reduces coalescence more. However, for the higher viscosity ratios, where the dispersed phase viscosity was changed the droplet size is larger due to greater resistance to deformation as the

viscosity of the dispersed phase increases. In summary, the droplet break-up in the HPH is dependent on both the dispersed and continuous phase viscosities.

There is no difference in emulsifier effect in the Microfluidizer for the highest pressure (with SDS, Tween 20 and sodium caseinate) however in the HPH with SDS the droplet size reaches the limiting value after 2 passes while with Tween 20 and sodium caseinate this occurs after 5 passes. Thus some coalescence still occurs in the HPH but SDS eliminates this as a consequence of the rapid adsorption onto the interface and the induced surface charge. This is evident at both pressures.

To summarise, it has been shown that the influence of the impinging jets within the Microfluidizer creates larger deformation stresses to cause more efficient droplet break-up, followed by extensional flow after impingement which reduces coalescence. Thus, compared to the valve homogeniser, the Microfluidizer is more resilient to: viscosity ratio changes and different emulsifier types. In contrast, the valve homogeniser is susceptible to coalescence after the main turbulent region when the stresses are not high enough to cause droplet break-up, the flow is still chaotic and forces to droplets to re-collide and coalesce. Thus the valve homogeniser produces wider droplet size distributions that are influenced by the viscosity ratio processed and the emulsifier type selected. This coalescence can be reduced by increasing the continuous phase viscosity.

CHAPTER 4: PRODUCTION OF WATER IN OIL (W/O) NANOEMULSIONS USING HIGH PRESSURE

4.1 Introduction

In the previous chapter, the emulsification performance of the two high pressure devices was investigated for water continuous emulsions; Microfluidizer compared to the HPH. It was identified that the droplet break-up of the simple O/W emulsions was turbulent inertial for both devices. The geometry differences promoted more efficient droplet break-up in the Microfluidizer, whereas, coalescence was prevalent in the HPH. It was found that by increasing the continuous phase viscosity, coalescence was reduced and the efficiency of the HPH increased.

This chapter will develop on these learnings and investigate the performance of the machines when the phases are reversed; in water-in-oil emulsions. The viscosity ratio, 0.04, (dispersed / continuous viscosity) is significantly lower than in the previous chapter and this is likely to produce different droplet break-up mechanisms. Formulation (emulsifier concentration and salt addition) and processing variables (passes, pressures and viscosity ratio) are investigated for the production of W/O nanoemulsions.

4.2 Material and methods

4.2.1 Materials

The oil soluble emulsifier, polyglycerol polyricinoleate (PGPR), was kindly provided by Palsgaard, Denmark (PGPR 4150). High oleic sunflower oil was supplied by PepsiCo Intl.

Calcium chloride (C8106), castor oil (259853) and glycerol (G7757) were purchased from Sigma Aldrich (UK). Double distilled de-ionised water was used for the preparation of all solutions.

4.2.2 Emulsion preparation

Water-in-oil emulsions were produced by homogenising 10 wt.% aqueous phase (with 0 – 10 wt.% $CaCl_2$ and 0 – 80 wt.% glycerol) with 90 wt.% sunflower oil (with 0.1-9 wt.% PGPR and 0 – 75 wt.% castor oil). The aqueous and oil phase were weighed out separately and stirred with a magnetic flea until all materials were dissolved and homogenous. The low weight per cent of water was selected to minimise effects of droplet collision and for the majority of experiments 9 wt.% PGPR was used to ensure that the emulsifier concentration was in excess to minimise coalescence.

Initially a coarse emulsion was prepared by using a Silverson mixer at 7500 rpm for 120 s at room temperature. Nanoemulsions were produced by passing the coarse emulsion through an air-driven Microfluidizer fitted with a cooling tube submerged in equal proportions of ice and water (M110S fitted with a Y-type chamber, Microfluidics, Newton, MA, USA) or a high pressure valve homogeniser (NS1001L PANDA, GEA Niro Soavi, Italy) for up to 5 passes for 50 & 100 MPa. See Table 4-1 for flowrates and inlet jet velocities for the Microfluidizer when sunflower oil only.

For more information on the high pressure valve homogeniser and the Microfluidizer see sections 3.2.2.1 and 3.2.2.2, respectively.

Table 4-1: Average flowrates in the Microfluidizer for sunflower oil at pressures 50 and 100 MPa measured experimentally.

Pressure (MPa)	Average flowrate (m^3/s)	Velocity of inlet (m/s)
50	3.97×10^{-6}	271
100	5.36×10^{-6}	494

4.2.3 Emulsion characterisation

4.2.3.1 Droplet size measurements by dynamic light scattering (DLS)

The droplet size distribution and droplet size average, z_{av}, was measured using a dynamic light scattering technique (HPPS 5001, Malvern, UK) at a scattering angle of 173° using a 633 nm laser with each measurement being the average of at least 11 runs with an initial equilibration time of 30 seconds. The samples were measured at 25 °C.

Before each measurement the emulsion sample was mixed by rotating the container around the horizontal axis 10 times to produce a homogenous distribution of droplets within the sample. Then 0.25 ml of emulsion sample was diluted in a sample pot with 25 ml of the continuous phase oil (in most cases this was sunflower oil). This sample pot was again rotated around the horizontal axis 10 times to disperse the particles within the sunflower oil. This dilution gives a scattering intensity of less than 500 cps (~0.001 wt.% of dispersed phase) to avoid effects of multiple scattering. This sample was then pipetted into a disposable borosilicate glass cuvette up to a height of between 1 cm and 1.5 cm and measured immediately. During handling of the cuvette it is important to only touch the top frosted edges to prevent transfer of oils from fingertips distorting measurements.

The refractive indices of the materials were measured using a Rudolph research refractometer J357 (New Jersey, USA).

4.2.3.2 Interfacial tension measurements

Interfacial tensions were measured using a K100 Tensiometer (Kruss, Germany) using the Wilhelmy plate method which is schematically shown in Figure 4.1.

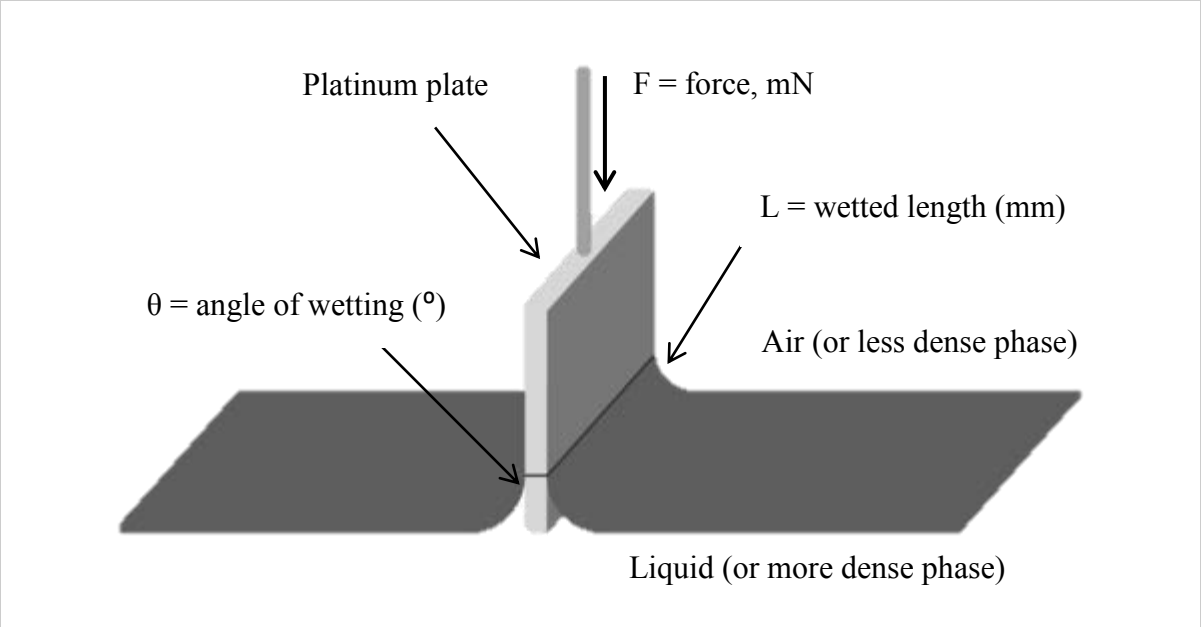

Figure 4.1: Schematic illustration of the Wilhelmy plate method for measuring the interfacial tension between two phases (Kruss, 2011).

As the plate is submerged into the less dense phase (Figure 4.1) a force (F) acts on the plate (measured by the tensiometer) and this is a function of both the wetting angle (θ) and the length (L) the plate is wetted. If the wetting angle can be reduced to 0°, $\cos(0) = 1$, then the interfacial tension (σ) can be calculated. Platinum plates are used because they are known to reduce the wetting angle to 0°.

$$\sigma = \frac{F}{LCos(\theta)}$$ **Equation 4-1**

To measure the interfacial tension of two liquids, the less dense liquid must be pipetted onto the more dense liquid being careful not to disturb the interface between the materials. The force is then measured over time to allow the interfacial tension to reach equilibrium. The measurements used an abraded platinum plate (height 10 mm, width 19.9 mm and thickness 0.2mm).

Interfacial tension results are sensitive to contamination therefore the cleaning protocol was strict to ensure no contamination from previous measurements. The glassware was thoroughly cleaned and dried, and the plate was cleaned and then heated. In preparation for measurements, the aqueous (higher density) and oil phases (lower density) were prepared separately. Initially, the plate is positioned at the aqueous phase interface and the balance which measures the force is locked. Then the oil phase is carefully pipetted on top of the aqueous phase surface. The balance is then unlocked and lowered to zero contact angle with the plate. The values for interfacial tension are then calculated using the Kruss software.

All interfacial tension measurements were performed in triplicate and at an ambient temperature of 25 ºC.

4.2.3.3 Viscosity measurements

Viscosity measurements of the aqueous and oil phases were performed using a dynamic shear rheometer with cup and vane geometry (cup diameter 25 mm, with vane width 23 mm and

clearance of 10 mm) in Bohlin Gemini Nano Rheometer (Malvern, UK), and viscosities were taken at 100 s^{-1}. All measurements were performed at 25 °C.

4.3 Results and discussion

4.3.1 Comparison of high pressure devices for effect of PGPR concentration

The influence of PGPR concentration was tested by making a series of water-in-oil emulsions with between 0.1 – 9 wt.% PGPR in the oil phase, and with 2 wt.% calcium chloride dissolved in the aqueous phase. Calcium chloride was used because it has been shown to reduce the droplet size with PGPR (Márquez *et al.*, 2010, Pawlik *et al.*, 2010). The effect of emulsifier concentration on droplet size was measured for both devices (Figure 4.2).

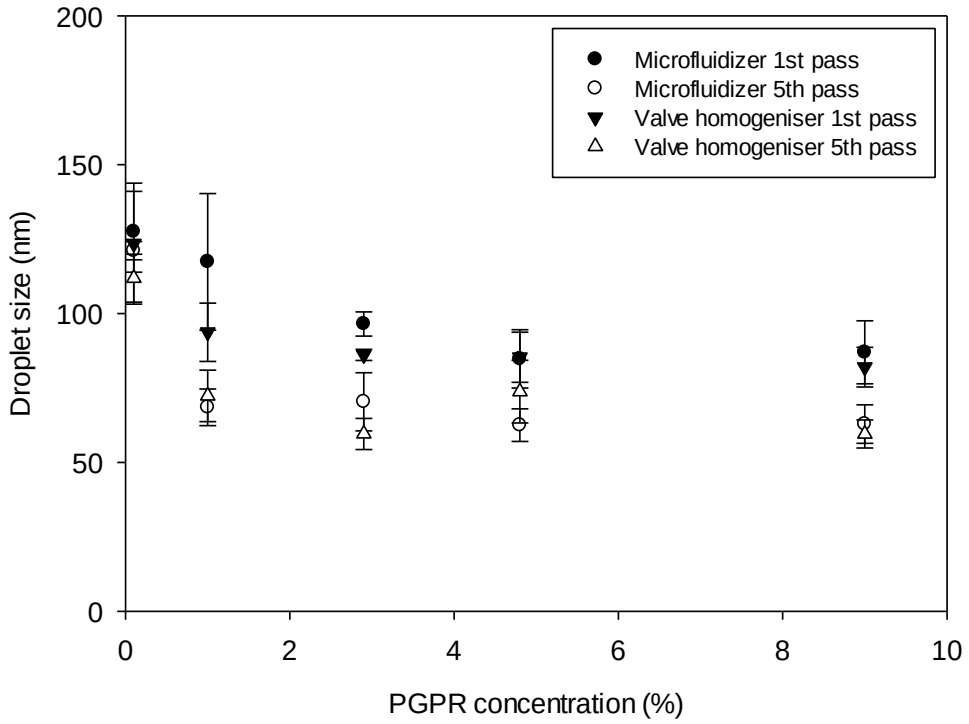

Figure 4.2: Effect of PGPR concentration on droplet size after 1st and 5th pass for 10 wt.% water dispersed phase (with 2 wt.% calcium chloride in the aqueous phase) in sunflower oil in the valve homogeniser and the Microfluidizer 50 MPa.

Figure 4.2 shows that by increasing the concentration of PGPR the droplet size of the emulsion decreases. This demonstrates the dynamic equilibrium in emulsification between droplet break-up and coalescence (Niknafs *et al.*, 2011); at low concentrations of PGPR there is not enough emulsifier to rapidly coat and stabilise newly formed droplets and therefore coalescence occurs. After one pass the difference in droplet size as a function of emulsifier concentration is more pronounced than after five passes. This indicates that at lower emulsifier concentrations the emulsifier requires several passes to completely adsorb to the interface of droplets. The minimum droplet size is seen at 9 wt.% PGPR after 5 passes. It is likely that at 1% PGPR there is enough emulsifier to cover and stabilise the droplets,

however, as the concentration of PGPR is increased further, the slight decrease in droplet size is due to reduced interfacial tension during droplet deformation (Feigl *et al.*, 2007).

As can be seen from Figure 4.2 there is no difference in homogenising performance between the two devices. This is in contrast to previous work with oil-in-water nanoemulsions (Lee and Norton, 2013, Lee *et al.*, 2013), where it was observed that the Microfluidizer produced smaller droplets than the HPH and the final droplet size was obtained after the first pass. This was attributed to the impinging jets creating uniform high shear in a timescale that allows a single pass to fully break-up the droplets (Qian and McClements, 2011, Lee and Norton, 2013). To further investigate this effect, the emulsions produced from different passes and pressures from both devices were compared.

4.3.2 Comparison of high pressure devices for effect of pass number and pressures

In order to determine the effect of pressure and passes on the formation of W/O emulsions a series of coarse emulsions were made with 10 wt.% water containing 2 wt.% calcium chloride in the aqueous phase and 9 wt.% PGPR in the oil continuous phase. The excess emulsifier concentration was selected to minimise coalescence in flow. These emulsions were passed up to five times through the high-pressure devices at 50 and 100 MPa (Figure 4.3 & Figure 4.4).

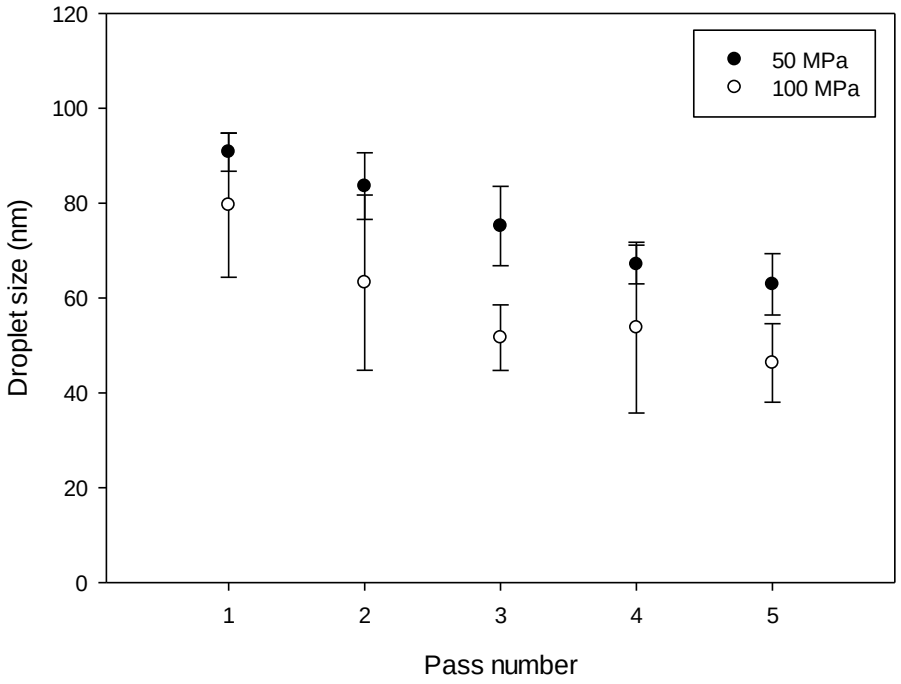

Figure 4.3: Effect of pass number on the emulsion droplet size for 10 wt.% water dispersed phase (with 2 wt.% calcium chloride in the aqueous phase) in sunflower oil with 9 wt.% PGPR in the Microfluidizer at 50 and 100 MPa.

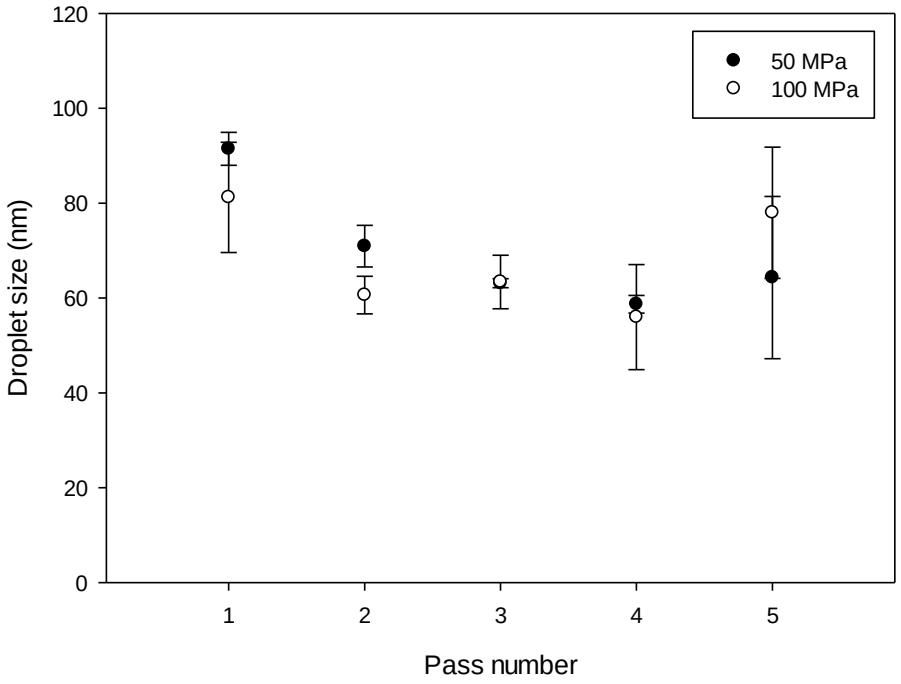

Figure 4.4: Effect of pass number on the emulsion droplet size for 10 wt.% water dispersed phase (with 2 wt.% calcium chloride in the aqueous phase) in sunflower oil with 9 wt.% PGPR in the Valve homogeniser at 50 and 100 MPa.

It can be seen from Figure 4.3 & Figure 4.4 that the homogenising efficiency of both devices is similar. With both producing 100 nm emulsions after the first pass and after five passes the emulsion droplet size has reduced to 60 nm for both pressures. This is in contrast to the work done on the Microfluidizer with O/W emulsions where it was shown that the minimum droplet size of ~110 nm was observed after the first pass and then subsequent passes narrowed the distribution around 110 nm (Qian and McClements, 2011, Lee and Norton, 2013, Lee *et al.*, 2013). To understand the difference the continuous phase viscosities of each emulsion need to be considered.

In the oil continuous emulsion the continuous phase viscosity is higher resulting in a higher energy dissipation rate (Vankova *et al.*, 2007a) but as a consequence of the higher viscosity the majority of the energy dissipates as viscous stresses rather than velocity fluctuations (i.e. the Kolmogorov length scale is significantly larger than the droplets being produced). This flow type is turbulent viscous. There have been few studies on turbulent viscous droplet break-up, however, it is known that whilst generally the flow type produces a faster energy dissipation rate it also requires a higher residence time (or more passes through the device) in the intense zone of energy dissipation to reduce the droplet size to the final droplet size (Vankova *et al.*, 2007a). These results (Figure 4.3 & Figure 4.4) further evidences turbulent viscous flow since the droplet size continues to decrease every time it is passed through the device.

Since turbulent viscous flow is suspected, the Kolmogorov length scale should be estimated. Table 4-2 shows this estimate.

Table 4-2: Energy dissipation rates for different pressures in the Microfluidizer from the k-epsilon model in Fluent using water as the fluid

	Homogenising pressure 100 MPa
Jet flow rate (m^3/s)	5.36E-06
Velocity of jet (m/s)*	494
Maximum energy dissipation (m^2/s^3)**	3.32E+12
Minimum Kolmogorov length scale (nm)	752

*this is calculated from the measured flowrate and dimensions of the inlet pipes, see Table 4-1 in Materials and Methods

**Values obtained from a Fluent simulation not fully published within this thesis

The minimum Kolmogorov length scale is 752 nm. This is 10 times larger than the droplet size obtained using the high pressure device, thus further indicating droplet break-up within turbulent viscous regime, i.e. break-up from the shearing forces within the turbulent eddies.

It was seen in the previous chapter, where the water continuous emulsions were broken up with turbulent inertial forces, the Microfluidizer produced smaller droplet sizes and distributions compared to the valve homogeniser. This was attributed to the intense deformation stresses as the jets impinge followed by the extensional flow which allows for longer emulsifier adsorption time. The results shown here do not show a difference between the Microfluidizer and valve homogeniser, this suggests that there is little or no affect from

the impinging jets indicating that the majority of energy dissipates before they impinge. Since energy dissipates faster at higher viscosities, this is likely.

The effect of increasing the pressure from 50 to 100 MPa is shown in Figure 4.3 & Figure 4.4, as expected there is a decrease in droplet size for both devices as the higher pressure energy input creates larger shearing stresses. However it can be seen for the HPH there is an increase in droplet size after 5 passes. The HPH used in this work had no temperature control during homogenisation, as a result the emulsion temperature after five passes was approximately 30^0C higher than the starting temperature, leading to an increased rate of coalescence or Ostwald ripening. Coalescence can be checked by comparing the overall droplet size distributions (Figure 4.5).

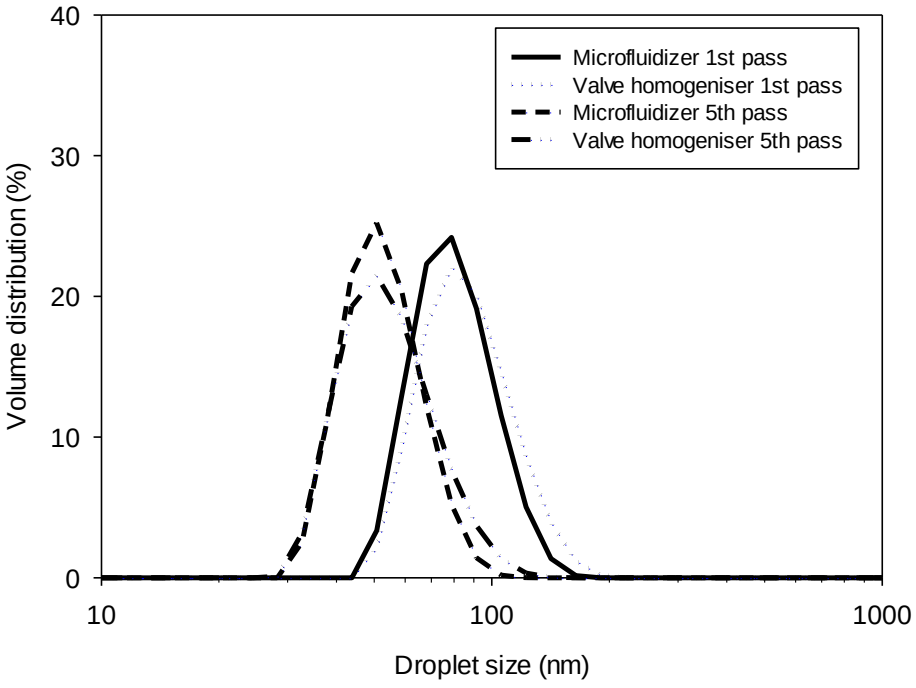

Figure 4.5: Effect of homogenising device, Microfluidizer and valve homogeniser, on the droplet size distribution after the first and fifth pass for 10 wt.% water dispersed phase (with 2 wt.% calcium chloride in the aqueous phase) in sunflower oil with 9 wt.% PGPR at 50 MPa

Figure 4.5 shows that for both devices, after one pass, the droplet size distribution is mono-modal and has no shoulders from coalescence or flow bypassing the main turbulent region. After five passes, the droplet size of the main peak has decreased from 100 nm to 60 nm. This is further evidence that the droplet break-up mechanism is due to turbulent viscous flow since viscous stresses create droplet break-up uniformly without creating the velocity fluctuations that cause in-processing coalescence. Multiple passes are required to produce the smallest droplet size, as the time for energy dissipation is shorter with the higher viscosity continuous phase; therefore the residence time for the shearing forces creating droplet break-up is also shorter.

A droplet size increase was observed, though not statistically significant, in Figure 4.4 after the 4^{th} pass. It was hypothesised that this could be due to the higher temperature causing coalescence or Ostwald ripening. Figure 4.5 shows a slightly larger tail of the distribution after the 5^{th} pass which could indicate Ostwald ripening of the emulsion however it appears that the increase is not distinguishable on the droplet size distribution.

In viscous flow, the dependency on emulsifier concentration is reduced since there is reduced coalescence. In order to determine the dependency of PGPR concentration on droplet size with different passes and pressures through the devices the emulsifier concentration was reduced to 1 wt.% of the continuous phase.

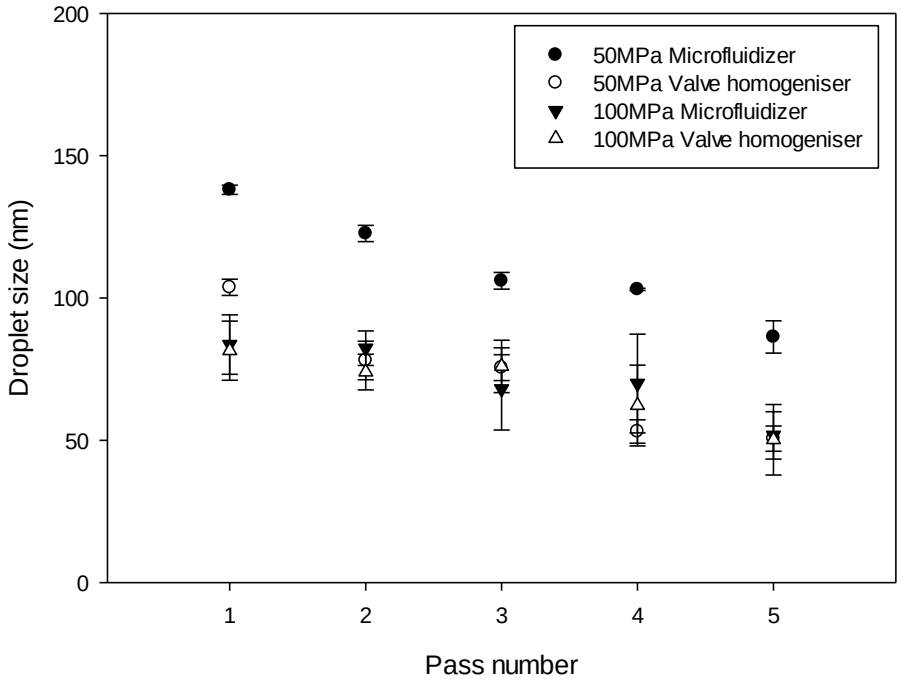

Figure 4.6: Effect of pass number on the emulsion droplet size for 10 wt.% water dispersed phase (with 2 wt.% calcium chloride in the aqueous phase) in sunflower oil with 1 wt.% PGPR in the valve homogeniser and the Microfluidizer at 50 and 100 MPa.

Figure 4.6 shows that by decreasing the emulsifier concentration there is minimal change in droplet size for the emulsions produced using the valve homogeniser at both pressures and the Microfluidizer at the higher pressure (100 MPa); with the first pass emulsion droplet size at 100 nm reducing to 60 nm after five passes. This indicates a similar droplet break-up mechanism to previously discussed for Figure 4.3 & Figure 4.4. However, for the Microfluidizer at the lower pressure (50 MPa) the droplet sizes are significantly higher producing 140 nm after the first pass refining to 100 nm after the fifth pass. This likely to be due to the lower concentration of emulsifier not adsorbing and stabilising the interface quickly enough as the droplets are deformed.

The next step in understanding W/O nanoemulsion production is to investigate the influence of salt in the aqueous phase on the interface and droplet size.

4.3.3 Effect of calcium chloride on droplet break-up

It has been proposed previously that adding salt into water in oil emulsions made by high shear mixing and stabilised by PGPR results in a smaller emulsion droplet size as a consequence of a reduction in interfacial tension (Márquez *et al.*, 2010, Pawlik *et al.*, 2010). To investigate this for high pressure homogenisation a series of water-in-oil emulsions were produced with 10 wt.% water in sunflower oil, and 9 wt.% PGPR in the oil continuous phase with the concentration of calcium chloride varied, Figure 4.7. The low volume fraction of water was chosen to minimise the effect of coalescence caused by droplets colliding before the interface is coated with emulsifier. PGPR was used as it is an elastic emulsifier that adsorbs onto the interface quickly (Gülseren and Corredig, 2012) and is very effective in producing W/O emulsions (Cheng *et al.*, 2006, Surh *et al.*, 2006, Pawlik *et al.*, 2010, Le Révérend *et al.*, 2011).

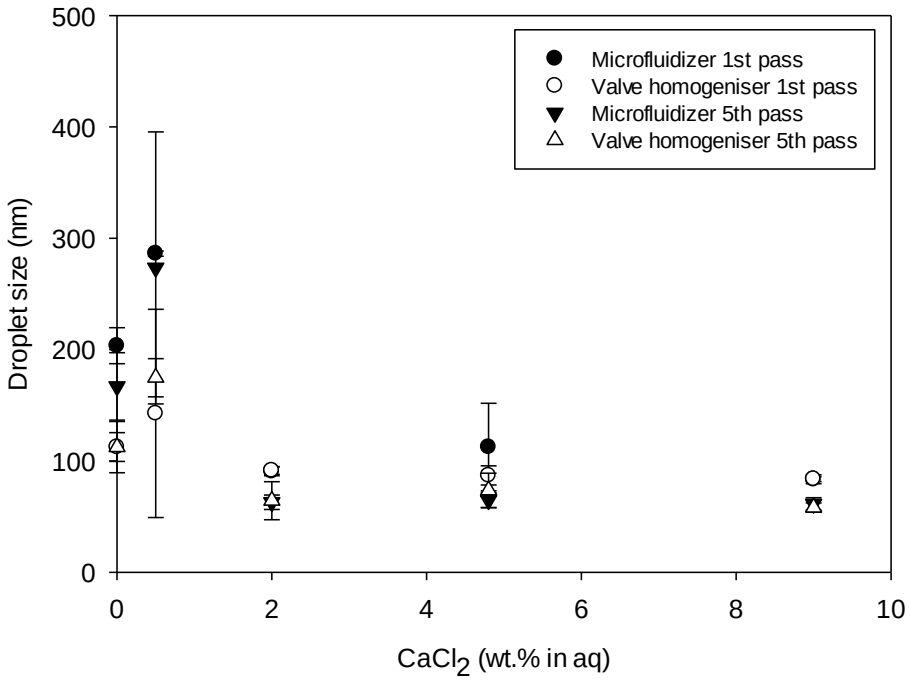

Figure 4.7: Effect of calcium chloride concentration on droplet size for 10 wt.% water dispersed phase in sunflower oil with 9 wt.% PGPR of the oil phase after the first and fifth pass at 50 MPa

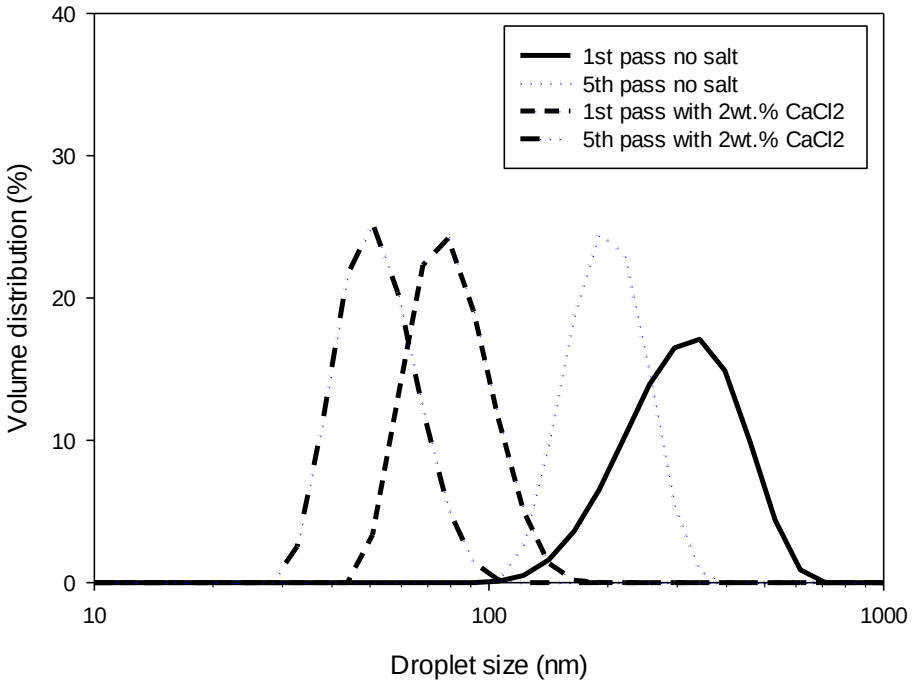

Figure 4.8: Effect of 2 wt.% calcium chloride addition into the aqueous phase on the droplet size distribution of a W/O emulsion, on the droplet size distribution after the first and fifth pass for 10 wt.% water dispersed phase in sunflower oil with 9 wt.% PGPR in a Microfluidizer at 50 MPa

Figure 4.7 shows that by increasing the concentration of calcium chloride the droplet size of the emulsions after one pass decreases from 200 nm to 80 nm in the Microfluidizer and from 130 nm to 80 nm in the HPH. The smallest droplet size was observed with 2 wt.% or greater calcium chloride. Figure 4.8 shows an example of the differences in droplet size distributions that are achieved by adding salt. It is shown that not only are the peak heights different as a result of differences in the average droplet size but also the emulsion with salt has a narrower droplet size distribution. These droplet size distributions reinforce the hypothesis that break-up is likely to be turbulent viscous since emulsions made without salt still show a reduction in mean peak height after multiple passes and the distribution is monomodal after the first pass (Vankova *et al.*, 2007a).

The reason for the reduction in droplet size with salt addition has been debated in the literature. Firstly, it could be due to the salt reducing the thickness of the electrical double layer and thus reducing the interfacial tension, thereby allowing tighter packing of emulsifier at the interface (Pawlik *et al.*, 2010, Bohinc *et al.*, 2001). Or the salt could reduce the interfacial activity of fatty acids in the oil which therefore creates tighter packing of PGPR, also reducing the interfacial tension (Márquez *et al.*, 2010). In order to consider the latter theory 1 wt.% of oleic acid was added into the sunflower oil to increase the fatty acid content.

Table 4-3: Effect of salt and oleic acid on the droplet size in A) valve homogeniser B) Microfluidizer

A) Valve homogeniser	**Oil only**		**1 wt.% oleic acid in oil phase**	
	1st pass (nm)	5th pass (nm)	1st pass (nm)	5th pass (nm)
Water only	112 ± 13	112 ± 23	218 ± 48	232 ± 7
Water with 2 wt.% CaCl2 in aqueous dispersed phase	91 ± 3	64 ± 17	180 ± 8	109 ± 2

B) Microfluidizer	**Oil only**		**1 wt.% oleic acid in oil phase**	
	1st pass (nm)	5th pass (nm)	1st pass (nm)	5th pass (nm)
Water only	203 ± 16	167 ± 30	190 ± 23	171 ± 12
Water with 2 wt.% CaCl2 in aqueous dispersed phase	91 ± 4	63 ± 6	167 ± 4	126 ± 18

Table 4-3 shows that the smallest droplet sizes are observed with salt added and no additional fatty acids. This suggests that presence of fatty acids in the oil phase can influence the final droplet size of an emulsion. As fatty acids are ionic and are expected to be active at the oil-water interface it might be expected that a mixed emulsifier layer is formed reducing the rate of PGPR adsorption and effectiveness. This increased absorption time leads to chance of droplet collision and an increase in emulsion droplet size.

It is unlikely that the reduction in droplet diameter with the addition of salt is solely due to reduction of the effect of fatty acids.

Table 4-4: Effect of calcium chloride and PGPR on the interfacial tension (mN/m) between water and sunflower oil

Calcium chloride wt.% in aqueous phase	Interfacial tension (mN/m)			
	Oil only	0.1% PGPR	1% PGPR	9% PGPR
0	24.7 ± 0.5	13.0 ±1.3	2.6 ±0.6	3.5 ±0.6
0.2	24.9 ±1.2	8.5 ±5.3	2.6 ±0.6	3.3 ±0.7
1	24.8 ±1.1	6.5 ±1.9	2.2 ±0.4	2.8 ±0.6
2	25.5 ±1.0	5.3 ±1.5	1.5 ±1.1	2.5 ±1.7

Table 4-4 shows that by increasing the salt concentration in the aqueous phase for a given concentration of PGPR the interfacial tension is reduced, this is evident at the lowest

concentration of PGPR (0.1%). This has been seen before and it is suggested that the addition of ions compresses the electrical double layer at the interface creating a lower interfacial tension (Márquez *et al.*, 2010), and as such there is a reduction in time required to deform a droplet and break up within the homogenisation process. This is observed as an overall reduction in emulsion droplet size.

In summary, addition of salt reduces the interfacial tension or resistance to droplet deformation and thus droplet size. Deformation rate is also dependent on the viscosity of the continuous and dispersed phases therefore this will be investigated next.

4.3.4 Effect of viscosity ratio on droplet size

The effect of viscosity ratio for oil continuous emulsions has been investigated. A low viscosity ratio was achieved by using a continuous oil phase modified by castor oil in order to increase the viscosity. Castor oil blends well with sunflower oil with minimal change to the interfacial tension (Quinchia *et al.*, 2010). To test at higher viscosity ratios the dispersed phase was modified with glycerol which is known not to significantly change the interfacial tension (Qian and McClements, 2011). The droplet sizes produced for the viscosity ratio range from 0.001 to 1 are shown in Figure 4.9 (excess emulsifier) and Figure 4.10 (lower emulsifier concentration).

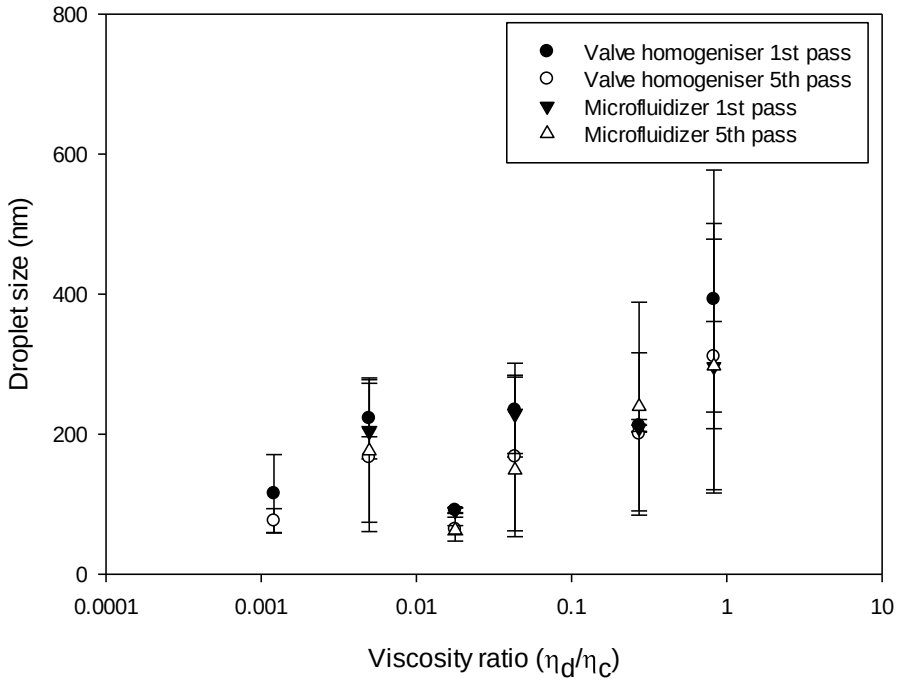

Figure 4.9: Effect of viscosity ratio on the emulsion droplet size for W/O emulsions with 10 wt.% water (with 2 wt.% $CaCl_2$ and between 20 - 80% glycerol, 0.002 - 0.04 Pa s, for viscosity ratios 0.04, 0.2 and 0.8 respectively) and sunflower oil (with 35 - 75% castor oil, 0.18 – 0.735 Pa s, for viscosity ratio 0.004 - 0.001 respectively) with 9 wt.% PGPR at 50 MPa. Note that for viscosity ratio 0.001 the Microfluidizer could not pump this due to its high viscosity.

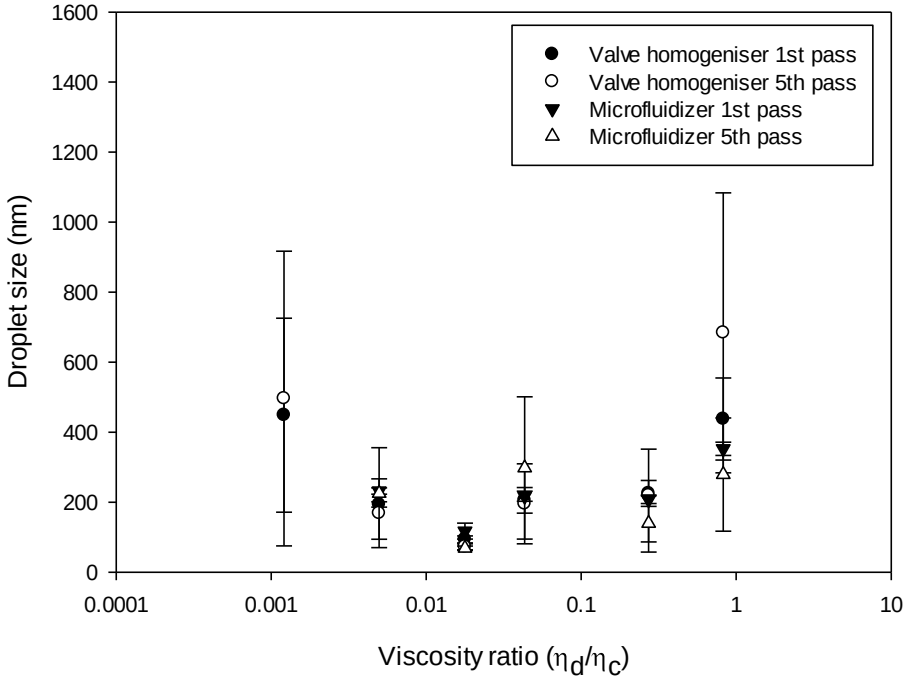

Figure 4.10: Effect of viscosity ratio on the emulsion droplet size for W/O emulsions with 10 wt.% water (with 2 wt.% $CaCl_2$ and between 20 - 80% glycerol, 0.002 - 0.04 Pa s, for viscosity ratios 0.04, 0.2 and 0.8 respectively) and sunflower oil (with 35 - 75% castor oil, 0.18 – 0.735 Pa s, for viscosity ratio 0.004 - 0.001 respectively) with 1 wt.% PGPR at 50 MPa. Note that for viscosity ratio 0.001 the Microfluidizer could not pump this due to its high viscosity.

It has been reported that the mechanism of droplet deformation and viscous break-up in turbulent flow will be largely dependent on the viscosity ratio of the dispersed to continuous phase (Grace, 1982, Walstra, 2005). As the ratio approaches 1 (turbulent viscous flow) the energy transfer from the continuous to dispersed phase to deform the droplet reaches a maximum resulting in a minimum in droplet size (Grace, 1982, Walstra, 2005). Figure 4.9 and Figure 4.10 shows that for viscosity ratios 0.001 – 1 the droplet sizes are similar (about 200 nm) with increasing error as the viscosity ratio increases. However, it is clear that for both the HPH and the Microfluidizer the droplet size does not go through a minimum at 1. This is consistent with the previous chapter for oil in water emulsions. These results imply that extensional flow is present in both devices, although it is unclear if the presence of this

flow creates droplet break-up or allows for increased time for emulsifier adsorption. The latter explanation is more likely since extensional flow is geometry dependent and both the devices used here have significantly different geometries so it is improbable that both devices will be capable of producing similar extensional flows.

4.4 Chapter conclusions

This chapter has shown that droplet sizes for water in sunflower oil emulsions as small as 50 nm can be produced using either a HPH or a Microfluidizer at pressures of 50 MPa and greater. However multiple passes are needed to reduce the mono-modal droplet size distribution from ~ 100 nm after the first pass down to 50 nm after the fifth pass. The higher viscosity continuous phase (in comparison to the O/W nanoemulsions produced in the previous chapter) increases the rate of energy dissipation and increases the Kolmogorov length scale thus changing the mechanism of droplet break-up to turbulent viscous break-up; where the droplet deformation for break-up is caused from viscous shearing forces. Within this flow type coalescence is minimal due to few velocity fluctuations in the flow. The Microfluidizer commonly has a higher homogenising efficiency, however, it has been shown here that both devices produce similar droplet sizes after each pass. This is probably a consequence of the majority of the energy dissipating before the jets impinge as a result of the higher viscosity continuous phase and thus the deformation forces caused by the impinging jets are significantly lower and do not cause droplet deformation and break-up.

Salt addition reduced the interfacial tension and slightly reduced the droplet size produced from both devices. It is proposed that salt has two functions in high pressure homogenisation: it reduces the interfacial activity of free fatty acids in the oil thereby shortening the adsorption

time of PGPR and it also compresses the electrical double layer inside the aqueous dispersed phase and reduces interfacial tension.

Adjusting the viscosity ratio showed limited dependence on droplet size (although the error was large). This may be due to extensional flow present; however, as the error is large this cannot be concluded.

CHAPTER 5: FLAVOUR RELEASE FROM O/W NANOEMULSIONS

5.1 Introduction

The purpose of this chapter is to test the claim that flavour release is faster from nanoemulsions by exploring the aroma release from the aqueous continuous phase and the oil dispersed phases of nano and micron sized emulsions. It has been previously highlighted (section 1.1.2) that nanoemulsions are receiving a lot of research interest because the replacement of micron-sized droplets with nano-sized droplets in existing products is commonly found to enhance the products acceptability, including the enhanced flavour release (de Roos, 2003).

Flavour release is expected to be faster in nanoemulsions from the dispersed phase due to the larger surface area for mass transfer of flavour compounds (Cussler, 2009, Paraskevopoulou *et al.*, 2009). In contrast, the continuous phase flavour release may be expected to reduce with smaller droplets, and a larger surface area, as there is more chance of the volatile being trapped at the oil-water interface (Doyen *et al.*, 2001). On the nanoemulsion scale the author knows of only one study that has investigated flavour release (Paraskevopoulou *et al.*, 2009). The series of emulsions tested were made using 15% ethanol which could alter the release properties of the flavour volatiles at the interface in comparison to a simple oil-in-water emulsion. This study indicated that there were some trends, though not significant, that indicated faster dispersed phase flavour release with smaller droplets (Paraskevopoulou *et al.*, 2009). This reinforces the need for a better understanding of flavour release within nanoemulsions.

In this chapter two techniques are being used to indicate flavour release from a series of emulsions tested: static headspace and in-*vivo* testing. The static equilibrium headspace test measures the availability of aroma compounds in the gas phase and thus the affinity of the aroma compounds to transfer, or partition, across the air-water interface. The in-*vivo* technique measures flavour release under dynamic and un-equilibrated conditions. Flavour release during oral processing is enhanced by the mixing conditions in the mouth and dilution with saliva thus reducing the mass transfer resistance across the liquid-air interface (McNulty and Karel, 1973).

This chapter will investigate continuous and dispersed phase volatile release as an indication of its flavour release from emulsions with different droplet sizes (0.15, 1, 10 and 40 μm) and oil phase volumes (10 and 30%). It is hypothesised that this work will show faster flavour release from the dispersed phase as the droplet size reduces, due to the larger oil-water interfacial area for transfer. However, continuous phase flavour release would be expected to reduce with decreasing droplet size because there is more interfacial area available for the aroma to adsorb into the oil-water interface.

5.2 Materials and methods

5.2.1 Materials

5.2.1.1 Oil phase

Sunflower oil was purchased from a local supermarket and the oil soluble flavour, limonene (product number W504505, purity ≥95%), was purchased from Sigma Aldrich (UK).

5.2.1.2 Aqueous phase

Distilled water was used for the preparation of all solutions, and dissolved within this was the emulsifier polysorbate 80 (W291706) and the aqueous soluble flavour, ethyl butyrate (W242713, purity ≥98%), both were purchased from Sigma Aldrich (UK).

5.2.2 Emulsion preparation

A series of emulsions were prepared by homogenising either 10 or 30 wt.% oil with the aqueous phase containing 1 wt.% polysorbate 80 (except for the emulsion with 30% sunflower oil and 150 nm droplet size where the emulsifier concentration had to be increased to 2 wt.% to stabilise all the interface and achieve 150 nm sized droplets). The concentration of the flavour compounds were calculated for the overall emulsion, with 200 mg/L of oil soluble limonene and 2 mg/L of aqueous soluble ethyl butyrate. The methods for producing the emulsions are summarised in Table 5-1, although all emulsions had the same first step in processing and were prepared using a high shear mixer (Silverson L5M, Chesham, UK) and for the smaller droplet sizes the emulsions were subsequently passed through a high pressure valve homogeniser (Panda PLUS 2000, GEA Niro Soavi, Italy) for up to 5 passes at the stated pressure.

Table 5-1: Emulsion production methods

Target droplet size (µm)	High shear mixer	High pressure valve homogeniser
0.15	10,000 rpm for 60 s	100 MPa for 5 passes
1	10,000 rpm for 60 s	10 MPa for 1 pass
10	4500 rpm for 5 mins	-
40	2000 rpm for 5 mins	-

It should be noted that the emulsion with the higher phase volume will have a higher viscosity due to the larger number of droplets. However, this was not adjusted for with a thickener in the continuous phase since it is important to keep the continuous phase viscosity the same (though not measured here) and thickeners are known to adsorb aroma compounds (de Roos, 2003).

5.2.3 Droplet size measurements

The droplet size distribution, span and surface weighted mean droplet diameter, $d_{3,2}$, were measured using light diffraction (Malvern Mastersizer MS2000, Malvern, UK) with a Hydro SM manual small volume sample dispersion unit attached. The sample was diluted with double distilled water (RI=1.33). The span of the emulsion is defined as:

$$Span = \frac{d_{90} - d_{10}}{d_{50}} \qquad \textbf{Equation 5-1}$$

Where d_{90}, d_{50} and d_{10} are the droplet sizes are the 90th, 50th and 10th percentile.

See section 3.2.3.1 for more details on this technique.

5.2.4 Flavour release measurement using mass spectroscopy

5.2.4.1 Headspace measurement

Three aliquots (30 ml) of each flavoured emulsion were placed in screw capped bottles (100 ml) and allowed to equilibrate for 20 minutes at 20 °C prior to headspace (HS) analysis. A portion of the headspace was sampled into the Atmospheric Pressure Chemical Ionization (APCI) source at 5.5 mL/min through a small port in the bottle cap. APCI was fitted to a Platform LCZ mass spectrometer (Micromass, Manchester, UK) through a heated (120 °C) deactivated fused silica transfer line 1 m x 0.53 mm ID. The source was heated to 75 °C and operated in positive ion mode (4 kV) at a cone voltage of 18 V. When the sample was placed through headspace analysis, the APCI-MS traces showed a rapid rise in signal to a plateau value which was maintained for about 10 s after which the bottle was resealed. The running order of the samples was randomised and data were collected in selected ion recording mode with a dwell time of 0.25 s monitoring m/z 117 for ethyl butyrate and 137 for limonene. Masslynx 4.1 (Micromass, Manchester, UK) was used to determine the peak height of the maximum signal observed for each sample (IMax).

5.2.4.2 In-*vivo* measurement

The flow rate of 30 mL/min for APCI measurement was set up because a faster sampling rate was required for in-*vivo* analysis to allow for quicker and more accurate measurement of results. Other instrument conditions were kept the same, except the dwell time was at 0.02 s to collect more data points for aroma release during breathing and provide more detailed

information on the release profiles. An additional ion, acetone with m/z 59, was added to monitor the breath pattern.

Three replicate samples (5 g) of each of the flavoured emulsions were consumed by three panellists. The running order of samples were randomised and consumed by each panellist in turn, so each panellist had 15-20 minutes between each run. Water was provided to cleanse the palate. To reduce the panellist variation during in-*vivo* analysis, controlled protocol was used: holding the sample in the mouth for 20 s with normal breathing and swallowing at 20 s, then the panellist was ask to continue normal breathing for another 20 s. In addition, the exhaled air from the nose of each volunteer was monitored before consuming any sample to ensure that there was no carry-over of aroma from the previous sample and that all compounds had returned to baseline levels.

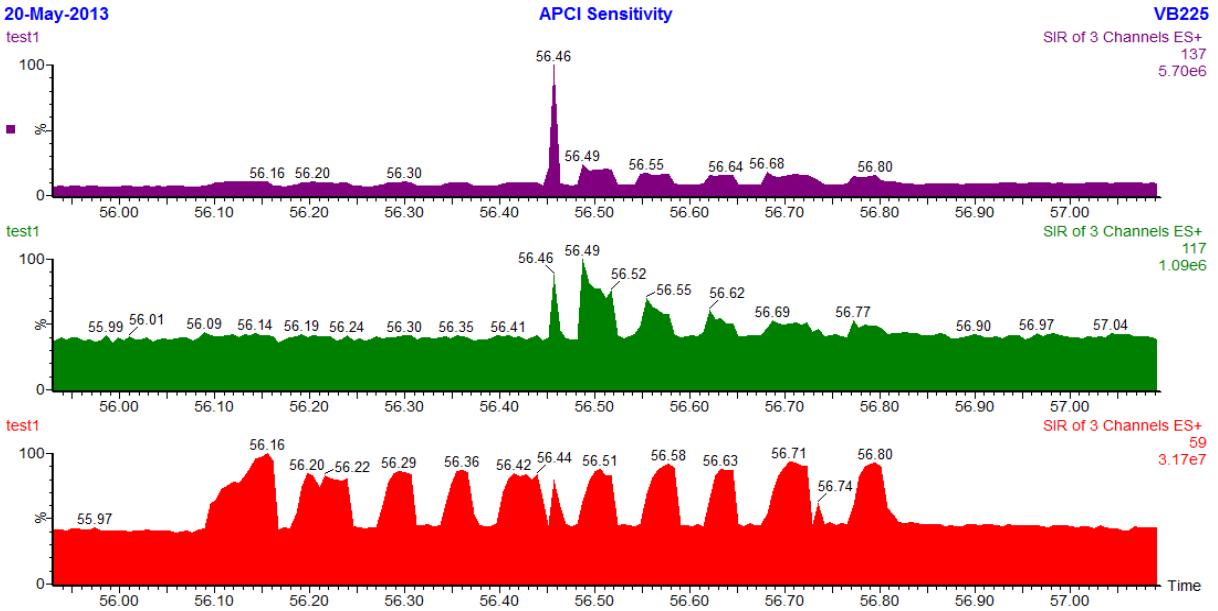

Figure 5.1: Selected ion mode (SIR) with electronspray positive mode (ES+) was set for in-*vivo* release of limonene (ion 137, top) and ethyl butyrate (ion 117, middle) with acetone from breath (ion 59, bottom). It is illustrated that the panellist held the nanoemulsion in mouth and breath from 56.10 min and swallowed before 56.50min and finished the test after 56.80 min. The maximum ion intensity (IMax) was at 5.70 e6 and 1.09 e6 for limonene and ethyl butyrate, respectively.

Figure 5.2: Photo demonstrating the experimental set-up on in-*vivo* measurement including a photo of the tube which carries a sample of the exhaled air to the mass spectromter.

An example of a panellist consuming one sample using the designed eating protocol is illustrated in Figure 5.1 following by an image showing the experimental set-up (Figure 5.2). From the release curves, the maximum ion intensity (IMax) for ethyl butyrate and limonene was recorded for each panellist, for each emulsion and for each replicate. As such, the average IMax values presented for the in-*vivo* studies are an average of nine results; with three panellists producing three runs.

5.2.5 Data analysis of flavour release

All results were analysed by SPSS16.0 (SPSS Inc., Chicago, USA) to calculate the mean IMax from replicates and perform statistical analysis. Multi-analysis of variance (MANOVA)

followed by Tukey's multiple comparison tests were applied where appropriate ($p < 0.05$), to determine statistical significance at 95% confidence level.

The average IMax values were used to calculate the lipid effect of the emulsions. This is calculated by dividing the IMax values measured at 10% oil by those at 30% oil fraction to compare the influence of oil fraction on flavour release.

Oral processing can vary depending on the panellist. Despite the flavour release results per panellist varying slightly, MANOVA analysis indicated that there was no significant difference between panellists for either of the aroma compounds ($p > 0.05$).

5.3 Results and discussion

5.3.1 Emulsion characterisation

In order to investigate the influence of droplet size on flavour partitioning and release a series of emulsions were made with target droplet sizes of 0.15, 1, 10 and 40 μm at 10% and 30% dispersed phase fraction. A combination of high shear mixing and high pressure homogenisation was used to achieve these droplet sizes (see Table 5-1 for more details). Figure 5.3 and Table 5-2 show the volume distributions, surface weighted mean droplet size and spans of the emulsions produced.

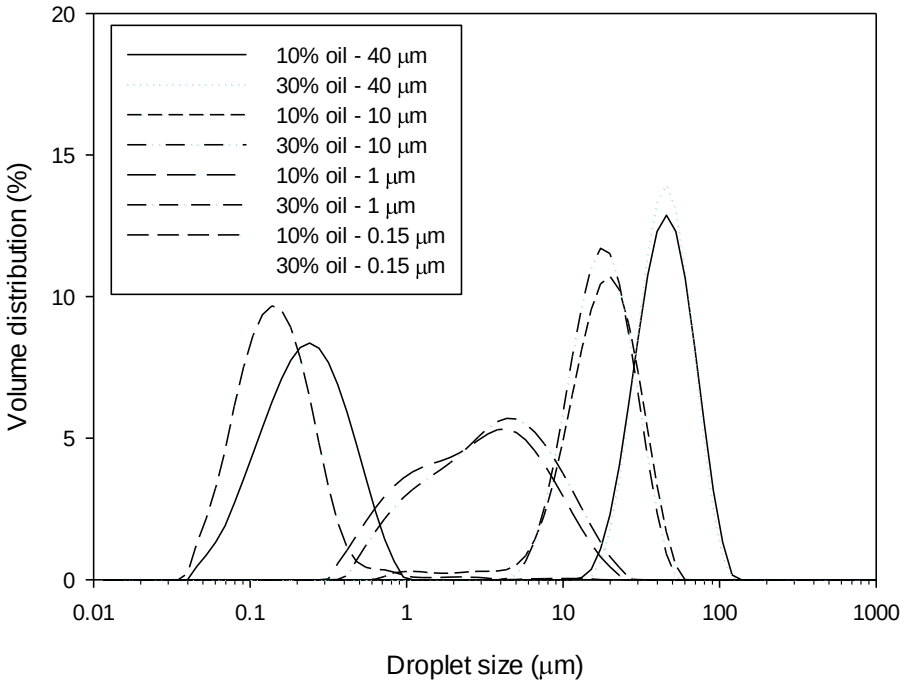

Figure 5.3: Droplet size distributions of sunflower oil in water emulsions stabilised with polysorbate 80 with 100 mg/L limonene and 2mg/L of ethyl butyrate.

Table 5-2: Surface weighted mean, d3,2, droplet diameters and span of sunflower oil in water emulsions stabilised with Tween 20 with 100 mg/L limonene and 2mg/L of ethyl butyrate.

Droplet size targeted (µm)	Actual $d_{3,2}$ (µm)		Span	
	10% oil dispersed phase	30% oil dispersed phase	10% oil dispersed phase	30% oil dispersed phase
0.15	0.11	0.17	1.55	1.74
1	1.70	2.14	2.92	2.73
10	11.4	14.7	1.34	1.20
40	38.0	38.4	1.09	1.00

As can be seen from Figure 5.3 and Table 5-2 the droplet sizes and distributions are similar for the two mass fractions of oil for each target droplet size. However, the span of the droplet size distributions ranged from ~1, for the droplet sizes at 0.15, 10 and 40 µm, to ~3 for the droplet size 1 µm. Whilst this difference should be considered in results analysis a previous study that investigated influence of droplet size distribution (spans ~ 1.5 – 3) on flavour release demonstrated that span was independent of the flavour release (Meynier *et al.*, 2005). Therefore, it is expected that the differences in the emulsion droplet size distributions will not influence the results.

5.3.2 Aqueous soluble flavour release from the aqueous continuous phase

Influence of oil phase fraction on flavour release

Initially the aqueous soluble flavour intensity was investigated from the continuous phase. Figure 5.4 and Figure 5.5 shows the headspace and in-*vivo* maximum intensities of ethyl butyrate, respectively, as a function of droplet size. Whilst the graphs show the results for both the influence of oil fraction and droplet size on flavour release, the results for oil fraction will be discussed first and then the discussion for the droplet size results will follow.

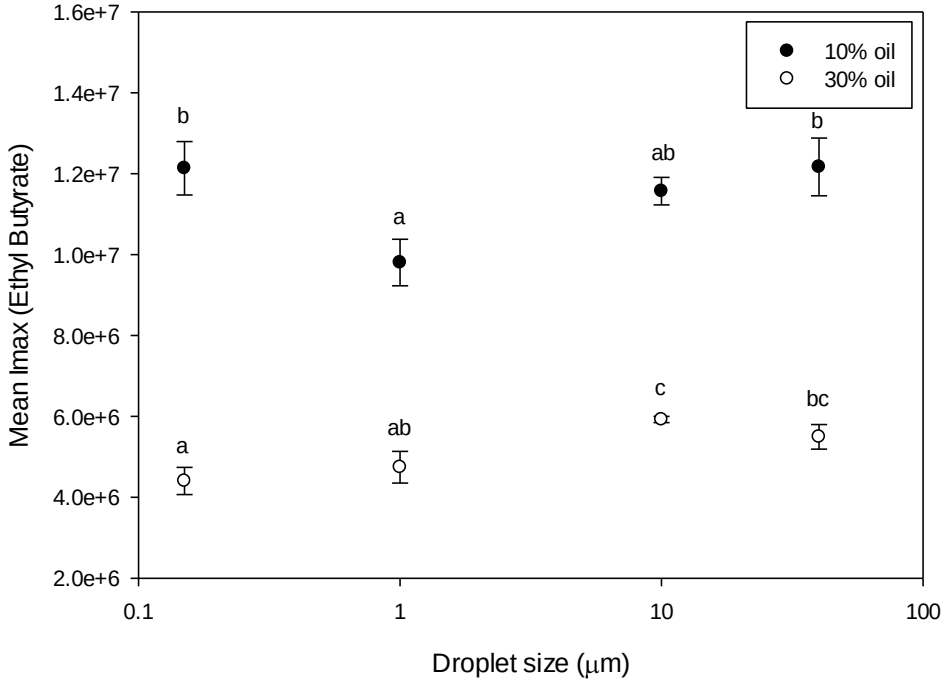

Figure 5.4: Average maximum measured concentrations of ethyl butyrate in the headspace from emulsions with different droplet sizes made with 10% oil mass fraction and 30% oil mass fraction. Different letters, 'a', 'b' and 'c', indicate significant differences ($p < 0.05$) across different droplet sizes.

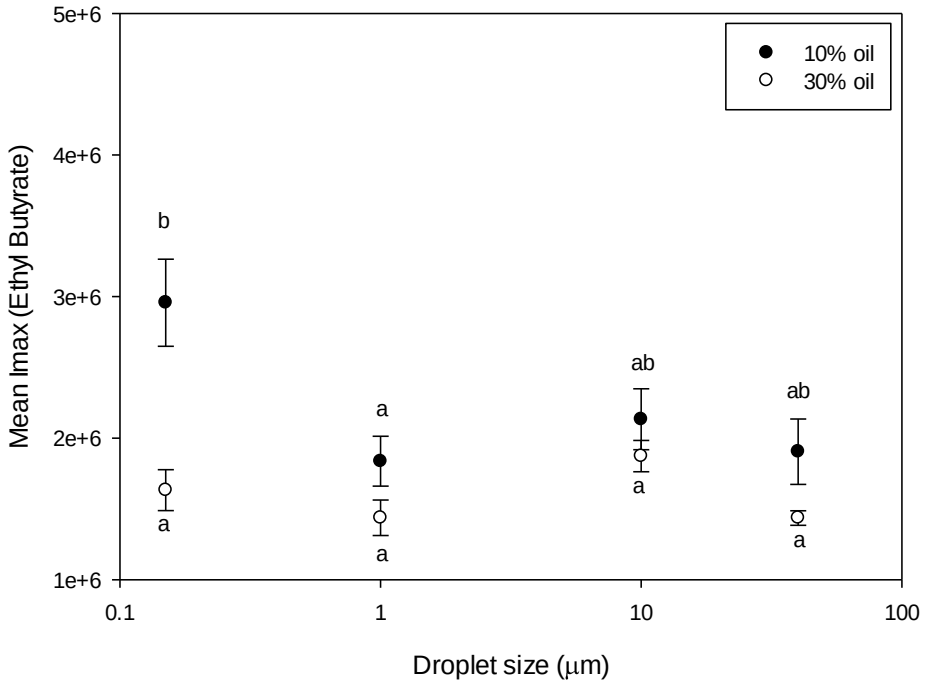

Figure 5.5: Average maximum measured concentrations of ethyl butyrate during in-*vivo* testing from emulsions with different droplet sizes made with 10% oil mass fraction and 30% oil mass fraction. Different letters, 'a', 'b' and 'c', indicate significant differences ($p < 0.05$) across different droplet sizes.

As can be seen in Figure 5.4 oil phase fraction has a significant effect on ethyl butyrate release ($p < 0.001$), with the lower oil fraction emulsion partitioning more of the aqueous soluble flavour into the headspace, despite having the same amount of flavour within the total emulsion. This reduction in flavour release with increased oil phase fraction has previously been attributed to the flavour molecule partitioning into the oil-water interface (Carey *et al.*, 2002).

The results for in-*vivo* release of ethyl butyrate, Figure 5.5, show that the dispersed phase fraction significantly affects the water continuous volatile release for in-*vivo* testing ($p < 0.001$), with 10% oil releasing more ethyl butyrate. These results agree with the static

headspace results and show that as the oil dispersed phase fraction is increased the amount of water continuous volatile release is reduced.

The lipid effect values (release at 10% oil divided by the release at 30% oil) are presented in Table 5-3. The lipid effect is used to indicate the role of the oil or lipid on the release of volatiles. For example, a lipid effect value of over 1 indicates that the oil/lipid traps more of the volatile at the interface for the higher oil fractions leading to a large difference between the volatile intensities measured by each technique.

Table 5-3: Lipid effect (LE) of ethyl butyrate by headspace and in-*vivo* analysis. The values were calculated by dividing their respective release at 10% oil fraction by the release at 30% oil for each droplet size.

Droplet Size	**Headspace**	**In-*vivo***
0.15 μm	2.76	1.37
1 μm	2.07	1.66
10 μm	1.95	1.31
40 μm	2.21	1.24
Average	*2.25 ± 0.36*	*1.39 ± 0.18*

The average lipid effect for ethyl butyrate for in-*vivo* was 1.39, and is much lower than the 2.25 observed during the headspace measurement. This indicates that a higher proportion of the flavour is released from the 30% oil emulsion during the in-*vivo* test compared to the headspace. The dynamic conditions in the mouth; the mixing, emulsion destabilisation and

higher temperature, promotes the release of flavour molecules that have partitioned into the oil-water interface. In practice, this may mean that the consumer will smell a difference in flavour volatile release with different oil phase fractions, however, once in the mouth the difference is less obvious.

Influence of droplet size on flavour release

The results from static headspace testing for ethyl butyrate at each droplet size are shown in Figure 5.4. MANOVA results for the emulsions with 10% oil fraction illustrated a significant effect of droplet size on the partitioning of ethyl butyrate within the headspace of the emulsions ($p < 0.001$), and Tukey's analysis showed that the droplet size of 1 μm had a significantly lower release than 150 nm and 40 μm. To consider the mechanism for continuous phase flavour release, the surface area and number of droplets in the emulsions at the different droplet sizes have been estimated and are presented in Table 5-4.

Table 5-4: Emulsion dimensions for variable droplet size assuming monomodal droplet size distributions including number of droplets and specific surface area for a given phase fraction.

Droplet size (μm)	Number of droplets in 10% (number/m^3)	Number of droplets in 30% (number/m^3)	Specific surface area in 10% oil (m^2/g)	Specific surface area in 30% oil (m^2/g)
0.15	5.69E+19	1.70E+20	5.28	10.89
1	1.91E+17	5.73E+17	0.356	1.068
10	1.91E+14	5.73E+14	0.0527	0.123
40	2.98E+12	8.95E+12	0.0158	0.0468

It has been claimed previously by Meynier *et al.* (2005) that the formation of an emulsion with a larger interfacial area (i.e. smaller droplet size or higher dispersed phase fractions) decreases the continuous phase flavour release because the aroma volatiles partition into the interface. If this were the sole mechanism for flavour release, it would be expected that flavour release would be lower for the emulsions with the highest surface areas (150 nm droplet sizes for both 10 and 30% oil phase fraction) and highest for the lowest interfacial area (40 μm droplets). This is not observed in this study and implies that continuous flavour release is unlikely to be solely dependent on the oil-water interfacial area.

For a given fraction of oil, as the droplet size decreases there are more droplets present (see Table 5-4), the presence of more droplets is likely to decrease the mass transfer of flavour volatiles through the continuous phase. The data in Figure 5.4 shows a trend, as the droplet size reduces from 40 μm down to 0.15 μm (except at 0.15 μm with 10% oil) the amount of

flavour partitioning into the headspace reduces too. There will be a higher number of droplets within the smaller sized emulsions compared to the 40 μm emulsion thus reducing mass transfer of flavour through the continuous phase. Also the larger interfacial area will reduce the release of volatiles as there is a larger area for volatile partitioning into the interface. On the nanoemulsion scale this trend is not seen for 10% oil.

The higher flavour release measured at 150 nm could indicate a different behaviour at the nanoemulsion scale. This data however, only shows one data point at higher release which could be an anomaly in the results. To test this, further work should be done on lower oil phase fractions.

The in-*vivo* results for ethyl butyrate release (Figure 5.5) show similar trends to those identified in the headspace results for 10% oil, with droplet size having a significant effect on flavour release ($p < 0.001$). Minimum release is observed at 1 μm, which is significantly lower than the release at 150 nm (Tukey's test). This increase in flavour release on the nanoscale was also observed for the 150 nm emulsion compared to 1 μm in the static headspace measurement. It is attributed to the nano-sized droplets restricting the amount of volatile being adsorbed into the oil-water interface, thus increasing the amount in the continuous aqueous phase available for release.

To emphasise, it is proposed that for decreasing droplet size both the increase in the interfacial area and number of oil droplets within the aqueous continuous phase reduces the intensity of flavour measured in either the headspace or in-*vivo* testing. When the emulsion

droplet size approaches the nanoscale the behaviour is unclear, and further work can be done on reducing the oil phase fraction.

5.3.3 Oil soluble flavour release from the dispersed oil phase

This section uses the same series of emulsions made and tested in section 5.3.2 to determine the influence of oil phase fraction and droplet size on the release of the oil soluble flavour, limonene.

Influence of oil phase fraction on flavour release

Figure 5.6 and Figure 5.7 show the flavour partitioning into the headspace and release from in-*vivo* testing, respectively, and the values of the lipid effect are presented in Table 5-5. Initially, the impact of oil phase fraction will be discussed for both headspace and in-*vivo* measurement then the results for droplet size will be evaluated.

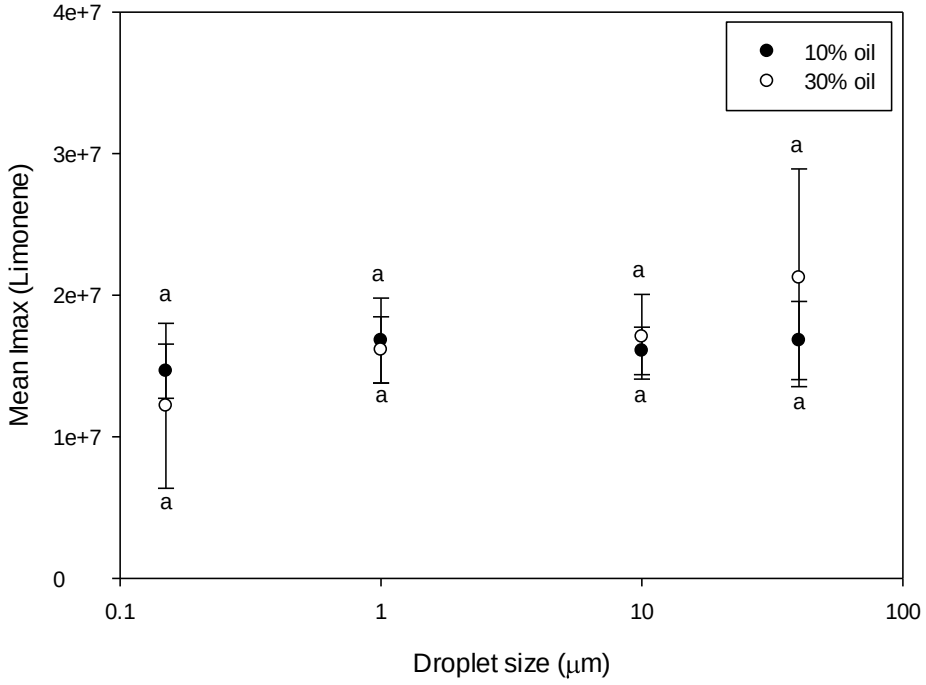

Figure 5.6: Average maximum measured concentrations of ethyl butyrate in the headspace from emulsions with different droplet sizes made with 10% oil mass fraction and 30% oil mass fraction. Different letters, 'a', 'b' and 'c', indicate significant differences ($p < 0.05$) across different droplet sizes.

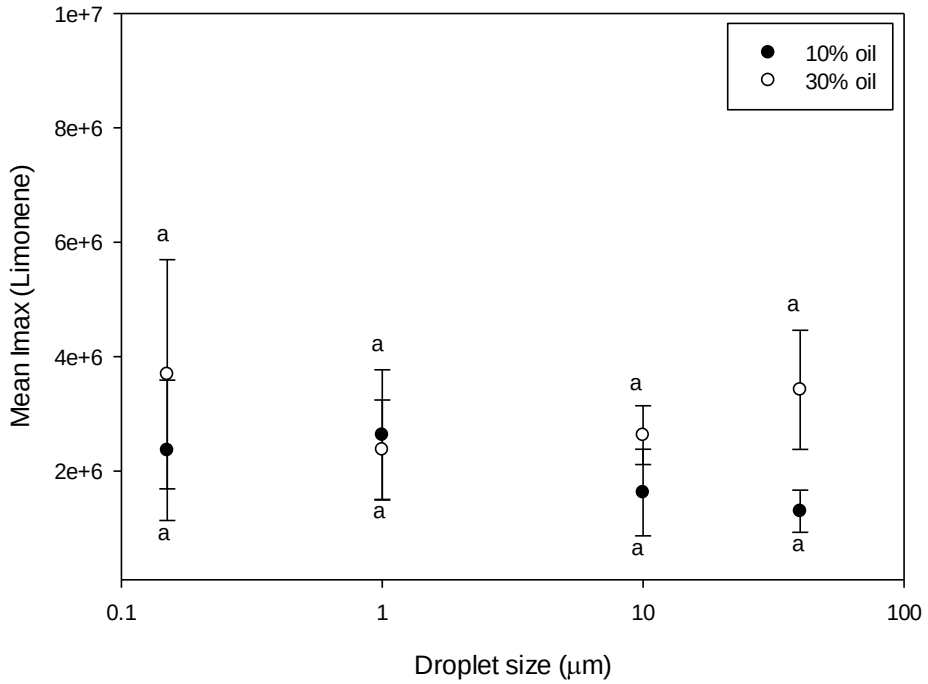

Figure 5.7: Average maximum measured concentrations of ethyl butyrate during in-*vivo* testing from emulsions with different droplet sizes made with 10% oil mass fraction and 30% oil mass fraction. Different letters, 'a', 'b' and 'c', indicate significant differences ($p < 0.05$) across different droplet sizes.

Table 5-5: Lipid effect (LE) of limonene by headspace and in-*vivo* analysis. The values were calculated by dividing their respective release at 10% oil fraction by the release at 30% oil for each droplet size.

Droplet Size	Headspace	In-*vivo*
0.15 μm	1.20	0.59
1 μm	1.04	1.11
10 μm	0.94	0.58
40 μm	0.79	0.38
Average	*0.99 ± 0.17*	*0.71 ± 0.16*

Figure 5.6 shows the results for limonene intensities partitioning into the emulsion headspace. It can be seen that the oil phase volume fraction does not have a significant effect on the limonene intensity detected in the headspace ($p > 0.05$). The average lipid effect for limonene was 0.99 which confirms that its release was very similar for 10% and 30% oil. This suggests that the limonene was dissolved in the dispersed oil phase and did not transfer between the oil/water interface during the static headspace analysis and therefore there was no effect on concentrations of flavour volatiles in the headspace for the oil phase volume or droplet size. Similar results have been observed before for lower oil dispersed phase volumes (0 – 0.2 wt.% oil) for three different oil soluble volatiles measured using a similar mass spectrometry technique to detect aroma (Carey *et al.*, 2002).

The in-nose data shown in Figure 5.7 shows that similar to the headspace results there is no difference in limonene detected for droplet sizes 0.15 to 10 μm. This is likely to be because a low concentration of limonene is released from the dispersed phase within the emulsion into the air.

Guinard *et al.* (2002) studied flavour detection from the dispersed phase by using a sensory panel and found a similar result. Phase volumes of 1.5 – 15% w/v were tested with varying concentrations of dispersed phase flavour. The sensory panel could not detect a difference in flavour intensity for either the variable phase volume or flavour concentration. The authors' reasoning was that the flavour was not partitioning out of the dispersed phase preventing the sensory panel from detecting it. When emulsifier is in excess and micelles are present within the continuous phase, these can trap the dispersed phase flavour compound which will also reduce the rate of flavour release.

At the 40 μm droplet size, the higher oil fraction has a significant effect on its in-nose release ($p < 0.01$ for the emulsions with 40 μm droplet sizes), showing limonene release at the higher volume fractions of oil. This increase in release with higher oil fractions is further reinforced, though not significant, with the average lipid effect for in-*vivo* reducing to 0.71 compared to 0.99 measured in the headspace. During oral processing emulsions may breakdown and destabilise in the mouth; this is more likely to happen if the oil phase fraction is high and the droplet size is large because the emulsion is less stable (Malone *et al.*, 2003, van Aken *et al.*, 2007). As the emulsion breaks down in the mouth it will start to phase separate, which increases flavour release by allowing the flavour to transfer directly from the oil phase to the air phase. This will be quicker than transferring into the aqueous phase and then into the air, which was shown to be unlikely and slow by the analysis of mass transfer coefficients (in Table 2-3 within section 2.3.3). Since the largest droplet sizes, at the higher oil phase fraction exhibit higher release than the lower oil phase fraction, destabilisation is more likely to occur in the emulsion with the highest mass fraction of oil and largest droplet size. To further evidence this theory, during experimentation this emulsion visually creamed but did not phase separate (at room temperature) and the participants had to redisperse the droplets by rotating the bottle 3 times immediately prior to measuring the sample out. Therefore the emulsion quickly creamed and after dilution with saliva and at mouth temperature this emulsion may be phase inverting.

Influence of emulsion droplet size on flavour release

The results for the detection of limonene in the headspace showed that droplet size did not have a significant effect on the aroma detection ($p > 0.05$) (Figure 5.6).

Similar to the results for limonene in the headspace, droplet size does not have a significant effect on in-*vivo* limonene release ($p > 0.05$).

To summarise, it is proposed that within this formulation, mass transfer of flavour across the oil-water interface limits the release of oil dispersed flavour, and not the difference in droplet size.

5.4 Chapter conclusions

This work has shown that the continuous phase volatile detection is highly dependent on the oil phase fraction, with more oil, less volatile is detected in the headspace or in the participant's breath (for the in-*vivo* testing). As the oil phase fraction is increased a larger amount of droplets are present for each droplet size, and a larger surface area is available for the volatile to partition into the interface thus less volatile is detected in either technique. The difference in volatile detection between the in-*vivo* test compared to the headspace was less because the dynamic conditions of the mouth promote release of volatile partitioning at the interface.

It was seen that when the droplet size of the emulsion decreased, and the overall number of droplets in the emulsion increased, the rate of water continuous phase flavour release was reduced (excluding 150 nm at 10% oil). The reduction in flavour release was as a consequence of having more droplets and more oil-water interfacial area in the emulsion, reducing the transfer of the flavour.

There was one anomaly to this trend, with more flavour being measured in the headspace and in-vivo for 150 nm droplets in 10% oil. If this were a true result it may indicate that nano-sized droplets are too small to hinder mass transfer of flavour through the continuous phase. However, more work should be done on this to determine if this is a real result.

Dispersed phase flavour partitioning or in-*vivo* release showed little difference with variable droplet size or phase volume. This indicates that the volatile did not transfer out of the dispersed phase in either of the testing methods. The exception to this was with the largest emulsion droplet size, where the volatile release was significantly higher. This result may indicate that the release is dependent on destabilisation and partial phase separation of the emulsion. Once the emulsion has phase separated, the limonene only needs to transfer across the oil-air interface, rather than transfer across into the water continuous phase of the emulsion and then into the air. Therefore, to summarise, these results would suggest that for oil soluble dispersed phase flavours nano-sized droplets should show the lowest flavour release unless there is another mechanism influencing release not identified here.

Previous results showed slight trends towards faster release with nanoemulsions (Paraskevopoulou *et al.*, 2009) and these results have highlighted some trends in release too, however, these are not large and thus for these conditions flavour release from nanoemulsions is no different than flavour release from micron sized emulsions.

CHAPTER 6: OIL INCLUSION INTO FLUID GELS FOR USE AS FAT MIMETIC

6.1 Introduction

This chapter explores an alternative method for reducing fat content in food, whilst still exploiting the longer physical stability and faster delivery of actives which nanoemulsions provides.

Biopolymers are being used in the food industry (along with other industries including cosmetics and personal care) to structure or stabilise emulsion based products. This is most commonly achieved either by forming a weak gel network or by thickening simply by the introduction of large polymeric molecules that interact thus increasing the viscosity (Gabriele, 2011).

Within foods these biopolymers can thicken to increase product stability and increase the perceived fattiness of the food. However, a more novel way of reducing fat in foods is to replace oil droplets with gel particulates that have similar sizes and mechanical properties to the fat or oil being replaced (Fernández Farrés *et al.*, 2014). These are produced using a cooled jacketed pin stirrer which forms spherical particles when a hot gel is cooled through its gelation temperature whilst being sheared. A common criticism of these gel particulates is that they do not have the flavour of oil. To overcome this complaint, and one of the novel aspects of this study; a small amount of oil will be incorporated within this hot gel solution with the aim of including oil within the fluid gel particles.

The primary reason for researching the inclusion of oil within fluid gel particles is to investigate the possibility of including oil within the fat mimicking fluid gels and thus enhance the flavour. The fluid gel technology can be used in other industries too, and therefore this research has a wider impact than solely fat mimetics.

The rheology of fluid gels can be easily tuned to increase: the physical stability of a product, suspending ability of particles (aids in uniform product functionality throughout use) or to tune the yield stress to suit the method of application (inducing a yield stress to allow the product to be applied over a targeted site) (Gabriele *et al.*, 2010, Fernández Farrés *et al.*, 2014).

If nanoemulsion droplets were incorporated within the gel particulates the resulting fluid gel can have the additional advantages that nanoemulsions pertain, notably the more efficient delivery of actives (McClements, 2011). The gel strength could be tuned to control the rate of release of the active until the desired target: gut for more efficient nutrient absorption of the body (in food), sustained rate of release of active on skin (pharmaceuticals or cosmetics) or slowed release of fertilisers (agriculture).

This chapter will investigate how the addition of 5, 10 and 30% oil into the fluid gel production process influences the gelation mechanism and the fluid gel properties. Following this, the oil content will be maintained at 10% oil and the properties will be measured as three different emulsifier types are used to stabilise the oil droplets.

6.2 Materials and methods

6.2.1 Materials

Tween 20 (P7949), sodium caseinate (C8654), κ-carrageenan (22048), potassium chloride (P9333), sodium azide (S2002) and PEG (81260) were purchased from Sigma Aldrich UK. Sunflower oil was provided by PepsiCo Intl. SDS (S/5200/53) was purchased from Fischer Scientific (Loughborough, UK). Double distilled water was used for the preparation of all solutions.

6.2.2 Emulsion and fluid gel preparation

6.2.2.1 Emulsion production

The fluid gel emulsions were produced by first making an emulsion with 50 wt.% oil with 5 wt.% emulsifier dissolved in the aqueous continuous phase and then later mixed with the gel solution to dilute the oil content to the desired oil fraction overall.

A coarse emulsion was initially prepared by using a Silverson mixer at 7500 rpm for 120 s at room temperature (23 °C). Nanoemulsions were produced by passing the coarse emulsion through an air-driven Microfluidizer fitted with a cooling tube submerged in equal proportions of ice and water (M110S fitted with a Y-type chamber, Microfluidics, Newton, MA, USA) for up to 3 passes through the device (Tween 20 – 3 passes, sodium caseinate – 1 pass and SDS – 2 passes). The droplet size distributions of the emulsions produced are shown in Figure 6.1. At each stage of production the oil droplet size distribution was measured and it was found that there was minimal change and therefore the results for this are not presented in this chapter.

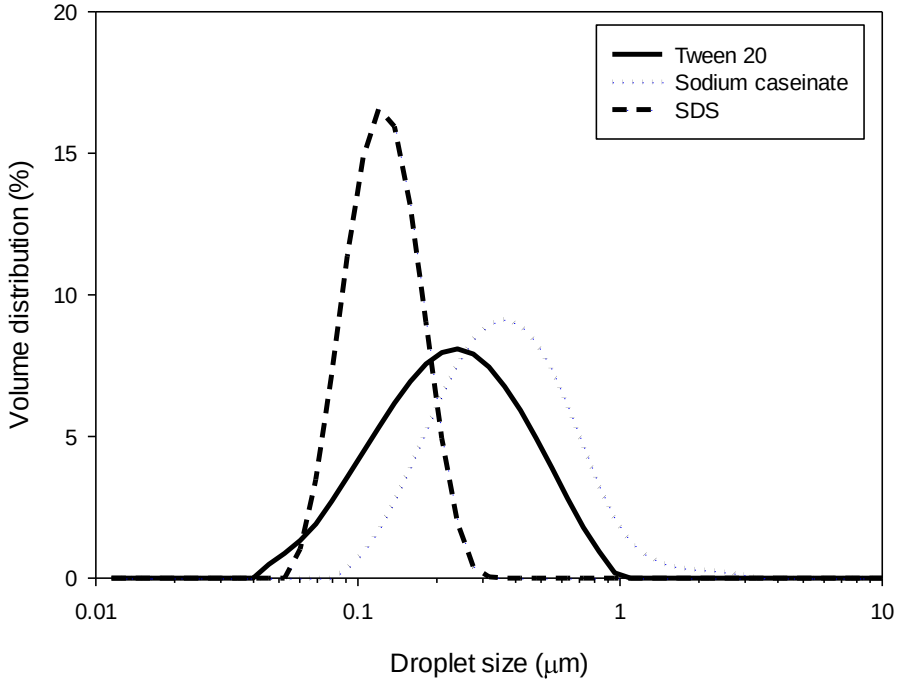

Figure 6.1: Droplet size distribution for 50 wt.% sunflower oil in water emulsions with 5 wt.% emulsifier from the Microfluidizer at an operating pressure of 150 MPa. Tween 20 was passed through the device three times, SDS twice and sodium caseinate only once.

6.2.2.2 Fluid gel and fluid gel emulsion production

A hot gel solution was prepared by heating to 80 °C for approximately an hour (or until all materials had dissolved and melted). Where fluid gel emulsions were produced the emulsion was added into the hot gel solution and left stirring for another half an hour. The concentration of the κ-c was, unless otherwise stated, 1.1wt.% in the aqueous phase, KCl was 0.2 wt.% and sodium azide was 0.01 wt.% overall, the latter was used for microbiological preservation of the samples. The droplet size of the emulsion was measured before and after addition into the gel.

In order to produce the fluid gel, the material was pumped through a non-sheared jacketed vessel which reduced the temperature of the gel to around 54 °C prior to entering the pin stirrer. The pin-stirrer was jacketed with counter current cooling maintained at 20 °C (inlet). See Figure 6.2 for the dimensions of the pin stirrer. Variable fluid gel flowrates were investigated but the pin stirrer rotation remained constant at 1500 rpm, this device's maximum, to produce the smallest fluid gel particles.

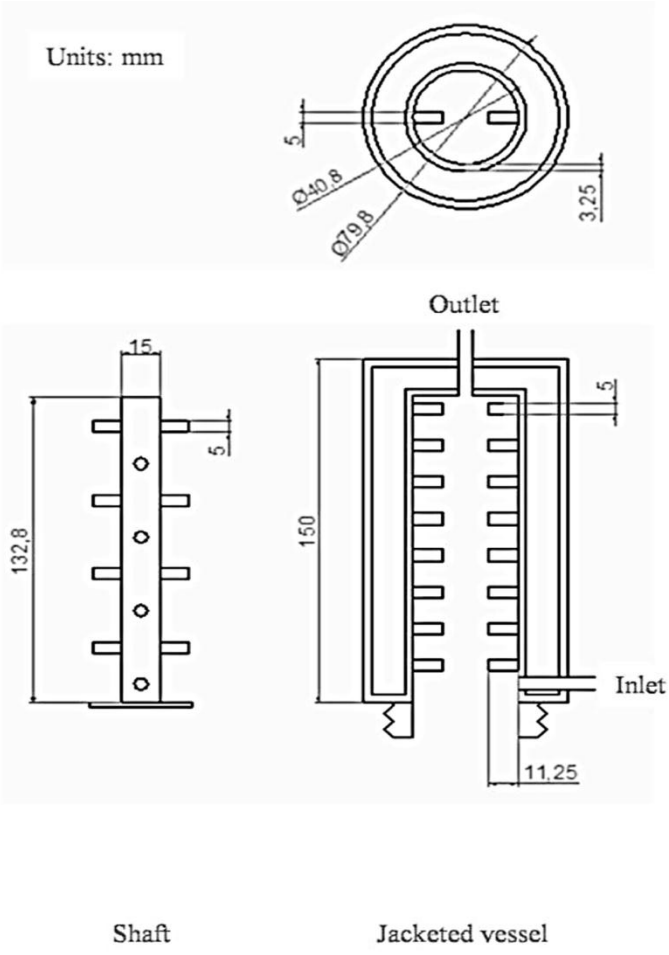

Figure 6.2: Dimensions of the jacketed pin-stirrer (Garrec, 2013)

The fluid gel exited the pin stirrer between 21 and 24 °C depending on the flowrate (10 – 100 ml/min) and was collected into sample pots submerged in ice. Actual temperature readings were recorded throughout all experiments. The samples were then transferred to a refrigerator

maintained at 5 °C. All samples were left for 24 hours before testing to allow post-processing effects to take place (Gabriele *et al.*, 2009).

6.2.3 Analytical methods

6.2.3.1 Fluid gel particle sizing

The fluid gel particle sizes were determined using a Malvern Mastersizer MS2000 (Malvern, UK) with a Hydro SM manual small volume sample dispersion unit attached. The refractive index of water and κ-carrageenan fluid gel particles are the same, therefore, the particles were dispersed within a 20% high molecular weight PEG solution. The purpose of this was to increase the refractive index of the continuous phase to 1.39 and differentiate between the continuous and dispersed phases for the laser scattering technique.

The sample was then pipetted into the Mastersizer. For the fluid gels only there was no need for post-processing of the results. However, for the fluid gels with oil droplets it was necessary to remove the peak that corresponds to the oil droplets and then scale the fluid gel peak until the cumulative volume adds to 100%.

The refractive indices were measured using a Rudolph research refractometer J357 (New Jersey, USA).

For more information on the Mastersizer see section 3.2.3.1.

6.2.3.2 Differential Scanning Calorimeter

Enthalpies and thermal transitions were detected using a Seteram μDSC3 evo differential scanning calorimeter (DSC). The device contains two screw-top cells containing the same weight of material as each other, one containing the sample and one the reference. For this work the reference was selected to be deionised and demineralised water to cancel out the temperature dependence of the specific heat capacity, thus providing non-sloping baselines. The samples were held isothermally at 20 °C for 10 minutes prior to ramping up to 70 °C at 1 °C/min. Before ramping down to 20 °C at the same rate, the sample was held isothermally at 70 °C for 10 minutes. The results shown within this chapter are only for the heating ramp.

6.2.3.3 Rheology

A Kinexus Pro rotational rheometer (Malvern, UK) was used for all rheology testing.

In order to understand the relationship between temperature and viscosity during cooling, gelation curves were measured. The temperature range measured was from 70 ^{0}C down to 20 ^{0}C at constant shear 200 s^{-1} with a cooling rate of 3 $^\circ$C/min. A 40 mm cone and plate with 4 degree angle was selected. A mid-point gelation temperature was correlated by determining the mid-point temperature half way between the temperature at which the gradient exceeded -0.01 Pa.s/$^\circ$C (assumed to be the onset of gelation) until it reduced past this value again.

To determine the rheological behaviour of the produced fluid gel and fluid gel emulsions two tests were carried out. Firstly, an oscillation test was carried out to determine the particle-particle interactions and therefore fluid gel's elastic modulus. A 60mm roughened parallel plate was used with a gap of 1mm and all tests were completed at 10 $^\circ$C. The material's elastic

properties were measured using a frequency sweep from 0.1 to 10 Hz. This was followed by a viscosity test to predict the fluid gels viscosity in the mouth, the viscosity of the samples were measured at a constant shear rate 50 s^{-1}, thought to be an average shear rate in the mouth (Wood, 1968), with a temperature ramp from 10 $^{\circ}$C up to 37 $^{\circ}$C.

6.2.3.4 Centrifugation

The volume of oil trapped within the gel particles was measured using a centrifugation technique. 5 g of fluid gel emulsion was diluted with 5 g of distilled water (exact weights were recorded) then vortex mixed for 30 s to disperse the fluid gel particles within the water and allow all free oil droplets to disperse within the continuous water phase. Following this the samples were then centrifuged for 1 hour at 4,000 rpm (24,000 rcf) in a Sigma Sci-Quip 2-5 centrifuge. The advantage of using a low acceleration is that it will separate off the fluid gel particles (they formed a compact layer at the top of the centrifuge tube) without centrifuging the nano-sized oil droplets out to the top too. The layer at the top of the centrifuge tube was removed and then the fluid from a few millimetres underneath this was pipetted off and weighed into a glass bottle. The glass bottle was then placed into an oven set at 100 ^{0}C to evaporate the water off. The bottle was then reweighed and the remaining weight was assumed to be the free oil (this was verified against a fluid gel only sample and the weight left was zero therefore there was minimal free polymer in the continuous phase interfering with the results). The free oil content was then calculated and by knowing the phase volume of particles it is possible to calculate the volume of oil included into the fluid gel particles.

6.3 Results and discussion

6.3.1 Influence of oil addition and fraction on fluid gel emulsion production

The effect of adding oil into the polysaccharide formulation during fluid gel production was tested. Each emulsion formulation change has been investigated methodically; firstly by measuring how the change in variable affects the gelation (using viscosity changes during gelation to indicate coil-coil reorganisation and DSC to indicate helix-helix aggregation), followed by investigating the final fluid gels and fluid gel emulsion's rheological properties (oscillation and viscosity testing) and the fluid gel particle size and oil inclusion efficiency. The fluid gel and fluid gel emulsions were made using a jacketed pin stirrer at 50 ml/min and 1500 rpm, whilst being cooled from 54 °C to ~21 °C.

To determine the influence of oil addition and fraction on the production of fluid gel emulsions the amount of κ-carrageenan was maintained at 1.1 wt.% in the aqueous continuous phase with the amount of KCl limited to 0.2 wt.% overall. The salt content in these experiments is restricted because the final salt content in a food product should be low due to its adverse implications on health (NHS, 2014). It should be noted that this means that as the amount of κ-c is decreased with increasing oil mass fraction, the KCl concentration in the continuous phase increases. Initially the changes during gelation were tested; the results are shown in Figure 6.3 and Table 6-1. The emulsions within this section are stabilised by Tween 20.

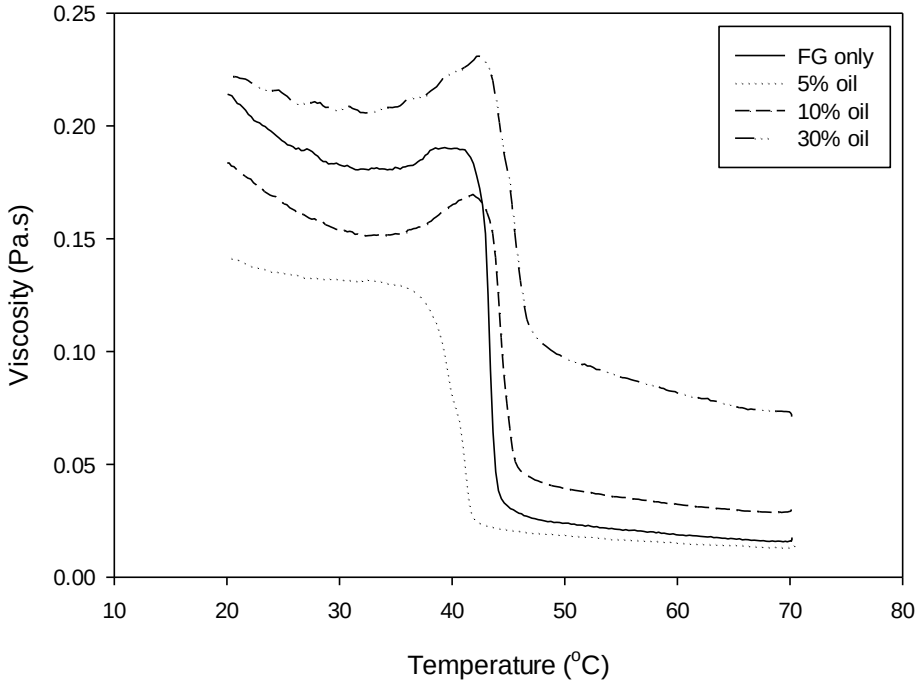

Figure 6.3: Fluid gel emulsion production viscosity profiles during the sheared cooling of 1.1 wt.% κ-c in the aqueous phase and 0.2 wt.% KCl at 3 °C/min and 200 s^{-1} for emulsions containing 5%, 10% and 30% oil compared to fluid gel only

Table 6-1: Peak areas for heat flow during cooling measured with DSC at 1 °C/min for 1.1 wt.% κ-c in the aqueous phase and 0.2 wt.% KCl for fluid gel (FG) only, 5%, 10% and 30%. All errors calculated from an average of three results.

Oil phase fraction	**Enthalpy of gelation (J/g)**	**Enthalpy of gelation* (J/g of FG)**	**Onset of gelation (°C)**	**End of gelation (°C)**
FG only	-0.30 ± 0.02	-0.30 ± 0.02	39.9 ± 0.9	30.6 ± 0.2
5% oil	-0.32 ± 0.01	-0.34 ± 0.01	41.0 ± 0.4	31.5 ± 0.3
10% oil	-0.28 ± 0.02	-0.31 ± 0.02	40.1 ± 0.8	32.1 ± 0.6
30% oil	-0.20 ± 0.01	-0.29 ± 0.01	40.8 ± 0.3	33.7 ± 0.3

* corrected per g of carrageenan

Figure 6.3 shows the onset of coil-helix ordering increases from 42 °C up to 47 °C as the oil fraction increases from 5% up to 30%. Since at the higher oil fractions, the continuous gel

phase has a higher salt concentration (κ-c:KCl reduces), this means that there are more K^+ ions to shield the repulsion between the sulphate groups on the κ-c polymer and this increases the onset of ordering (Morris *et al.*, 1980, Goodall and Norton, 1987). Despite this, the fluid gel only formulation (which has the lowest κ-c:KCl) shows similar gelation behaviour to the fluid gel with 10% oil. This suggests that the presence of the oil in the system also reduces the temperature at which the coils arrange into helices.

Analysis of the DSC results (Table 6-1) showed that the enthalpy of gelation decreases as the oil content increases, thus there is less aggregation of κ-c as the oil content increases. Since the overall mass fraction of κ-c decreases with increasing oil fraction this result would be expected as there is less κ-c to aggregate. To determine the influence of oil droplets, the third column in Table 6-1 is the enthalpy normalised to show the enthalpy per gram of κ-c present. Accounting for this, the same trend is still visible, but to less of an extent; the higher oil contents have a lower enthalpy for gelation.

To summarise, both the coil to helix transition (inferred by the gelation curves) and helix to helix transition (inferred by the DSC) is slowed by the presence of oil droplets.

The properties of these fluid gel emulsions were further tested, to investigate how the reduction in aggregation with addition of oil affects the fluid gel particle size and elastic modulus. The data for these will now be discussed (shown in Figure 6.4, Figure 6.5, Figure 6.6 and the oil inclusion is shown in Table 6-2).

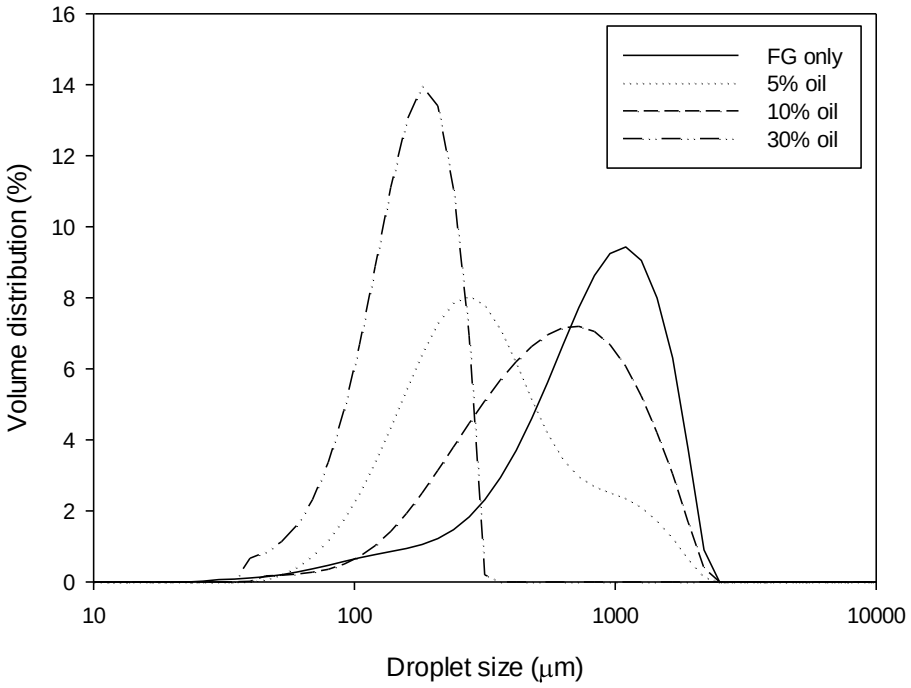

Figure 6.4: Fluid gel emulsion particle size distribution for fluid gel (FG) only, 5%, 10% and 30% oil made with 1.1 wt.% κ-carrageenan in the aqueous phase and 0.2 wt.% KCl at 50 ml/min (note that the peak for the oil droplet size has been removed).

It can be seen from Figure 6.4 that the distribution of fluid gel particle sizes produced in this work range from 0.2 to 1.2 mm. This particle size is larger than has previously been cited in literature, with the smallest cited at 1 μm (Garrec and Norton, 2012b, Garrec, 2013) up to ~0.05 mm (Gabriele *et al.*, 2009). The fluid gel particle size will depend strongly on the cooling and shearing conditions during the aggregation step of gelation as this will affect the extent of aggregation between gel nuclei and thus the final size of the fluid gel particles formed (Gabriele *et al.*, 2009). Figure 6.3 shows that the viscosity continues to rise as the temperature reduces down to 20 °C indicating that the helix-helix aggregation will not have fully completed and continues after exiting the pin stirrer (measured to be at 21 °C), where the gelation below these temperatures will be quiescent (Garrec, 2013). It is therefore believed that the fluid gel particles would aggregate to the order of 0.1 – 1 mm.

Figure 6.4 shows that the fluid gel particle sizes and distributions for 30% oil are smaller than the lower oil contents and fluid gel only. The smaller particle size is because the higher content of oil reduces aggregation between particles and thus the final fluid gel particle size is smaller. It is proposed that the oil blocks aggregation between particles by reducing the chance of the polysaccharide particles cross-linking with others. The fluid gel only, 5% and 10% oil have similar particle sizes, and, therefore, similar aggregation during the final quiescent cooling step.

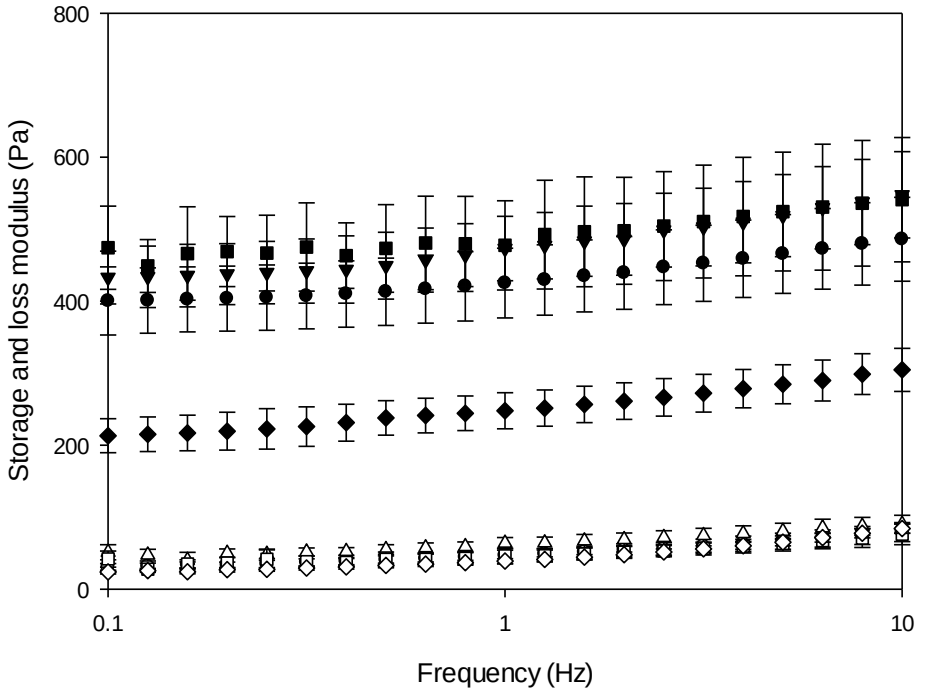

Figure 6.5: Measured storage and loss modulus, G' and G'', through a frequency sweep (0.1 – 10 Hz) of fluid gels (● for G' and ○ for G'') and fluid gel emulsions containing 5% (▼ for G' and △ for G''), 10% (■ for G' and □ for G'') and 30% (◆ for G' and ◇ for G'') oil made with 1.1wt.% κ-c in the aqueous phase and 0.2 wt.% KCl at 50 ml/min

It was shown from the oscillation rheology (Figure 6.5) that the fluid gel emulsion with 30% oil has the lowest elastic modulus thus agreeing with the hypothesis that the increased oil content reduces the aggregation between particles and therefore the elastic modulus of the

fluid gel. For the lower oil fractions and fluid gel only, the oscillation behaviour is similar indicating that the particle-particle interactions are also similar.

Table 6-2: Oil inclusion in fluid gel particles for the fluid gel emulsions containing 5%, 10% and 30% oil

Oil phase volume	Oil inclusion (%)	Overall weight % of oil droplets not trapped in the fluid gel particles
5%	78.8 ± 2.4	1.06 ± 0.12
10%	91.5 ± 0.7	0.41 ± 0.53
30%	98.8 ± 1.4	0.35 ± 0.41

Contrasting the fluid gel particle sizes (~0.1 – 1 mm) shown in Figure 6.4 with the oil droplet sizes (~200 nm), the fluid gel particles are over 100 times larger. This difference in scale makes it difficult to image the fluid gels to determine the location of oil droplets. Alternatively, a centrifuge technique was used to determine the oil inclusion efficiency. Table 6-2 shows the oil inclusion efficiency of the fluid gels, from the lowest efficiency at 5% oil, with approximately 80% oil inclusion, up to 99% for 30% oil. Comparing these results to the viscosity and enthalpy changes during gelation (Figure 6.3 and Table 6-1) the oil inclusion efficiency appears to be dependent on the temperature for onset of ordering. At the higher oil content the ordering is faster and therefore the oil is more likely to be trapped within the polymers as they order, whereas, the reverse is seen at the lower oil contents.

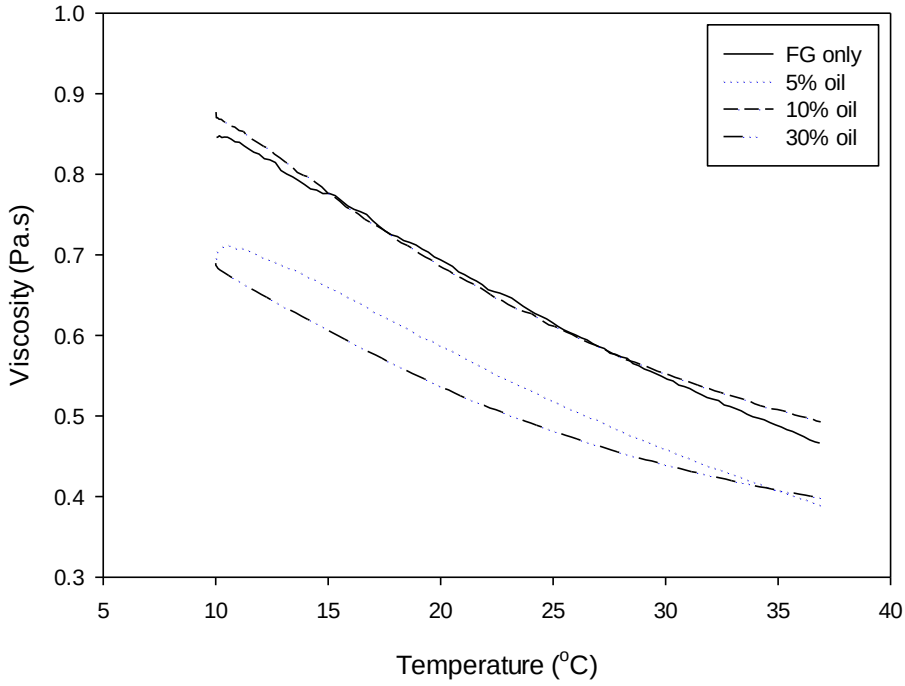

Figure 6.6: Viscosity profiles for fluid gel emulsions containing 5%, 10% and 30% oil made with 1.1 wt.% κ-carrageenan in the aqueous phase and 0.2 wt.% KCl at 50 ml/min measured at 200 s^{-1} starting at 10^0C and increasing to 37^0C (mouth temperature). Lines shown are an average of three repeats.

The viscosity curves (Figure 6.6) show 30% oil and 5% oil to have a lower viscosity than fluid gel only and 10% oil. The fluid gel emulsion with 30% oil has a high fraction of oil trapped in each fluid gel particle which reduces the resistance of the particles to flow, thereby decreasing the viscosity. The lower viscosity at 5% oil compared to 10% is likely to be due to the higher weight percent of oil droplets free within the continuous phase between the fluid gel particles. These oil droplets will be 'lubricating' the fluid gel particles and decreasing the viscosity. It is proposed that the 10% oil and fluid gel only system have similar viscosities because they have similar fluid gel particle sizes, and particle interactions. Also the free oil within the 10% oil sample is not high enough to lubricate the particles and reduce the viscosity.

To summarise, reducing κ-c:KCl increases the onset of gelation which increases oil inclusion. However, it was also observed that the onset of gelation can be reduced by the presence of oil droplets blocking helix-helix aggregation. At the highest oil content the reduction in aggregation produced a fluid gel emulsion with a lower elastic modulus and particle size. Additionally, when the oil inclusion is low (80%) the viscosity of the fluid gel emulsion is lower as the free oil lubricates the particles and decreases viscosity.

6.3.2 Influence of emulsifier choice used for stabilising the emulsions on fluid gel emulsion production

A series of fluid gel emulsions were produced using the same formulation and processing conditions as in the previous section except that the emulsifier type was changed: Tween 20 (non-ionic emulsifier), sodium caseinate (linear protein) and SDS (anionic emulsifier). The droplet sizes of the emulsions ranged from ~110 nm for SDS, ~200 nm for sodium caseinate and ~230 nm for Tween 20. It is expected that the presence of the emulsifier in the fluid gel emulsions will both affect the way the droplets interact within the gel and also affect the gelation from the free emulsifier in the continuous phase. All emulsion fluid gels produced here were plotted against the data from the fluid gel only systems also presented in the previous section. Initially the gelation behaviour of these fluid gel emulsions was tested.

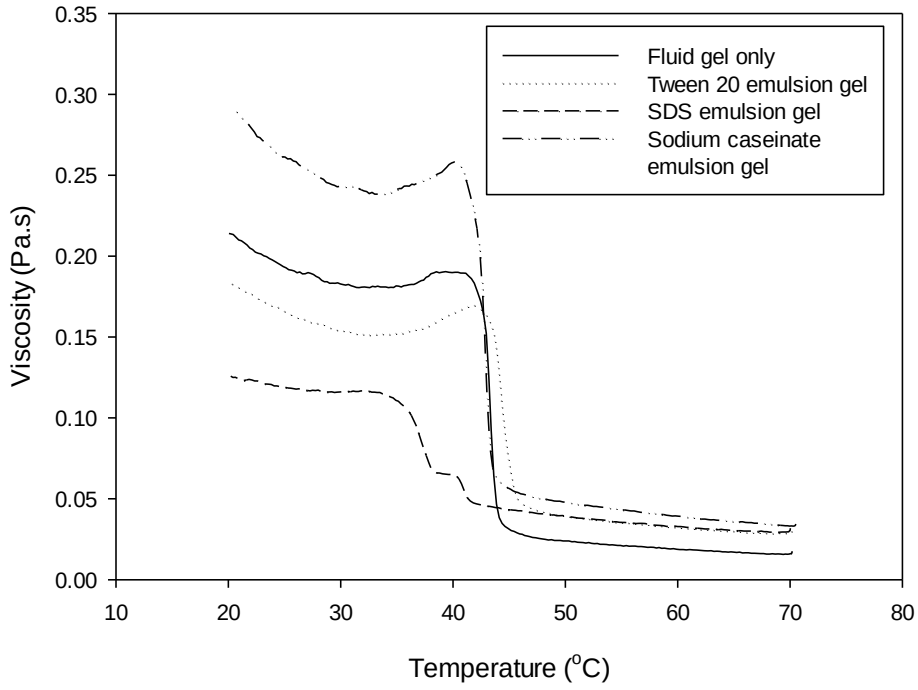

Figure 6.7: Fluid gel emulsion production viscosity profiles during the sheared cooling of 1.1 wt.% κ-c in the aqueous phase and 0.2 wt.% KCl at 3 ^{0}C/min and 200 s^{-1} for fluid gel only and 10% oil emulsions stabilised with Tween 20, SDS and sodium caseinate

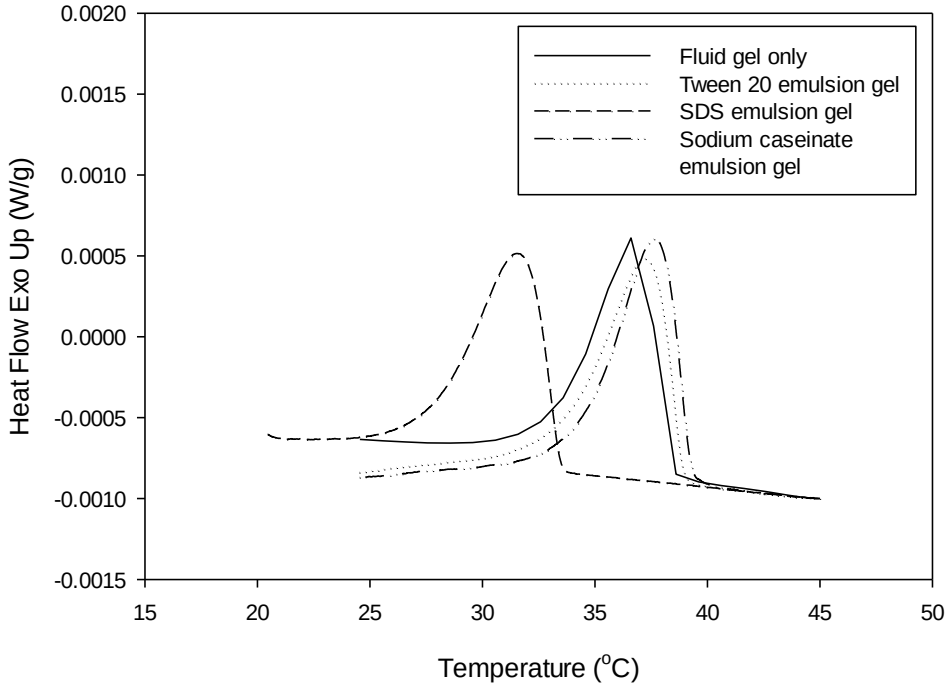

Figure 6.8: Cooling heat flow profile measured with DSC at 1 ^{0}C/min for 1.1 wt.% k-carrageenan in the aqueous phase and 0.2 wt.% KCl for fluid gel only and 10% oil emulsions stabilized with Tween 20, SDS and sodium caseinate.

Table 6-3: Peak areas for heat flow during cooling measured with DSC at 1°C/min for 1.1 wt.% κ-c in the aqueous phase and 0.2 wt.% KCl for 10% oil emulsions stabilised with Tween 20, SDS and sodium caseinate

	Enthalpy for gelation (J/g)	Midpoint of gelation (°C)
Fluid gel only	-0.30 ± 0.02	39.9 ± 0.9
Tween 20	-0.28 ± 0.02	36.1 ± 0.7
SDS	-0.27 ± 0.01	29.6 ± 0.2
Sodium caseinate	-0.28 ± 0.00	36.0 ± 0.2

It is observed from the gelation data that the temperature for viscosity increase and heat flow during gelation are similar for the emulsions stabilised by sodium caseinate and Tween 20 suggesting that the formation of the fluid gel is dominated by the gelation of the κ-c network for these emulsifier types. This agrees with previous work done on milk gels with κ-c and sodium caseinate (Nono *et al.*, 2011). In contrast, SDS shows a lower enthalpy for gelation suggesting less aggregation in the SDS fluid gel and a gelation temperature 6 °C lower. SDS is an anionic molecule used to stabilised oil droplets and when in excess forms micelles that will encapsulate the cationic potassium ions in solution and reduce salt binding helix-helix aggregation, thus reducing the temperature of gelation. Figure 6.7 shows that SDS has two stages where the viscosity increases. Since the helix-helix aggregation step is delayed by the reduced salt availability, the coil-helix ordering occurs before the helix-helix aggregation step.

To further investigate the rheological properties the oscillation and viscosity behaviour were measured, along with the fluid gel particle sizes and oil inclusion and these are shown in Figure 6.9, Figure 6.10, Figure 6.11 and Table 6-4.

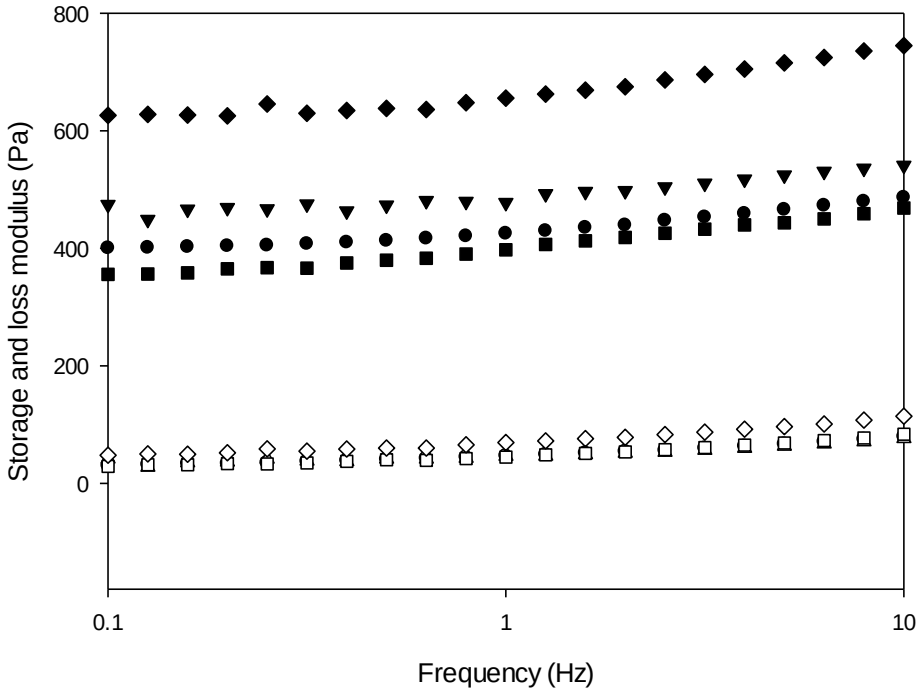

Figure 6.9: Measured storage and loss modulus, G' and G'', through a frequency sweep (0.1 – 10 Hz) for fluid gel only (● for G' and ○ for G'') of fluid gel emulsions (10% oil) containing emulsions stabilised by Tween 20 (▼ for G' and ▵ for G''), SDS (■ for G' and □ for G'') and sodium caseinate (♦ for G' and ◊ for G'') made with 1.1wt.% κ-c in the aqueous phase and 0.2 wt.% KCl at 50 ml/min

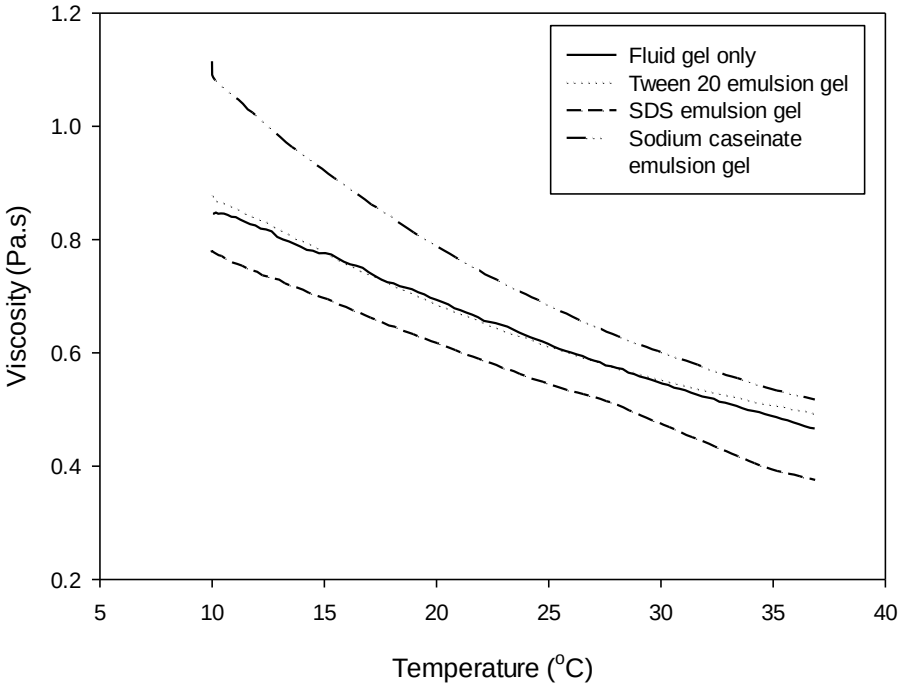

Figure 6.10: Viscosity profiles for fluid gel only and fluid gel emulsions (10% oil) containing emulsions stabilized by Tween 20, SDS and sodium caseinate made with 1.1 wt.% k-carrageenan in the aqueous phase and 0.2 wt.% KCl at 50 ml/min measured at 200 s^{-1} starting at 10^{0}C and increasing to 37^{0}C (mouth temperature). Lines shown are an average of three repeats.

Table 6-4: Oil inclusion in fluid gel particles for the fluid gel emulsions stabilised by Tween 20, SDS and sodium caseinate

Emulsifier type	Oil inclusion
Tween 20	91.5 ± 0.7%
SDS	56.8 ± 1.0%
Sodium caseinate	87.6 ± 4.5%

The fluid gel emulsions with SDS had a lower elastic modulus and viscosity than the emulsions stabilised with Tween 20 or sodium caseinate. The lower elastic modulus is due to the weaker gel that is formed as a consequence of the lower salt availability and the reduced aggregation (evidence in Table 6-3). The weaker particulate gel will result in a lower viscosity

product since when force is applied to cause the particles to flow they will deform more easily (Figure 6.10). In addition, the oil inclusion efficiency is greatly reduced to 55% which could be a result of the lower gelation temperature thus reducing the oil entrapment efficiency within the particles. The high content of free oil between the particles will further reduce the viscosity by lubricating the fluid gel particles under flow.

The fluid gel emulsions with sodium caseinate present exhibited a higher G' and higher viscosity compared to the other emulsifiers. Addition of sodium caseinate will strengthen the gel by interacting with the sulphate groups on the κ-c chains via the predominantly positive regions of the protein (Ribeiro *et al.*, 2004). This will result in a higher viscosity since the particles will be harder to deform and flow. Additionally, the association of sodium caseinate and κ-c will result in more free chains at the particle surfaces creating a larger interaction between particles than the low molecular weight Tween 20 system and thus increasing the elastic modulus. The oil inclusion efficiency (Table 6-4) is similar to when Tween 20 is used. This therefore agrees with the hypothesis that the gel network is dependent on the κ-c and not on the selection of either Tween 20 or sodium caseinate and does not affect the oil entrapment during ordering and formation of the gel network.

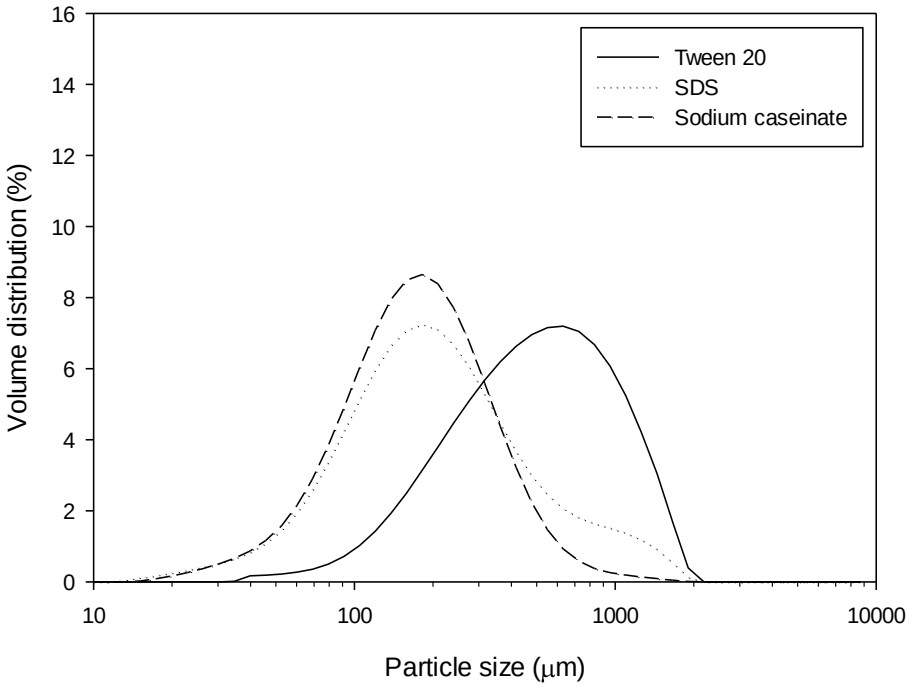

Figure 6.11: Fluid gel emulsion particle size distributions for emulsions stabilised by Tween 20, SDS and sodium caseinate made with 1.1 wt.% κ-c in the aqueous phase and 0.2 wt.% KCl at 50 ml/min (the peak for the oil droplet size has been removed)

Analysis of the particle size distributions, Figure 6.11, showed smaller fluid gel particle sizes when sodium caseinate was used compared to Tween 20. This shows that during the quiescent cooling step there was less inter particle aggregation when sodium caseinate was present. Sodium caseinate has negatively charged regions and consequently it is thought that the extent of aggregation is reduced. The same lower fluid gel size is observed with the anionic SDS.

6.4 Chapter conclusions

The main conclusion is that a fluid gel can be produced with nanoemulsion droplets trapped within the gel particles. This will enhance the flavour acceptance of fluid gels for their use as

fat mimetics. It was shown that the properties of these fluid gel emulsions can be manipulated be changing the polysaccharide or salt concentration to manipulate the gelation behaviour.

The temperature for onset of gelation is increased by increasing the salt concentration, which also increases the rate of gelation and traps more oil within the fluid gel particles. The presence of more oil droplets blocks the extent of aggregation during gelation and produces a fluid gel with lower elasticity. The results for emulsions stabilised by SDS reinforced the link between gelation rate and oil entrapment. SDS reduced salt availability thus reducing the rate of gelation and the oil entrapment was significantly reduced from 90% with Tween 20 to 55% with SDS. The viscosity of the fluid gel emulsions were then lower than would be expected if the gelation rate was slow and this was because less oil was trapped and was then free between the particles to lubricate the flow. Viscosity was also a function of the oil phase volume, as this was increased to 30% oil the viscosity reduced because the particles were more easily deformed due to the high oil content within the gel particles.

The enthalpy of gelation (dependent on salt concentration) appears to influence the final particle size and elastic modulus. A higher enthalpy of gelation indicates more helix-helix aggregation which increases the extent of particle growth during quiescent cooling thus producing a larger particle size and a fluid gel emulsion with a higher elastic modulus. The elastic modulus was also shown to be increased by addition of sodium caseinate, the polymer associates with the sulphate groups on the κ-c via the negative regions on the polymer to form a stronger gel with more particle-particle interactions.

This work has shown it is possible make fluid gels with oil incorporated into the structure and the properties can be manipulated by changing the formulation to tune into the desired fat properties.

CHAPTER 7. CONCLUSIONS AND FURTHER WORK

7.1 Main conclusions

Although the individual conclusions are summarised at the end of each chapter, the main findings are reiterated here with emphasis on the industrial applications of the results.

The overall purpose of this work was to further the process engineering knowledge for the production of fat mimetic products with the intention of reducing obesity in the western world. Nanoemulsions were of particular interest compared to micron sized emulsions as they are perceived as creamier thus the content of fat can be reduced and still match the fattiness that is perceived by the consumer. Another advantage is that oil soluble vitamins and minerals when solubilised with the dispersed phase of a nanoemulsion once consumed they are absorbed more efficiently into the blood stream. This targeted delivery may be used to incorporate known vitamins and minerals that are absent or low in the target consumer's diet.

Chapters 3 and 4 have extended the current knowledge of nanoemulsion production for a much broader range of viscosities for both emulsion types using high pressure homogenisers. It has been highlighted that the highest inefficiency related to the industrially applicable valve homogeniser is from droplet coalescence. Once the viscosity of the continuous phase is increased the rate of coalescence is significantly reduced. By extending this theory further, when the continuous phase viscosity is increased and the turbulence regime is fully turbulent viscous, the efficiencies of the two devices are matched. In practice, this means that if the continuous phase of the emulsion were more viscous the production costs would be less as less processing would be required. For the situations where it is unacceptable to manipulate

the formulation this thesis has highlighted the need to research different homogeniser valve geometries.

Whilst predominantly the aim of chapters 3 and 4 was to explore the processing efficiency of nanoemulsion production, the W/O nanoemulsion produced in Chapter 4 could find industrial application as an oil mimetic product.

Chapter 5 explored the potential advantage that flavour/volatile release is faster in nanoemulsions. The data contradicted this theory, with both continuous and dispersed phase volatile release being higher for the larger droplet sizes. The difference was not too large however, the implication would be that for nanoemulsion products more flavour would have to be added to match a micron emulsion alternative.

Chapter 6 tested an application for nanoemulsion technology. Fluid gels are currently used as fat mimetics, however, one of the common criticisms of them are the bland taste, this chapter has shown that up to 30% oil can be included within the particles to potentially promote its consumer acceptance. Additionally, it was shown that the rheological properties can still be manipulated to match the fat properties it is mimicking.

7.2 Further work

7.2.1 O/W nanoemulsions

The chapter on O/W nanoemulsion production extended the understanding of how the HPH and Microfluidizer cause droplet break-up for viscosity ratios 0.1 – 100. Although after

conducting the research for this chapter, the main area for further work was to understand how the two high pressure devices cause droplet break-up at viscosity ratios below 0.1. This work was completed in chapter 3.

Extending the CFD work on the Microfluidizer to model two phase flow would be useful for verifying which areas of the geometry are crucial for producing a tight distribution of shearing forces and minimising coalescence. The droplet size distributions made from the HPH were wider than the Microfluidizer and it would be useful to invest in developing new geometries that will reduce coalescence and produce a more uniform distribution of shearing forces. If the HPH was redesigned to allow the jets produced at the exit of the valve gap to impinge this would increase the uniformity of shearing forces and cause extensional flow in a similar way to the Microfluidizer. See Figure 7.1.

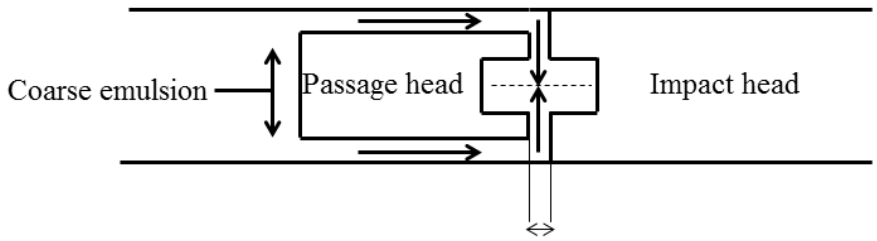

Figure 7.1: Schematic diagram of a proposed alternative geometry for a valve homogeniser to reduce the chance of coalescence (note the diagram is not drawn to scale)

It should be noted that Figure 7.1 is not drawn to scale and the impinging region would have to be smaller than the diagram would suggest.

7.2.2 W/O nanoemulsions

High pressure homogenisation to produce W/O nanoemulsions was novel and consequently there are several areas for future research. PGPR was the only emulsifier investigated in this work thus looking at different emulsifier types to investigate how different adsorption times and interfacial properties influence the break-up would be important for thorough investigation before commercialisation. Theoretically emulsifier adsorption time should be less influential in viscous flow (Walstra, 2005), and the interfacial tension and elasticity would be more important. Since lecithin is commonly used in W/O emulsions and produces an elastic interface it should be the next to be explored.

Although homogenisation of water-in-sunflower oil emulsions was shown to be independent of geometry (HPH or Microfluidizer) the transition to this independence should be investigated. The work done on varying viscosity ratio attempted to develop this understanding however these results had large variability. These results should be repeated for another emulsifier to see if the error is reduced and a trend is more distinguishable.

The W/O nanoemulsion produced in this work would be a good oil mimetic which could be developed further to be used as an oil mimetic coating for savoury food surfaces e.g. a potato crisp. A potential disadvantage of this application is that the water droplets may absorb into the low moisture surface and soften the product. If it is possible to sinter fat crystals at the interface of these nano-sized water droplets, this problem would be overcome. These fat shells should also promote the creaminess of the product.

7.2.3 Flavour release

It has been shown to more of an extent than any research preceding it that droplet size may be a function of both continuous and dispersed phase flavour release within O/W emulsions. An option for further work is to test if the trends for flavour release are similar for W/O emulsions, and determine with a sensory panel if the differences in flavour release can be detected by humans.

It was interesting to see that as the droplet size approached 150 nm from 1 μm for 10% oil, the aqueous continuous phase flavour release rate increased. Further research should investigate the change in flavour release mechanisms for droplet sizes within this range and phase volumes lower than 10% to determine if this is a linear relationship, or if it is dependent on a critical droplet size.

The relationship between the dispersed oil soluble flavour and its release was less apparent, although the results indicated that if the emulsion destabilised the release was higher. Therefore it would be good to investigate the influence of emulsion stability on release by changing the emulsifier type and concentration. Additionally, investigating different oil soluble volatiles should change the release rate and give a more thorough indication on the release behaviour.

The testing protocol measured release within equilibrium conditions, as once the participant swallows the emulsion the release is likely to have neared equilibrium. Future work should test more dynamic conditions. This could be by using trained panellists to rate through seconds in time the intensity of flavour detected.

7.2.4 Nanoemulsions within fluid gels

As this was the first study on introducing oil droplets into fluid gels with κ-carrageenan there are many opportunities for further work.

The fraction of quiescent cooling was high for this work leading to fluid gel particles of 500 μm. There was evidence that this amount of quiescent cooling was not required for entrapping oil within the gel particles, this should be investigated further by shearing to temperatures lower than 20 °C: 15, 10 and 5 °C and therefore producing smaller particle sizes and then measuring the oil inclusion.

Fluid gels and fluid gel emulsions were produced in this chapter and the resulting microstructural changes were measured. The next step is to verify the sensory properties of these fluid gels in particular the fat mimicking properties (lubrication) using a tribometer and a sensory panel. Fluid gels, fluid gel emulsions and fluid gels with emulsion stirred into them should be compared.

One of the reasons for using nanoemulsion droplets, instead of emulsion droplet sizes more commonly found in industrial food products (1 – 10 μm), is they should enhance the creaminess perception along with providing the other benefits associated with nanoemulsions (Lett *et al.*, 2014). This hypothesis should be verified by testing the lubrication of fluid gel emulsions with different droplet sizes. Although when comparing these fluid gel emulsions the extent of aggregation may alter as the droplet sizes become larger thus also changing the lubricative properties.

κ-carrageenan was selected as the biopolymer used within this work because the relatively slow gelation rate produces small particle sizes similar to oil droplets ~1 μm (Gabriele *et al.*, 2009) and therefore mimic oil or fat better than alternative biopolymers. However, the disadvantage of using κ-carrageenan is that it requires salt to gel, and many food manufacturers are aiming to reduce salt from their ingredients list as it is known to increase blood pressure (NHS, 2014). Other biopolymers such as agarose or gellan should be compared to the results with κ-carrageenan.

CHAPTER 8. REFERENCES

ANDERSON, N. S., CAMPBELL, J. W., HARDING, M. M., REES, D. A. & SAMUEL, J. W. 1969. X-ray diffraction studies of polysaccharide sulphates: double helix models for k- and l-carrageenans. *J Mol Biol,* 45**,** 85-99.

ARONSON, M. P. & PETKO, M. F. 1993. Highly Concentrated Water-in-Oil Emulsions: Influence of Electrolyte on Their Properties and Stability. *Journal of Colloid and Interface Science,* 159**,** 134-149.

BALSON, T. G. 1999. HLB: Is It a Valuable Concept or a Curiosity? *In:* KARSA, D. R. (ed.) *Industrial Applications of Surfactants IV.* Woodhead Publishing.

BINKS, B. P. 1998. Modern Advances in Emulsion Science. *Royal Society of Chemistry.*

BINKS, B. P. & FLETCHER, P. D. I. 2001. Particles Adsorbed at the Oil−Water Interface: A Theoretical Comparison between Spheres of Uniform Wettability and "Janus" Particles. *Langmuir,* 17**,** 4708-4710.

BIRDI, E. 1977. *Micellization, Solubilization and Microemulsions,* New York and London, Plenum Press.

BOHINC, K., KRALJ-IGLIČ, V. & IGLIČ, A. 2001. Thickness of electrical double layer. Effect of ion size. *Electrochimica Acta,* 46**,** 3033-3040.

BROWN, C. R. T., CUTLER, A. N. & NORTON, I. T. 1995. Liquid based composition comprising a gelling polysaccharide capable of forming a reversible gel and a method of preparing such composition. Google Patents.

BROWN, C. R. T., FAIRLEY, P. & LAM, S. 1999. *Hair treatment compositions*.

BRYCE, T. A., CLARK, A. H., REES, D. A. & REID, D. S. 1982. Concentration dependence of the order-disorder transition of carrageenans. Further confirmatory evidence for the double helix in solution. *Eur J Biochem,* 122**,** 63-9.

CAREY, M., ASQUITH, T., LINFORTH, R. & TAYLOR, A. 2002. Modeling the Partitiion of Volatile Aroma Compounds from a Cloud Emulsion. *Journal of Agricultural and Food Chemistry***,** 1985-1990.

CASOLI, P., VACCA, A. & BERTA, G. L. 2010. A numerical procedure for predicting the performance of high pressure homogenizing valves. *Simulation Modelling Practice and Theory,* 18**,** 125-138.

CHAN, C. K., PERROT, F. & BEYSENS, D. 1988. Effects of Hydrodynamics on Growth: Spinodal Decomposition under Uniform Shear Flow. *Physical Review Letters,* 61**,** 412-415.

CHENG, C.-J., CHU, L.-Y. & XIE, R. 2006. Preparation of highly monodisperse W/O emulsions with hydrophobically modified SPG membranes. *Journal of Colloid and Interface Science,* 300**,** 375-382.

COOK, E. J. & LAGACE, A. P. 1985. *Apparatus for forming emulsions*. Aug 6, 1985.

COURTHAUDON, J.-L., DICKINSON, E. & DALGLEISH, D. G. 1991. Competitive adsorption of β-casein and nonionic surfactants in oil-in-water emulsions. *Journal of Colloid and Interface Science,* 145**,** 390-395.

CUSSLER, E. L. 2009. *Fundamentals of Mass Transfer*

Diffusion, Cambridge University Press.

DE ROOS, K. B. 2003. Effect of texture and microstructure on flavour retention and release. *International Dairy Journal,* 13**,** 593-605.

DICKINSON, E. 2009. 2 - Hydrocolloids and emulsion stability. *In:* PHILLIPS, G. O. & WILLIAMS, P. A. (eds.) *Handbook of Hydrocolloids (Second edition).* Woodhead Publishing.

DICKINSON, E., EVISON, J., GRAMSHAW, J. W. & SCHWOPE, D. 1994. Flavour release from a protein-stabilized water-in-oil-in-water emulsion. *Food Hydrocolloids,* 8**,** 63-67.

DONSÌ, F., SESSA, M. & FERRARI, G. 2011a. Effect of Emulsifier Type and Disruption Chamber Geometry on the Fabrication of Food Nanoemulsions by High Pressure Homogenization. *Industrial & Engineering Chemistry Research,* 51**,** 7606-7618.

DONSÌ, F., SESSA, M. & FERRARI, G. 2011b. Effect of Emulsifier Type and Disruption Chamber Geometry on the Fabrication of Food Nanoemulsions by High Pressure Homogenization. *Industrial & Engineering Chemistry Research*.

DOWLING, P. K. K. M. C., DAVID R. 2012. Chapter 8 - Laminar Flow. *In:* DOWLING, P. K. K. M. C., DAVID R. (ed.) *Fluid Mechanics (Fifth Edition).* Boston: Academic Press.

DOYEN, K., CAREY, M., LINFORTH, R. S. T., MARIN, M. & TAYLOR, A. J. 2001. Volatile Release from an Emulsion: Headspace and In-Mouth Studies. *Journal of Agricultural and Food Chemistry,* 49**,** 804-810.

FEIGL, K., MEGIAS-ALGUACIL, D., FISCHER, P. & WINDHAB, E. J. 2007. Simulation and experiments of droplet deformation and orientation in simple shear flow with surfactants. *Chemical Engineering Science,* 62**,** 3242-3258.

FERNÁNDEZ FARRÉS, I., MOAKES, R. J. A. & NORTON, I. T. 2014. Designing biopolymer fluid gels: A microstructural approach. *Food Hydrocolloids*.

FLOURY, J., BELLETTRE, J., LEGRAND, J. & DESRUMAUX, A. 2004a. Analysis of a new type of high pressure homogeniser. A study of the flow pattern. *Chemical Engineering Science,* 59**,** 843-853.

FLOURY, J., DESRUMAUX, A. & LARDIÈRES, J. 2000. Effect of high-pressure homogenization on droplet size distributions and rheological properties of model oil-in-water emulsions. *Innovative Food Science & Emerging Technologies,* 1**,** 127-134.

FLOURY, J., LEGRAND, J. & DESRUMAUX, A. 2004b. Analysis of a new type of high pressure homogeniser. Part B. study of droplet break-up and recoalescence phenomena. *Chemical Engineering Science,* 59**,** 1285-1294.

FRASCH-MELNIK, S., NORTON, I. T. & SPYROPOULOS, F. 2010. Fat-crystal stabilised w/o emulsions for controlled salt release. *Journal of Food Engineering,* 98**,** 437-442.

GABRIELE, A. 2011. *Fluid gels: Formation, production and lubrication.* Formulation Engineering, The University of Birmingham.

GABRIELE, A., SPYROPOULOS, F. & NORTON, I. T. 2009. Kinetic study of fluid gel formation and viscoelastic response with kappa-carrageenan. *Food Hydrocolloids,* 23**,** 2054-2061.

GABRIELE, A., SPYROPOULOS, F. & NORTON, I. T. 2010. A conceptual model for fluid gel lubrication. *Soft Matter,* 6**,** 4205-4213.

GARREC, D. A. 2013. *Understanding Fliud Gels and Hydrocolloid Technology.* Doctor of Engineering, The University of Birmingham.

GARREC, D. A., GUTHRIE, B. & NORTON, I. T. 2013. Kappa carrageenan fluid gel material properties. Part 1: Rheology. *Food Hydrocolloids,* 33**,** 151-159.

GARREC, D. A. & NORTON, I. T. 2012a. The influence of hydrocolloid hydrodynamics on lubrication. *Food Hydrocolloids,* 26**,** 389-397.

GARREC, D. A. & NORTON, I. T. 2012b. Understanding fluid gel formation and properties. *Journal of Food Engineering,* 112**,** 175-182.

GAVI, E., MARCHISIO, D. L. & BARRESI, A. A. 2007. CFD modelling and scale-up of Confined Impinging Jet Reactors. *Chemical Engineering Science,* 62**,** 2228-2241.

GHOSH, S. & ROUSSEAU, D. 2011. Fat crystals and water-in-oil emulsion stability. *Current Opinion in Colloid & Interface Science,* 16**,** 421-431.

GOODALL, D. M. & NORTON, I. T. 1987. Polysaccharide conformations and kinetics. *Accounts of Chemical Research***,** 59-65.

GOV.UK. 2013. *Reducing obesity and improving diet* [Online]. Available: https://www.gov.uk/government/policies/reducing-obesity-and-improving-diet [Accessed 05/08/2014 2014].

GRACE, H. P. 1982. Dispersion phenomena in high-viscosity immiscible fluid systems and application of static mixers as dispersion devices in such systems. *Chemical Engineering Communications,* 14**,** 225-277.

GRIFFIN, W. C. 1949. Classification of surface-active agents by HLB. *J. Soc. Cosmet. Chem. 1 (1949)***,** pp 311 - 326.

GUINARD, J.-X., WEE, C., MCSUNAS, A. & FRITTER, D. 2002. Flavor release from salad dressing varying in fat and garlic flavor. *Food Quality and Preference,* 13**,** 129-137.

GÜLSEREN, İ. & CORREDIG, M. 2012. Interactions at the interface between hydrophobic and hydrophilic emulsifiers: Polyglycerol polyricinoleate (PGPR) and milk proteins, studied by drop shape tensiometry. *Food Hydrocolloids,* 29**,** 193-198.

HÅKANSSON, A., FUCHS, L., INNINGS, F., REVSTEDT, J., TRÄGÅRDH, C. & BERGENSTÅHL, B. 2011. High resolution experimental measurement of turbulent flow field in a high pressure homogenizer model and its implications on turbulent drop fragmentation. *Chemical Engineering Science,* 66**,** 1790-1801.

HÅKANSSON, A., FUCHS, L., INNINGS, F., REVSTEDT, J., TRÄGÅRDH, C. & BERGENSTÅHL, B. 2012a. Experimental validation of k–ε RANS-CFD on a high-pressure homogenizer valve. *Chemical Engineering Science,* 71**,** 264-273.

HÅKANSSON, A., INNINGS, F., REVSTEDT, J., TRÄGÅRDH, C. & BERGENSTÅHL, B. 2012b. Estimation of turbulent fragmenting forces in a high-pressure homogenizer from computational fluid dynamics. *Chemical Engineering Science,* 75**,** 309-317.

HÅKANSSON, A., INNINGS, F., TRÄGÅRDH, C. & BERGENSTÅHL, B. 2013. A high-pressure homogenization emulsification model—Improved emulsifier transport and hydrodynamic coupling. *Chemical Engineering Science,* 91**,** 44-53.

HÅKANSSON, A., TRÄGÅRDH, C. & BERGENSTÅHL, B. 2009. Dynamic simulation of emulsion formation in a high pressure homogenizer. *Chemical Engineering Science,* 64**,** 2915-2925.

HANCOCKS, R. D., SPYROPOULOS, F. & NORTON, I. T. 2012. Products of membrane emulsification. *In preparation*.

HARRISON, M., HILLS, B. P., BAKKER, J. & CLOTHIER, T. 1997. Mathematical Models of Flavor Release from Liquid Emulsions. *Journal of Food Science,* 62**,** 653-664.

HEFFERNAN, S. P., KELLY, A. L. & MULVIHILL, D. M. 2009. High-pressure-homogenised cream liqueurs: Emulsification and stabilization efficiency. *Journal of Food Engineering,* 95**,** 525-531.

HEMAR, Y., HALL, C. E., MUNRO, P. A. & SINGH, H. 2002. Small and large deformation rheology and microstructure of κ-carrageenan gels containing commercial milk protein products. *International Dairy Journal,* 12**,** 371-381.

HENRY, J. 2007. *The Formation and Characterisation of Edible Nano-emulsions.* Engineering Doctorate, The University of Birmingham.

HENRY, J. V. L., FRYER, P. J., FRITH, W. J. & NORTON, I. T. 2009. Emulsification mechanism and storage instabilities of hydrocarbon-in-water sub-micron emulsions stabilised with Tweens (20 and 80), Brij 96v and sucrose monoesters. *Journal of Colloid and Interface Science,* 338**,** 201-206.

HENRY, J. V. L., FRYER, P. J., FRITH, W. J. & NORTON, I. T. 2010. The influence of phospholipids and food proteins on the size and stability of model sub-micron emulsions. *Food Hydrocolloids,* 24**,** 66-71.

HINZE, J. 1955. Fundamentals of the hydrodynamic mechanism of splitting in dispersion processes. *AIChE Journal,* 1**,** 289-295.

HODGE, S. M. & ROUSSEAU, D. 2003. Flocculation and coalescence in water-in-oil emulsions stabilized by paraffin wax crystals. *Food Research International,* 36**,** 695-702.

HODKINSON, J. & GREENLEAVES, I. 1963. Computations of light-scattering and extinction by spheres according to diffraction and geometrical optics, and some comparisons with the Mie theory. *JOSA,* 53**,** 577-588.

HÖHLER, R., COHEN-ADDAD, S. & DURIAN, D. J. 2014. Multiple light scattering as a probe of foams and emulsions. *Current Opinion in Colloid & Interface Science,* 19**,** 242-252.

HOWARTH, W. J. 1964. Coalescence of drops in a turbulent flow field. *Chemical Engineering Science,* 19**,** 33-38.

HSCIC.GOV. 2014. *Statistics on Obesity, Physical Activity and Diet - England, 2014* [Online]. Available: http://www.hscic.gov.uk/catalogue/PUB13648.

INNINGS, F. & TRÄGÅRDH, C. 2007. Analysis of the flow field in a high-pressure homogenizer. *Experimental Thermal and Fluid Science,* 32**,** 345-354.

JAFARI, S., HE, Y. & BHANDARI, B. 2007a. Optimization of nano-emulsions production by microfluidization. *European Food Research and Technology,* 225**,** 733-741.

JAFARI, S. M., ASSADPOOR, E., HE, Y. & BHANDARI, B. 2008. Re-coalescence of emulsion droplets during high-energy emulsification. *Food Hydrocolloids,* 22**,** 1191-1202.

JAFARI, S. M., HE, Y. & BHANDARI, B. 2007b. Production of sub-micron emulsions by ultrasound and microfluidization techniques. *Journal of Food Engineering,* 82**,** 478-488.

JOSCELYNE, S. M. & TRÄGÅRDH, G. 2000. Membrane emulsification — a literature review. *Journal of Membrane Science,* 169**,** 107-117.

KABALNOV, A. 1998. Thermodynamic and theoretical aspects of emulsions and their stability. *Current Opinion in Colloid & Interface Science,* 3**,** 270-275.

KELLY, W. & MUSKE, K. 2004. Optimal operation of high-pressure homogenization for intracellular product recovery. *Bioprocess and Biosystems Engineering,* 27**,** 25-37.

KOLMOGOROV, A. N. 1949. On the breakage of drops in a turbulent flow. *Mathematics and mechanics,* 1**,** 339-343.

KUMAR, A. & VENKATESU, P. 2014. Does the stability of proteins in ionic liquids obey the Hofmeister series? *International Journal of Biological Macromolecules,* 63**,** 244-253.

LANGRIDGE, J. 2004. *Correlating Instrumental and Sensory Analyses of Flavour.* The University of Nottingham.

LE RÉVÉREND, B. J. D., TAYLOR, M. S. & NORTON, I. T. 2011. Design and application of water-in-oil emulsions for use in lipstick formulations. *International Journal of Cosmetic Science***,** no-no.

LEE, L., NIKNAFS, N., HANCOCKS, R. & NORTON, I. T. 2013. Emulsification: Mechanistic Understanding. *Trends in Food Science & Technology,* 31**,** 72-78.

LEE, L. & NORTON, I. T. 2013. Comparing droplet breakup for a high-pressure valve homogeniser and a Microfluidizer for the potential production of food-grade nanoemulsions. *Journal of Food Engineering,* 114**,** 158-163.

LEONG, T. S. H., WOOSTER, T. J., KENTISH, S. E. & ASHOKKUMAR, M. 2009. Minimising oil droplet size using ultrasonic emulsification. *Ultrasonics Sonochemistry,* 16**,** 721-727.

LETT, A. M., NORTON, J. E., YEOMANS, M. R. & NORTON, I. T. 2014. Influence of oil droplet size on the rheological and tribological properties of oil-in-water emulsion systems in relation to sensory perception (Under submission).

LIFSHITZ;, M. & SLYOZOV, J. V. 1961. *Journal Physics and Chemistry of Solids,* 19**,** 35-50.

LINFORTH, R., CABANNES, M., HEWSON, L., YANG, N. & TAYLOR, A. 2010. Effect of Fat Content on Flavor Delivery during Consumption: an in Vivo Model. *Journal of Agricultural and Food Chemistry***,** 6905-6911.

LINFORTH, R. & TAYLOR, A. J. 2000. Persistence of Volatile Compounds in the Breath after Their Consumption in Aqueous Solutions. *Journal of Agricultural and Food Chemistry,* 48**,** 5419-5423.

LORIG, T. S. 2000. The application of electroencephalographic techniques to the study of human olfaction: a review and tutorial. *International Journal of Psychophysiology,* 36**,** 91-104.

MALONE, M. E., APPELQVIST, I. A. M. & NORTON, I. T. 2003. Oral behaviour of food hydrocolloids and emulsions. Part 2. Taste and aroma release. *Food Hydrocolloids,* 17**,** 775-784.

MÁRQUEZ, A. L., MEDRANO, A., PANIZZOLO, L. A. & WAGNER, J. R. 2010. Effect of calcium salts and surfactant concentration on the stability of water-in-oil (w/o) emulsions prepared with polyglycerol polyricinoleate. *Journal of Colloid and Interface Science,* 341**,** 101-108.

MARZE, S. B. 2009. Relaxation Processes of PGPR at the Water/Oil Interface Inferred by Oscillatory or Transient Viscoelasticity Measurements. *Langmuir,* 25**,** 12066-12072.

MATALANIS, A. & MCCLEMENTS, D. J. 2012. Factors Influencing the Formation and Stability of Filled Hydrogel Particles Fabricated by Protein/Polysaccharide Phase Separation and Enzymatic Cross-Linking. *Food Biophysics,* 7**,** 72-83.

MCCLEMENTS, D. J. 2004. *Food Emulsions: Principles, Practices, and Techniques,* London, CRC Press, Boca Raton.

MCCLEMENTS, D. J. 2011. Edible nanoemulsions: fabrication, properties, and functional performance. *Soft Matter,* 7**,** 2297-2316.

MCNULTY, P. B. & KAREL, M. 1973. Factors affecting flavour release and uptake in O/W emulsion. *International Journal of Food Science & Technology,* 8**,** 415-427.

MEYNIER, A., LECOQ, C. & GENOT, C. 2005. Emulsification enhances the retention of esters and aldehydes to a greater extent than changes in the droplet size distribution of the emulsion. *Food Chemistry,* 93**,** 153-159.

MILLS, T. B. & NORTON, I. T. 2013. 11 - Tribology measurement and analysis: applications to food microstructures. *In:* MORRIS, V. J. & GROVES, K. (eds.) *Food Microstructures.* Woodhead Publishing.

MORRIS, E. R., REES, D. A. & ROBINSON, G. 1980. Cation-specific aggregation of carrageenan helices: Domain model of polymer gel structure. *Journal of Molecular Biology,* 138**,** 349-362.

NAKASHIMA, T., SHIMIZU, M. & KUKIZAKI, M. 1991. Membrane emulsification by microporous glass. *Proceedings of the 2nd International Conference on Inorganic Membranes, Montpellier, France***,** 513.

NHS. 2012. *Obesity* [Online]. Available: https://www.evidence.nhs.uk/topic/obesity [Accessed 03/08/2014 2014].

NHS. 2014. *Salt: the facts* [Online]. Available: http://www.nhs.uk/Livewell/Goodfood/Pages/salt.aspx [Accessed 25/06/2014.

NIKNAFS, N., SPYROPOULOS, F. & NORTON, I. T. 2011. Development of a new reflectance technique to investigate the mechanism of emulsification. *Journal of Food Engineering,* 104**,** 603-611.

NONO, M., NICOLAI, T. & DURAND, D. 2011. Gel formation of mixtures of κ-carrageenan and sodium caseinate. *Food Hydrocolloids,* 25**,** 750-757.

NORTON, I. T., FRITH, W. J. & ABLETT, S. 2006. Fluid gels, mixed fluid gels and satiety. *Food Hydrocolloids,* 20**,** 229-239.

NORTON, I. T., JARVIS, D. A. & FOSTER, T. J. 1999. A molecular model for the formation and properties of fluid gels. *International Journal of Biological Macromolecules,* 26**,** 255-261.

NORTON, I. T., SPYROPOULOS, F. & COX, P. W. 2009. Effect of emulsifiers and fat crystals on shear induced droplet break-up, coalescence and phase inversion. *Food Hydrocolloids,* 23**,** 1521-1526.

NORTON, J. 2011. *Fat reduction in chocolate: a multidisciplinary approach considering emulsion science and consumer expectations.*

O'SULLIVAN, J., ARELLANO, M., PICHOT, R. & NORTON, I. 2014. The effect of ultrasound treatment on the structural, physical and emulsifying properties of dairy proteins. *Food Hydrocolloids*.

OAKENFULL, D., MIYOSHI, E., NISHINARI, K. & SCOTT, A. 1999. Rheological and thermal properties of milk gels formed with κ-carrageenan. I. Sodium caseinate. *Food Hydrocolloids,* 13**,** 525-533.

PAN, L., TOMÁS, M. & AÑÓN, M. 2002. Effect of sunflower lecithins on the stability of water-in-oil and oil-in-water emulsions. *Journal of Surfactants and Detergents,* 5**,** 135-143.

PAOLETTI, S., SMIDSROD, O. & GRASDALEN, H. 1984. Thermodynamic stability of the ordered conformations of carrageenan polyelectrolytes. *Biopolymers,* 23**,** 1771-1794.

PARASKEVOPOULOU, A., TSOUKALA, A. & KIOSSEOGLOU, V. 2009. Monitoring air/liquid partition of mastic gum oil volatiles in model alcoholic beverage emulsions: Effect of emulsion composition and oil droplet size. *Food Hydrocolloids,* 23**,** 1139-1148.

PAWLIK, A., COX, P. W. & NORTON, I. T. 2010. Food grade duplex emulsions designed and stabilised with different osmotic pressures. *Journal of Colloid and Interface Science,* 352**,** 59-67.

PELAN, B. M. C., WATTS, K. M., CAMPBELL, I. J. & LIPS, A. 1997. The Stability of Aerated Milk Protein Emulsions in the Presence of Small Molecule Surfactants. *Journal of Dairy Science,* 80**,** 2631-2638.

PRADRAYUTTAWAT, A., YOSHIZAH, T., TAMURA, H. & TOKUNAGA, T. 1997. Optical Isomers and Odor Thresholds of Volatile Constituents in Citrus sudachi. *Food Science and Technology Intl,* 3**,** 402-408.

PRAJAPATI, V. D., MAHERIYA, P. M., JANI, G. K. & SOLANKI, H. K. 2014. Carrageenan: A natural seaweed polysaccharide and its applications. *Carbohydrate Polymers,* 105**,** 97-112.

QIAN, C. & MCCLEMENTS, D. J. 2011. Formation of nanoemulsions stabilized by model food-grade emulsifiers using high-pressure homogenization: Factors affecting particle size. *Food Hydrocolloids,* 25**,** 1000-1008.

QUINCHIA, L. A., DELGADO, M. A., VALENCIA, C., FRANCO, J. M. & GALLEGOS, C. 2010. Viscosity modification of different vegetable oils with EVA copolymer for lubricant applications. *Industrial Crops and Products,* 32**,** 607-612.

REYNOLDS, O. 1883. An Experimental Investigation of the Circumstances Which Determine Whether the Motion of Water Shall Be Direct or Sinuous, and of the Law of Resistance in Parallel Channels. *Royal Society of London,* Vol. 35 no. 224-226**,** 84-99.

RIBEIRO, K. O., RODRIGUES, M. I., SABADINI, E. & CUNHA, R. L. 2004. Mechanical properties of acid sodium caseinate-κ-carrageenan gels: effect of co-solute addition. *Food Hydrocolloids,* 18**,** 71-79.

RICHARDS, T. 2014. Interfacial rheology: Principle, applications and implementation.

SANKARAN, S., KHOT, L. R. & PANIGRAHI, S. 2012. Biology and applications of olfactory sensing system: A review. *Sensors and Actuators B: Chemical,* 171–172**,** 1-17.

SCHRÖDER, V., BEHREND, O. & SCHUBERT, H. 1998. Effect of Dynamic Interfacial Tension on the Emulsification Process Using Microporous, Ceramic Membranes. *Journal of Colloid and Interface Science,* 202**,** 334-340.

SHAW, D. J. 1991. *Introduction to colloid and surface chemistry,* London, Butterworth.

SIDDIQUI, S. W., UNWIN, P. J., XU, Z. & KRESTA, S. M. 2009. The effect of stabilizer addition and sonication on nanoparticle agglomeration in a confined impinging jet reactor. *Colloids and Surfaces A: Physicochemical and Engineering Aspects,* 350**,** 38-50.

SMIDSRØD, O., ANDRESEN, I.-L., GRASDALEN, H., LARSEN, B. & PAINTER, T. 1980. Evidence for a salt-promoted "freeze-out" of linkage conformations in carrageenans as a prerequisite for gel-formation. *Carbohydrate Research,* 80**,** C11-C16.

SOLANS, C., IZQUIERDO, P., NOLLA, J., AZEMAR, N. & GARCIA-CELMA, M. J. 2005. Nano-emulsions. *Current Opinion in Colloid & Interface Science,* 10**,** 102-110.

STEGEMAN, Y. W. 2002. Time dependent behavior of droplets in elongational flows.

STEGEMAN, Y. W., VAN DE VOSSE, F. N. & MEIJER, H. E. H. 2002. On the Applicability of the Grace Curve in Practical Mixing Operations. *The Canadian Journal of Chemical Engineering,* 80**,** 1-6.

STEVENSON, M. J. & CHEN, X. D. 1997. Visualization of the flow patterns in a high-pressure homogenizing valve using a CFD package. *Journal of Food Engineering,* 33**,** 151-165.

SULMONT, C., ISSANCHOU, S. & KÖSTER, E. P. 2002. Selection of Odorants for Memory Tests on the Basis of Familiarity, Perceived Complexity, Pleasantness, Similarity and Identification. *Chemical Senses,* 27**,** 307-317.

SUN, J. Z., ERICKSON, M. C. E. & PARR, J. W. 2005. Refractive index matching and clear emulsions. *Journal of cosmetic science,* 56**,** 253-265.

SURH, J., VLADISAVLJEVIĆ, G. T., MUN, S. & MCCLEMENTS, D. J. 2006. Preparation and Characterization of Water/Oil and Water/Oil/Water Emulsions Containing Biopolymer-Gelled Water Droplets. *Journal of Agricultural and Food Chemistry,* 55**,** 175-184.

TADROS, T., IZQUIERDO, P., ESQUENA, J. & SOLANS, C. 2004. Formation and stability of nano-emulsions. *Advances in Colloid and Interface Science,* 108-109**,** 303-318.

TAYLOR, A. J. & LINFORTH, R. S. T. 2001. Modelling Flavour Release through Quantitative Structure Property Relationships (QSPR). *CHIMIA International Journal for Chemistry,* 55**,** 448-452.

TAYLOR, A. J. & ROOZEN, J. P. 1996. Volatile flavor release from foods during eating. *Critical Reviews in Food Science and Nutrition,* 36**,** 765-784.

TAYLOR, G. I. 1935. Statistical theory of turbulence III - Distribution of dissipation of energy in a pipe over its cross-section. *Proceedings of the Royal Society of London Series a-Mathematical and Physical Sciences,* 151**,** 0455-0464.

TCHOLAKOVA, S., DENKOV, N. D. & DANNER, T. 2004. Role of Surfactant Type and Concentration for the Mean Drop Size during Emulsification in Turbulent Flow. *Langmuir,* 20**,** 7444-7458.

TCHOLAKOVA, S., VANKOVA, N., DENKOV, N. D. & DANNER, T. 2007. Emulsification in turbulent flow:: 3. Daughter drop-size distribution. *Journal of Colloid and Interface Science,* 310**,** 570-589.

TISSERAND, R. & YOUNG, R. 2014. 14 - Constituent profiles. *In:* YOUNG, R. T. (ed.) *Essential Oil Safety (Second Edition).* St. Louis: Churchill Livingstone.

TUORILA, H. & CARDELLO, A. V. 2002. Consumer responses to an off-flavor in juice in the presence of specific health claims. *Food Quality and Preference,* 13**,** 561-569.

VAN AKEN, G. A., VINGERHOEDS, M. H. & DE HOOG, E. H. A. 2007. Food colloids under oral conditions. *Current Opinion in Colloid & Interface Science,* 12**,** 251-262.

VANKOVA, N., TCHOLAKOVA, S., DENKOV, N. D., IVANOV, I. B., VULCHEV, V. D. & DANNER, T. 2007a. Emulsification in turbulent flow: 1. Mean and maximum drop diameters in inertial and viscous regimes. *Journal of Colloid and Interface Science,* 312**,** 363-380.

VANKOVA, N., TCHOLAKOVA, S., DENKOV, N. D., VULCHEV, V. D. & DANNER, T. 2007b. Emulsification in turbulent flow: 2. Breakage rate constants. *Journal of Colloid and Interface Science,* 313**,** 612-629.

VIA, M. 2012. The Malnutrition of Obesity: Micronutrient Deficiencies That Promote Diabetes. *ISRN Endocrinology,* 2012**,** 8.

VLIET, T. V. 2000. 1 Interfacial tension: Measurement. *In:* J. LYKLEMA, G. J. F. J. M. K. F. A. M. L. W. N. & VLIET, T. V. (eds.) *Fundamentals of Interface and Colloid Science.* Academic Press.

VOLLHARDT, J., MALKAN, N. & MANZO, R. P. 2002. *Process for producing cosmetic and pharmaceutical formulations, and products comprising same*.

WALSTRA, P. 2003. *Physical Chemistry of Foods,* New York, Marcel Dekker, Inc.

WALSTRA, P. 2005. 8 Emulsions. *In:* LYKLEMA, J. (ed.) *Fundamentals of Interface and Colloid Science.* Academic Press.

WALSTRA, P. & SMULDERS, P. E. A. 1998. Emulsion Formation. *In:* BINKS, B. P. (ed.) *Modern Aspects of Emulsion Science.* Cambridge: Royal Society of Chemistry.

WILDE, P., MACKIE, A., HUSBAND, F., GUNNING, P. & MORRIS, V. 2004. Proteins and emulsifiers at liquid interfaces. *Advances in Colloid and Interface Science,* 108-109**,** 63-71.

WINDHAB, E. J., DRESSLER, M., FEIGL, K., FISCHER, P. & MEGIAS-ALGUACIL, D. 2005. Emulsion processing—from single-drop deformation to design of complex processes and products. *Chemical Engineering Science,* 60**,** 2101-2113.

WOOD, F. W. 1968. Psychophysical studies on the consistency of liquid foods. *S.C.I Monograph***,** 40-49.

WOOSTER, T. J., GOLDING, M. & SANGUANSRI, P. 2008. Impact of Oil Type on Nanoemulsion Formation and Ostwald Ripening Stability. *Langmuir,* 24**,** 12758-12765.

WRIGHT, H. & RAMKRISHNA, D. 1994. Factors affecting coalescence frequency of droplets in a stirred liquid-liquid dispersion. *AIChE Journal,* 40**,** 767-776.

YANG, H., FAN, M., LIU, A. & DONG, L. 2015. General formulas for drag coefficient and settling velocity of sphere based on theoretical law. *International Journal of Mining Science and Technology,* 25**,** 219-223.

YUGUCHI, Y., THU THUY, T. T., URAKAWA, H. & KAJIWARA, K. 2002. Structural characteristics of carrageenan gels: temperature and concentration dependence. *Food Hydrocolloids,* 16**,** 515-522.